

AD-757 273

FUNDAMENTAL RESEARCH ON ADVANCED
TECHNIQUES FOR SONIC BOOM SUPPRESSION

B. H. Geothert, et al

Tennessee University

Prepared for:

Federal Aviation Administration

November 1972

DISTRIBUTED BY:

NTIS

National Technical Information Service
U. S. DEPARTMENT OF COMMERCE
5285 Port Royal Road, Springfield Va. 22151

FUNDAMENTAL RESEARCH ON ADVANCED TECHNIQUES FOR SONIC BOOM SUPPRESSION

AD 757273

**Dr. B. H. Goethert
The University of Tennessee
Space Institute
Tullahoma, Tennessee 37388**



NOVEMBER 1972

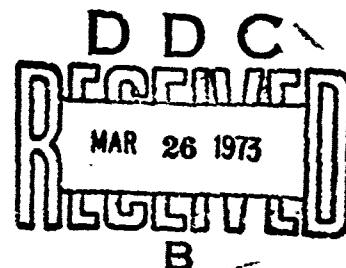
FINAL REPORT

Document is available to the public through the
National Technical Information Service,
Springfield, Virginia 22151


Reproduced by
**NATIONAL TECHNICAL
INFORMATION SERVICE**
U S Department of Commerce
Springfield VA 22151

Prepared for

**DEPARTMENT OF TRANSPORTATION
FEDERAL AVIATION ADMINISTRATION
Systems Research and Development Service
Washington, D. C. 20591**



The contents of this report reflect the views of the University of Tennessee Space Institute which is responsible for the facts and the accuracy of the data presented herein. The contents do not necessarily reflect the official views or policy of the Department of Transportation. This report does not constitute a standard, specification or regulation.

ACCESSION NO.	
NTIS	White Section <input type="checkbox"/>
D.C.	Buff Section <input type="checkbox"/>
UNAF OFFICE	<input type="checkbox"/>
JUSTIFICATION	
BY	
DISTRIBUTION/AVAILABILITY CODE	
DECL. A.C.M. AND/OR SPECIAL	
A	

TECHNICAL REPORT STANDARD TITLE PAGE

1. Report No. FAA-RD-73-4	2. Government Accession No.	3. Recipient's Catalog No.	
4. Title and Subtitle Fundamental Research on Advanced Techniques for Sonic Boom Suppression		5. Report Date November 1972	
		6. Performing Organization Code	
7. Author(s) Dr. B. H. Goethert		8. Performing Organization Report No.	
9. Performing Organization Name and Address The University of Tennessee Space Institute Tullahoma, Tennessee 37388		10. Work Unit No.	
		11. Contract or Grant No. DOT-FA 70 WA-2260	
12. Sponsoring Agency Name and Address Department of Transportation Federal Aviation Administration Systems Research and Development Service Washington, D. C. 20591		13. Type of Report and Period Covered Final Report	
		14. Sponsoring Agency Code	
15. Supplementary Notes Co-authors were: Dr. Y. S. Fan, Dr. S. N. Chaudhuri, Mr. R. Kohl, Dr. H. Gruschka and Mr. Philip Kessel.			
16. Abstract A multiphase theoretical investigation on predicting and alleviating sonic boom intensity is described. A new theory to predict sonic boom intensity on the ground from wind tunnel tests using normal size models (as opposed to the very small models presently used) was developed. A relatively easy method to determine aircraft contours with desirable finite pressure rise times is presented, as is a method to determine phantom body shapes with desirable pressure rise times which can be simulated by heat addition to the flow upstream of the aircraft. It is shown that a slotted nozzle engine exhaust has the unique capability to shift lift from the solid surface of the wing to the region behind the wing, with a resulting reduction in sonic boom intensity.			
17. Key Words Sonic Boom, Aero-acoustics, Slot Nozzle		18. Distribution Statement Document is available to the public through the National Technical Information Service, Springfield, Virginia 22151	
19. Security Classif. (of this report) Unclassified	20. Security Classif. (of this page) Unclassified	21. No. of Pages 209	22. Price

TABLE OF CONTENTS

	Page
1. INTRODUCTION	1.1
2. DISCUSSION	2.1
2.1 Extension of the Current Sonic Boom Theory and Development of a Wind Tunnel Testing Method Based on Large Models	2.1
2.2 Fundamental Theories, Applicability and Extensions	2.64
2.3 Sonic Boom Reduction by Focused Laser Beam Techniques	2.127
2.4 Engine-Airframe Integration with Special Emphasis on Non-Circular Engine Exhaust and Jet Flaps	2.157
3. CONCLUSIONS AND RECOMMENDATIONS	3.1
4. REFERENCES	4.1

PREFACE

The research described herein was performed by The University of Tennessee Space Institute, Tullahoma, Tennessee, for the Federal Aviation Agency, Washington, D. C., under Contract No. DOT-FA70WA-2260.

The Federal Aviation Agency project monitor was Mr. J. K. Power. The work reported herein was performed during the time period November 21, 1969 through November 21, 1971.

This research project encompassed four main areas. The principal investigator was Dr. P. H. Goethert, Dean of The University of Tennessee Space Institute and Professor of Aerospace and Mechanical Engineering. Mr. Robert W. Kamm, Executive Assistant to Dr. Goethert, was overall administrative coordinator for the project.

The various areas investigated and the main investigators involved were:

Fundamental Theories - Dr. Y. S. Pan, Associate Professor of Aerospace Engineering and Dr. S. N. Chaudhuri, Associate Professor of Aerospace Engineering.

Sonic Boom Reduction by Focused Laser Beam Techniques - Mr. Ronald Kohl, Assistant Professor of Physics.

Sonic Boom Reduction by Cryogenic Cooling of Air - Dr. Marcel K. Newman, Professor of Mechanical Engineering.

Engine Airframe Integration with Special Emphasis on Noncircular Engine Exhausts and Jet Flaps - Dr. Heinz Gruschka, Associate Professor of Physics and Mr. Philip Kessel, Ph.D. Candidate in Aerospace Engineering.

1. INTRODUCTION

Even though the U.S. recently discontinued the SST project, the problem of sonic boom attenuation is still of decisive importance because of supersonic flights of present and future military aircraft and future generations of space-flight vehicles, as well as future commercial aircraft. Flight routes, particularly of both domestic and foreign supersonic commercial transports will be restricted to over-water routes if the boom attenuation efforts are not sufficiently successful; whereas the entire air space, both over land and over water can be opened for supersonic air transportation if effective and economical attenuation of the sonic boom can be achieved. Thus the entire future of civilian supersonic air transportation is at stake.

Numerous theoretical and design studies as well as extensive experiments have been conducted to gain an understanding of the physical phenomena involved, and to develop methods for predicting and influencing the boom signature shape and intensity through appropriate aircraft design and operation. Mainly during the late 1960's, systematic efforts with the above objectives in mind have gained momentum and much progress has been made.

For instance, it is possible today to predict satisfactorily well the sonic boom intensity and shape in the near, mid, and far field for current supersonic aircraft designs, and to estimate with adequate accuracy the influence of design changes and of environmental parameters within the framework of today's conventional aircraft designs.

Because of the pressing urgency for finding an immediate solution for the sonic boom problem, most of the recent investigations and analysis methods were directed towards the problems associated with the planned first-generation of supersonic transports. As a result, unconventional supersonic transport designs, employing novel configurations of volume displacement, lifting surfaces, engines and exhaust jets (jet flaps) and integration of such components from the viewpoint of optimum sonic boom suppression have not received much emphasis. The University of Tennessee Space Institute and the Federal Aviation Administration recognized, however, that from a long-range viewpoint the gap in our knowledge concerning unconventional configurations must be filled by appropriate research. It was also recognized that such research would not only guide the designers and operators in devising effective evolutionary modifications of the first-generation supersonic aircraft for the purpose of better noise suppression. It would also, and probably more importantly, provide the design base for the next generation of supersonic and hypersonic transports for coping with the sonic boom problem more effectively than can be expected for the first-generation supersonic aircraft, even after successive evolutionary improvements.

The University of Tennessee Space Institute therefore undertook a multiphase investigation for the Federal Aviation Administration, the objectives of which were defined in the contract as follows:

"Fundamental Theories

This task will be to assess the numerous theories and programs presently available with an objective of defining regions of applicability and areas of limitation. Summary descriptions of near, mid and far field theories will be compiled with statements on the fundamental physical assumptions and simple verifications of limiting factors. The formulation of improved potential solutions for the far field will be explored, which are currently visualized as utilizing not only displacement singularities in a potential flow. Particular emphasis will be placed on defining the limitations of two-dimensional theory in predicting sonic boom signatures of aircraft. An exploration and evaluation of potential solutions in the vicinity of caustics will also be made. To supplement the theoretical approach into the right direction, some orientating wind tunnel tests will be conducted in the later phases of this program area."

Dr. Y. S. Pan and Dr. S. N. Chaudhuri each assisted by several graduate students, investigated separate phases of this task. Details of their findings are reported in Sections 2.1 and 2.2 respectively, of this report.

"Sonic Boom Reduction by Focused Laser-Beam Techniques

A feasibility study supported by wind tunnel experiments will be conducted to determine whether focused-laser beam techniques can be used to produce changes in the flow which may be relatable to equivalent airframe shapes. Realistic analyses of weight penalties associated with focused laser apparatus will be included to evaluate the feasibility with respect to aircraft application."

Dr. Ronald Kohl conducted this feasibility study, which is reported in Section 2.3 of this report.

"Sonic Boom Reduction by Cryogenic Cooling of Air

This task will be to assess briefly the quantitative improvement potential and the penalties associated with a radically new boom suppression technique by making use of air-liquidization effects. Disregarding the final practicability of this novel scheme, such studies will stimulate thinking along unorthodox lines and thus will have significant indirect benefits which can only be discovered by deviating greatly from the path of accepted conventional designs."

Dr. Marcel K. Newman determined during the first period of the contract that the additional power required to maintain large external surfaces at cryogenic temperatures in the Mach No. 3 flow field was excessive. Thus, with the concurrence of the FAA Project Monitor, this work was discontinued and is not reported in detail.

It is believed, however, that cryogenic cooling of the air would be feasible in a configuration known as "space-plane". The "space-plane" concept received much attention, and extensive performance and design studies were conducted in the early 1960 period. The propulsion system of the space-plane is of the liquid - air-type in which air is liquified before it is burned in the combustor. By means of the liquification of the air, the solid displacement of a major part of the airframe structure can be eliminated, and the sonic boom correspondingly reduced.

"Engine-Airframe Integration with Special Emphasis on Noncircular Engine Exhausts and Jet Flaps"

This task will be to explore the potential and feasibility of unconventional aircraft configurations, in which the complete integration of fuselage-wing-propulsion units is approached. Special emphasis will be placed on examining in depth the potential of noncircular engine exhausts, possibly in combination with variable jet plumes, for boom reduction. Besides other advantages of jet flaps, exhausting the processed air at the trailing edge of the wing either over the entire wing span or only over part span, the reduction of the rate of area increase of the stream tube air passing through the engine may be conveniently integrated with the air frame displacement and the equivalent displacement due to lift. A large number of such highly integrated engine-airframe configurations may become feasible especially if stability considerations of the aircraft would be eliminated, and instead artificial stability and control relied upon."

Dr. B. H. Goethert, principal investigator for this project, assisted by Dr. Heinz Gruschka and Mr. Philip Kessel (A UTSI Doctoral Candidate) studied this task. Their findings are reported in Section 2.4.

-Publications in professional journals based on the research work of this contract were:

Pan, Y. S. (1970), "Application of Whitham's theory to sonic boom in the mid-or near-field", AIAA Journal, Vol. 8, No. 11, pp 2080-2082

Pan, Y. S. (1971), "A method for wind tunnel investigations of sonic boom based on large models", AIAA Paper No. 71-184

Chaudhuri, S. N. and Praharaj, S. C. (1971), "The near-field flow pattern of an inclined slender body of revolution", AIAA Paper No. 71-626.

In addition to these publications, Dr. Pan presented Paper No. 71-184 at the 9th AIAA Aerospace Sciences Meeting, January 25-27, 1971, New York; and Mr. Praharaj presented Paper No. 71-626 at the 4th Fluid and Plasma Dynamics Conference of the American Institute of Aeronautics and Astronautics, June 21-23, 1971, Palo Alto, California.

Additional publications and presentations are also in preparation.

2. DISCUSSION

2.1 EXTENSION OF THE CURRENT SONIC BOOM THEORY AND DEVELOPMENT OF A WIND TUNNEL TESTING METHOD BASED ON LARGE MODELS by Dr. Y. S. Pan and UTSI students K. T. Wang and M. O. Varner

2.1.1 INTRODUCTION

Because of the development of supersonic transports, the sonic boom problem has been receiving considerable attention in the past decade. Calculations of sonic boom pressure signature of a supersonic aircraft have been based mainly on Whitham's supersonic projectile theory (Whitham, 1952) and the supersonic area rule of Hayes (1947) and Lomax (1955). The supersonic area rule shows that the pressure disturbance for a complex three-dimensional configuration can be reduced to the calculation of the pressure disturbance due to an equivalent body of revolution, provided that the position of interest is sufficiently far from the body. Whitham's theory, on the other hand, describes an asymptotic flow behavior at a distance sufficiently far from a body of revolution. This asymptotic flow obeys the geometric acoustic laws. That is, the flow disturbances are linearly proportional to a local F function, which is related to the shape of the body and to the flow conditions. The values of the F function are constant along the characteristic curves emitted from the body. Consequently, the sonic boom signature at a distance far from an aircraft can be calculated from the F function of an equivalent body of revolution of the aircraft.

In experimental investigations of the sonic boom in wind tunnels, it is usually necessary to use very small models in order to obtain direct measurements of the far-field pressure signature in the vicinity of a wind tunnel wall (see, for example,

Carlson (1964)). With these small models, inaccuracies with respect to model contours, vibration of model, boundary layer development, interferences of the sting supports, small non-uniformities of the free stream, etc. usually arise. The present proposed wind tunnel testing method is directed towards an alleviation of this very small model restriction.

The present proposed method is based on large models in wind tunnels, where only the near or the mid-field is simulated. By measuring the pressure distribution at the vicinity of the wind tunnel wall, it is possible to determine the signature of the sonic boom at large distances in the outer mid-field or in the far-field. This method is expected to have great significance in making wind tunnel tests more reliable by avoiding the use of extremely small models as is usually done today.

It is well known that, in the near field of an aircraft, the flow field is fully three-dimensional. The supersonic area rule may not be applied there and, hence, Whitham's supersonic projectile theory may not be employed directly. Moreover, the flow disturbances in the near field may not be generally described by Whitham's asymptotic relations even within the assumption of the linearized supersonic flow (Pan 1970 a,b, 1971). Indeed, recent wind tunnel experiments (Morris, Lamb and Carlson, 1970) have shown that Whitham's theory does not give good predictions of pressure signature shape in the near field especially at large Mach numbers and at large angles of attack.

Consequently, the calculation of flow disturbances in a not-so-far field from an aircraft or the extrapolation of a sonic boom pressure signature from a known pressure disturbance at a nearer field must be examined.

In this section, based on the well-known quasi-linear assumptions, we shall extend the current sonic boom theory to the near field. We shall be particularly concerned with the non-axisymmetric and non-geometric-acoustic effects in the flow field. Based on the new extended theory, we shall present a new wind tunnel testing method for sonic boom based on large models.

2.1.2 EXTENSION OF THE CURRENT SONIC BOOM THEORY

As discussed in the preceding sub-section, the current sonic boom theory is limited to predict the pressure disturbance at a distance sufficiently far from a supersonic aircraft. In this sub-section, we shall develop a theory to be applicable almost in the entire flow field.

GENERAL CONSIDERATION

Let us consider a steady, homogeneous, irrotational, supersonic flow over a three-dimensional configuration such as an aircraft (Figure 2.1.1). The flow disturbance generated by the aircraft in the supersonic flow propagates along characteristic surfaces to the far field in the downstream. It is clear physically that the flow disturbance in the far field due to the presence of this aircraft is equivalent to the flow disturbance

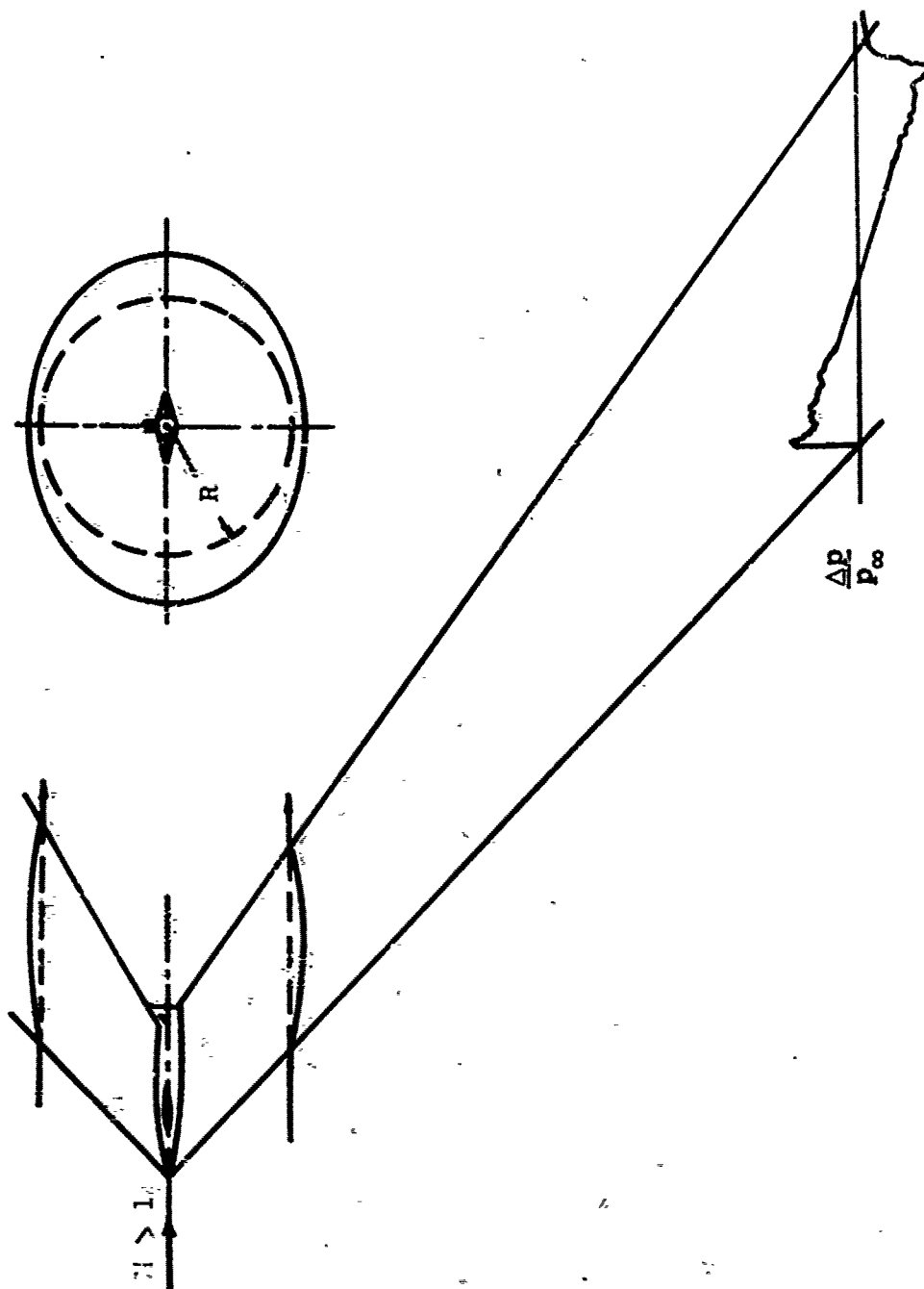


FIGURE 2.1.1.1 Supersonic Aircraft and Sonic Boom Propagation

generated from a streamtube of upstream radius R , or any other streamtubes, enclosing this aircraft in the nearer field.

A streamtube of upstream circular cross section with radius R is chosen arbitrarily but not too close to the aircraft (Figure 2.1.1), the flow disturbance over this streamtube is generally weak and this streamtube is of quasi-cylindrical shape with a mean radius R . The flow field over this streamtube can be treated by the well known linearized supersonic flow theory. The shape of this streamtube and the flow disturbance over this streamtube at R can be represented by a superposition of various multipole distributions. By defining a Whitham type F function in terms of these multipole distributions, we can obtain the F function for this streamtube of upstream radius R , which, in turn, can be related to the various flow disturbances at R .

The propagation of the known F function representing flow disturbance from one streamtube to another one further afield may be treated based on Whitham's hypothesis on the improvement of characteristics; that is, the values of the F function, are constant along bicharacteristics in the three-dimensional flow. Thus the new F function is obtained for a streamtube further afield. However, the new F function may generally have multiple values in certain regions of its arguments; these are due to the intersection of characteristic surfaces in the physical space where values of physical quantities cease to be unique. This failure of the linearized supersonic flow theory as a description of the flow is known to be remedied by the presence of shock surfaces. The positions of shock surfaces

may be determined by the usual simple geometric property; that is, to the first order of shock strength, the shock surface bisects the angle between the two intersecting characteristic surfaces. Having fixed the positions of the shocks, the new F function becomes single valued, which actually is the Whitham type local F function of the corresponding streamtube further afield. Finally, from the new single valued F function for this streamtube further afield, the corresponding flow disturbances may be obtained.

GOVERNING EQUATION AND ITS SOLUTION

Let us choose the body axis to be the x -axis coinciding with the free stream direction (Figure 2.1.2). Enclosing this body we choose a co-axial quasi-cylindrical streamtube with an arbitrary upstream radius R ($R=0$ corresponds to a general point-nosed slender body). On the surface of this streamtube the flow is assumed to be disturbed at $x=0$ where the origin of the x -axis is located. The r -axis perpendicular to the x -axis is the radial coordinate and θ is the polar coordinate measured counter-clockwise from the vertical downward r -direction. We further assume that the entire problem is symmetric with respect to $\theta=0$ (or π) plane.

Let the free stream velocity and Mach number be U and M respectively, and at a general point (x,r,θ) the local velocity be $(U+U_u, U_v, U_w)$. The flow is assumed to be irrotational, hence the velocity disturbances u, v , and w may be deduced from a velocity potential ϕ . On the linearized flow theory, ϕ satisfies the equation,

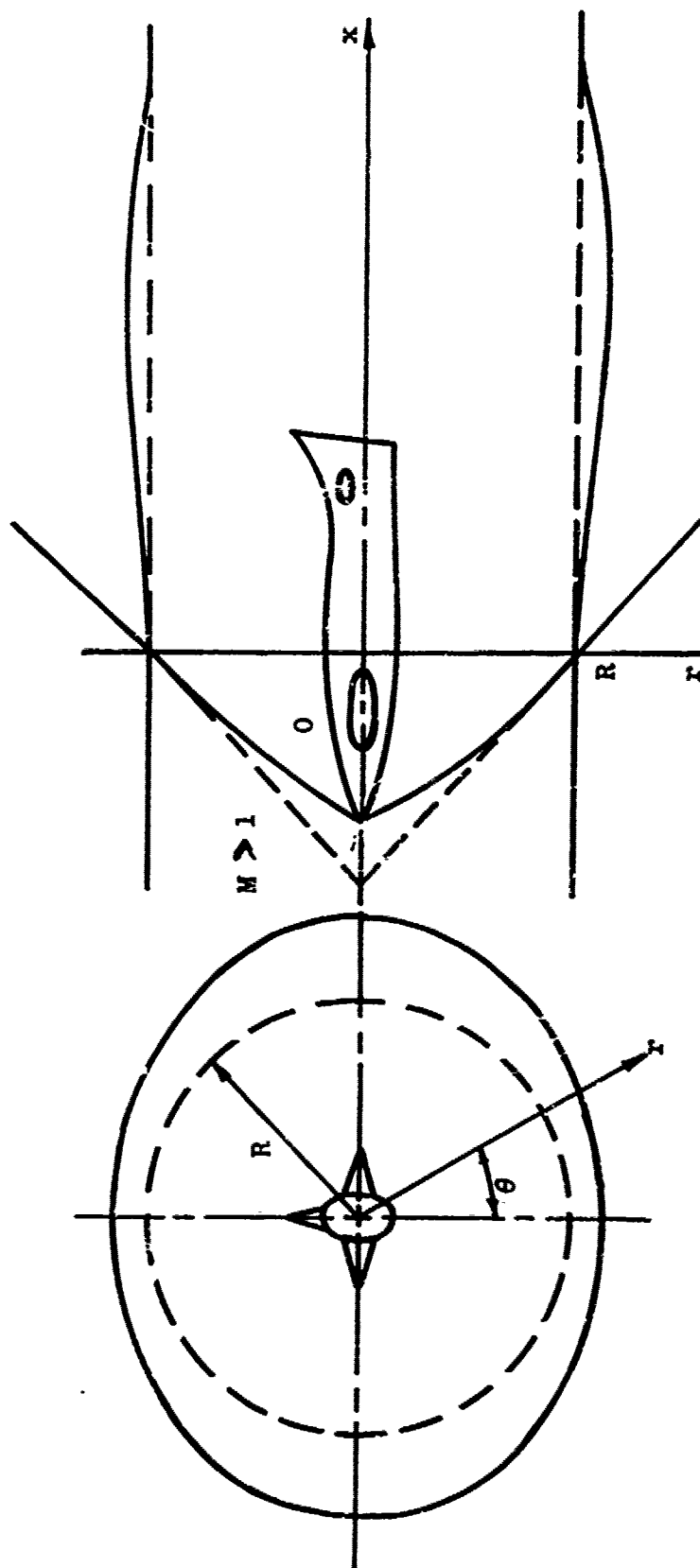


FIGURE 2.1.2 Quasi-Cylindrical Streamtube and Coordinate System

$$\frac{\partial^2 \phi}{\partial r^2} + \frac{1}{r} \frac{\partial \phi}{\partial r} + \frac{1}{r^2} \frac{\partial^2 \phi}{\partial \theta^2} - \beta^2 \frac{\partial^2 \phi}{\partial x^2} = 0, \quad (2.1.1)$$

where $\beta = (M^2 - 1)^{1/2}$

A general solution of Eq. (2.1.1) which represents a disturbance propagating downstream from the quasi-cylinder is, (Ward 1955),

$$\phi = - \sum_n \cos n\theta \int_{-\beta R}^{x-\beta r} \frac{h_n \left(\frac{x-t}{\beta r} \right) f_n(t) dt}{[(x-t)^2 - \beta^2 r^2]^{1/2}} \quad (2.1.2)$$

disturbance velocity components deduced from Eq. (2.1.2) are,

$$u = - \sum_n \cos n\theta \int_{-\beta R}^{x-\beta r} \frac{h_n \left(\frac{x-t}{\beta r} \right) f'_n(t) dt}{[(x-t)^2 - \beta^2 r^2]^{1/2}}, \quad (2.1.3)$$

$$v = \sum_n \cos n\theta \int_{-\beta R}^{x-\beta r} \frac{x-t}{r} \frac{h_n \left(\frac{x-t}{\beta r} \right) f'_n(t) dt}{[(x-t)^2 - \beta^2 r^2]^{1/2}} \quad (2.1.4)$$

and

$$w = \sum_n n \sin n\theta \int_{-\beta R}^{x-\beta r} \frac{h_n \left(\frac{x-t}{\beta r} \right) f_n(t) dt}{r [(x-t)^2 - \beta^2 r^2]^{1/2}}. \quad (2.1.5)$$

Here,

$$h_n(t) = \cosh [n \cosh^{-1} t], \quad (2.1.6)$$

and $f_n(t)$ are the multipole distributions and may be related to the shape of the quasi-cylindrical streamtube (Lomax and Heaslet, 1956). We shall solve for $f_n(t)$ in terms of the flow

disturbances later. The pressure disturbance relates to the velocity disturbances by the linearized Bernoulli's equation (Ward 1955),

$$p \equiv \frac{\Delta p}{\rho_{\infty} U^2} = \frac{p - p_{\infty}}{\rho_{\infty} U^2} = -u \quad (2.1.7)$$

F FUNCTION AND ITS FOURIER COMPONENTS

By changing the integration variables and by replacing $x - \beta r = y - \beta R$ in Eqs. (2.1.4)-(2.1.6), we have

$$u = - \sum_n \cos n \theta \int_0^y \frac{h_n (1 + \frac{y-t}{\beta r}) f'_n(t - \beta R) dt}{[(y-t)(y-t + 2\beta r)]^{1/2}} \quad (2.1.8)$$

$$r = \sum_n \cos n \theta \int_0^y \frac{y-t + \beta r}{r} \frac{h_n (1 + \frac{y-t}{\beta r}) f'_n(t - \beta R) dt}{[(y-t)(y-t + 2\beta r)]^{1/2}} \quad (2.1.9)$$

$$w = \sum_n \sin n \theta \int_0^y \frac{1}{r} \frac{h_n (1 + \frac{y-t}{\beta r}) f_n(t - \beta R) dt}{[(y-t)(y-t + 2\beta r)]^{1/2}} \quad (2.1.10)$$

Here, y is the characteristic parameter of a linearized characteristic curve from the surface of the streamtube of upstream radius R .

To define a Whitham type F function, we make a far-field approximation, i.e., $\beta r/y \gg 1$ and write velocity components in Fourier series expansions. The expressions (2.1.8) to (2.1.10) are reduced respectively to,

$$u = \sum_n u_n \cos n \theta = - \frac{1}{(2\beta r)^{1/2}} \sum_n F_n(y) \cos n \theta, \quad (2.1.11)$$

$$v = \sum_n v_n \cos n \theta = \frac{\alpha}{(2\beta r)^{1/2}} \sum_n F_n(y) \cos n \theta \quad (2.1.12)$$

$$w = \sum_n w_n \sin n \theta = \frac{1}{r(2\beta r)^{1/2}} \sum_n n G_n(y) \sin n \theta \quad (2.1.13)$$

Here,

$$F_n(y) = \int_0^y \frac{f'_n(t - \beta R) dt}{(y-t)^{1/2}} \quad (2.1.14)$$

being the Fourier components of the F function of the stream-tube with upstream radius R

$$F(y, \theta) = \sum_n F_n(y) \cos n \theta \quad (2.1.15)$$

and

$$G_n(y) = \int_0^y F_n(t) dt. \quad (2.1.16)$$

It may be noted that for bodies of revolution ($n=0$), the above relations are those asymptotic linear relations of Whitham (1952); for bodies of revolution at small angles of attack ($n=0$ and 1), the above relations reduce to those of Siegelman (1967). It may also be pointed out that in the above relations u and v vary as $r^{-1/2}$ and w varies as $r^{-3/2}$ to the far field; hence, in the far-field, w may be neglected in comparison with

u or v. Consequently, u, v and P may be related only to the F function of an equivalent body of revolution. This is the basis on which the current sonic boom calculations are made.

RELATIONS BETWEEN THE F FUNCTION AND FLOW DISTURBANCES

It has been shown by Pan (1970 a,b) that it is possible, within the linearized supersonic flow theory, to obtain exact relations between the flow disturbances and the corresponding local F function on an arbitrary streamtube enclosing an axisymmetric body. These relations are valid in the entire flow field of an axisymmetric slender body in the supersonic flow. Now we shall obtain similar relations for the flow over a non-axisymmetric quasi-cylindrical streamtube of upstream radius R (Figure 2.1.2). At large R, these relations reduce to Eqs. (2.1.11)-(2.1.13).

As stated previously, the shape of the streamtube of upstream radius R is represented by the superposition of the various multipole distributions f_n , where f_n may be determined in terms of the flow disturbances on the surface of the streamtube by the boundary conditions of Eq. (2.1.1). By setting $r=R$ in Eqs. (2.1.3)-(2.1.5) [or Eqs. (2.1.8)-(2.1.10)], using Eq. (2.1.7), and expanding the flow disturbances in Fourier series in θ [See, Eqs. (2.1.11)-(2.1.13)], the multipole distributions may be related to the Fourier components of the flow disturbances by the following integral equations; at (x,R) ,

$$P_n = -u_n = \int_0^x \frac{h_n \left(\frac{x-t}{\beta R} + 1 \right) f'_n(t - \beta R) dt}{[(x-t)(x-t + 2\beta R)]^{1/2}}, \quad (2.1.17)$$

$$v_n = \int_0^x \frac{x-t+\beta R}{R} \frac{h_n \left(\frac{x-t}{\beta R} + 1 \right) f'_n(t - \beta R) dt}{[(x-t)(x-t+2\beta R)]^{1/2}}, \quad (2.1.18)$$

and

$$w_n = \int_0^x \frac{n}{R} \frac{h_n \left(\frac{x-t}{\beta R} + 1 \right) f_n(t - \beta R) dt}{[(x-t)(x-t+2\beta R)]^{1/2}} \quad (2.1.19)$$

These are integral equations for f'_n of f_n and can be solved. Either f_n or f'_n can be found in terms of the Fourier components of the flow disturbance \dot{P}_n, u_n, v_n or w_n . Solutions have been obtained and reported by Pan (1971).

By substituting the solutions of f_n and f'_n into the definitions of F_n and G_n [Eqs. (2.1.14) and (2.1.16)], F_n and G_n can be written in terms of the flow disturbances (Pan, 1971), at R

$$\frac{F_n(x)}{(2\beta R)^{1/2}} = \begin{Bmatrix} P_n(x) \\ -u_n(x) \end{Bmatrix} - \frac{1}{\beta R} \int_0^x \begin{Bmatrix} P_n(t) \\ -u_n(t) \end{Bmatrix} S_n \left(\frac{x-t}{\beta R} \right) dt. \quad (2.1.20)$$

$$\frac{\beta F_n(x)}{(2\beta R)^{1/2}} = v_n(x) - \frac{1}{\beta R} \int_0^x v_n(t) T_n \left(\frac{x-t}{\beta R} \right) dt, \quad (2.1.21)$$

and

$$\frac{nG_n(x)}{R(2\beta R)^{1/2}} = w_n(x) - \frac{1}{\beta R} \int_0^x w_n(t) S_n \left(\frac{x-t}{\beta R} \right) dt. \quad (2.1.22)$$

Here S_n and T_n are resolvent kernels of K'_n and J'_n , respectively.

K'_n and J'_n are the differentiations of K_n and J_n , respectively, with respect to their arguments, where

$$K_n(x) = \frac{2^{3/2}}{\pi} \int_0^{\pi/2} \frac{h_n(x \cos^2 z + 1) dz}{(2 + x \cos^2 z)^{1/2}}, \quad (2.1.23)$$

and

$$J_n(x) = \frac{2^{3/2}}{\pi} \int_0^{\pi/2} \frac{(x \cos^2 z + 1) h_n(x \cos^2 z + 1) dz}{(2 + x \cos^2 z)^{1/2}} \quad (2.1.24)$$

S_n, T_n, K'_n and J'_n , have been computed on the UTSI computer IBM 1130 and are tabulated respectively in Tables 2.1.1 to 2.1.4 for x from 0 to 2.0 and for n from 0 to 5. [S_0, T_0, K'_0 and J'_0 were denoted respectively, as $S, S_1, K',$ and K'_1 previously by Pan (1970a)].

The Fourier components of the flow disturbances may also be expressed in terms of the corresponding F_n or G_n , at R (Pan 1971),

$$\begin{Bmatrix} P_n(x) \\ -u_n(x) \end{Bmatrix} = \frac{1}{(2\beta R)^{1/2}} \left[F_n(x) + \frac{1}{\beta R} \int_0^x F_n(t) K'_n\left(\frac{x-t}{\beta R}\right) dt \right] \quad (2.1.25)$$

$$v_n(x) = \frac{\beta}{(2\beta R)^{1/2}} \left[F_n(x) + \frac{1}{\beta R} \int_0^x F_n(t) J'_n\left(\frac{x-t}{\beta R}\right) dt \right] \quad (2.1.26)$$

$$w_n(x) = \frac{n}{R(2\beta R)^{1/2}} \left[G_n(x) + \frac{1}{\beta R} \int_0^x G_n(t) K'_n\left(\frac{x-t}{\beta R}\right) dt \right] \quad (2.1.27)$$

Since the streamtube of upstream radius R was chosen

TABLE 2.1.1 FUNCTIONS $S_n(x)$

x	n					
	0	1	2	3	4	5
0	- 0.1250 E+0 ^a	0.3750 E+0	0.1875 E+1	0.4375 E+1	0.7875 E+1	0.1237 E+2
0.1	- 0.1198 E+0	0.3503 E+0	0.1621 E+1	0.3307 E+1	0.4875 E+1	0.5780 E+1
0.2	- 0.1151 E+0	0.3279 E+0	0.1396 E+1	0.2437 E+1	0.2733 E+1	0.1877 E+0
0.3	- 0.1108 E+0	0.3073 E+0	0.1198 E+1	0.1738 E+1	0.1266 E+1	-0.1047 E+1
0.4	- 0.1069 E+0	0.2885 E+0	0.1024 E+1	0.1186 E+1	0.3170 E+0	-0.1208 E+1
0.5	- 0.1033 E+0	0.2712 E+0	0.8908 E+0	0.7568 E+0	-0.2484 E+0	-0.1003 E+1
0.6	- 0.1000 E+0	0.2553 E+0	0.7374 E+0	0.4306 E+0	-0.5394 E+0	-0.6563 E+0
0.7	- 0.9700 E-1	0.2406 E+0	0.6210 E+0	0.1888 E+0	-0.6433 E+0	-0.3005 E+0
0.8	- 0.9417 E-1	0.2270 E+0	0.5199 E+0	0.1532 E-1	-0.6278 E+0	-0.1352 E-1 ^b
0.9	- 0.9154 E-1	0.2144 E+0	0.4325 E+0	-0.1037 E+0	-0.5435 E+0	
1.0	- 0.8910 E-1	0.2028 E+0	0.3570 E+0	-0.1802 E+0	-0.4270 E+0	
1.1	- 0.8681 E-1	0.1919 E+0	0.2921 E+0	-0.2240 E+0	-0.3028 E+0	
1.2	- 0.8466 E-1	0.1819 E+0	0.2365 E+0	-0.2433 E+0	-0.1867 E+0	
1.3	- 0.8264 E-1	0.1725 E+0	0.1890 E+0	-0.2453 E+0	-0.8987 E-1	
1.4	- 0.8075 E-1	0.1638 E+0	0.1486 E+0	-0.2348 E-0	-0.1189 E-1 ^b	
1.5	- 0.7896 E-1	0.1556 E+0	0.1145 E+0	-0.2163 E+0		
1.6	- 0.7726 E-1	0.1480 E+0	0.8586 E-1	-0.1931 E+0		
1.7	- 0.7566 E-1	0.1409 E+0	0.6183 E-1	-0.1677 E+0		
1.8	- 0.7414 E-1	0.1343 E+0	0.4847 E-1	-0.1419 E+0		
1.9	- 0.7270 E-1	0.1280 E+0	0.2534 E-1	-0.1168 E+0		
2.0	- 0.7133 E-1	0.1222 E+0	0.1182 E-1	-0.9367 E-1		

^a Data are presented in the Floating-Point form used in the FORTRAN program language.
For example, -0.7133×10^{-1} is printed as -0.7133 E-1 .

^b values of data beyond this point cannot be accurately obtained at present.

TABLE 2.1.2 FUNCTION $T_n(x)$

x	n					
	0	1	2	3	4	5
0	0.3750 E+0 ^a	0.8750 E+0	0.2375 E+1	0.4875 E+1	0.8375 E+1	0.1287 E+2
0.1	0.3504 E+0	0.8146 E+0	0.2165 E+1	0.3907 E+1	0.5496 E+1	0.6351 E+1
0.2	0.3279 E+0	0.8059 E+0	0.1941 E+1	0.2987 E+1	0.3136 E+1	0.1954 E+1
0.3	0.3074 E+0	0.7686 E+0	0.1709 E+1	0.2141 E+1	0.1309 E+1	-0.6443 E+0
0.4	0.2885 E+0	0.7301 E+0	0.1476 E+1	0.1390 E+1	0.1540 E-1	-0.1825 E+1
0.5	0.2712 E+0	0.6911 E+0	0.1247 E+1	0.7482 E+0	-0.8312 E+0	-0.1991 E+1
0.6	0.2553 E+0	0.6518 E+0	0.1027 E+1	0.2233 E+0	-0.1254 E+1	-0.1529 E+1
0.7	0.2406 E+0	0.6126 E+0	0.8183 E+0	-0.1833 E+0	-0.1350 E+1	-0.7782 E+0 ^b
0.8	0.2270 E+0	0.5738 E+0	0.6242 E+0	-0.4761 E+0	-0.1207 E+1	0.3780 E-1 ^b
0.9	0.2144 E+0	0.5357 E+0	0.4483 E+0	-0.6639 E+0	-0.9122 E+0	
1.0	0.2027 E+0	0.4983 E+0	0.2904 E+0	-0.7590 E+0	-0.5456 E+0	
1.1	0.1919 E+0	0.4621 E+0	0.1518 E+0	-0.7763 E+0	-0.1735 E+0	
1.2	0.1819 E+0	0.4269 E+0	0.3261 E-1	-0.7318 E+0	0.1526 E+0	
1.3	0.1725 E+0	0.3931 E+0	-0.6684 E-1	-0.6416 E+0	0.3382 E+0	
1.4	0.1638 E+0	0.3606 E+0	-0.1478 E+0	-0.5215 E+0	0.5213 E+0 ^b	
1.5	0.1556 E+0	0.3295 E+0	-0.2112 E+0	-0.3854 E+0		
1.6	0.1481 E+0	0.2998 E+0	-0.2581 E+0	-0.2457 E+0		
1.7	0.1409 E+0	0.2717 E+0	-0.2902 E+0	-0.1126 E+0		
1.8	0.1340 E+0	0.2450 E+0	-0.3089 E+0	0.6930 E-1		
1.9	0.1281 E+0	0.2199 E+0	-0.3161 E+0	0.1052 E+0		
2.0	0.1222 E+0	0.1961 E+0	-0.3134 E+0	0.2283 E+0		

^a Data are present in the Floating-Point form used in the FORTRAN program language.
For example, -0.1350 x 10 is printed as -0.1350 E+1.

^b Values of data beyond this point cannot be accurately obtained at present.

TABLE 2.1.3 FUNCTION $K'_n(x)$

x	n					
	0	1	2	3	4	5
0	-0.1250 E+0 ^a	0.3750 E+0	0.1875 E+1	0.4375 E+1	0.7875 E+1	0.1237 E+2
0.1	-0.1183 E+0	0.3638 E+0	0.1955 E+1	0.5130 E+1	0.1080 E+2	0.2057 E+2
0.2	-0.1122 E+0	0.3534 E+0	0.2033 E+1	0.5917 E+1	0.1419 E+2	0.3133 E+2
0.3	-0.1067 E+0	0.3439 E+0	0.2108 E+1	0.6736 E+1	0.1806 E+2	0.4502 E+2
0.4	-0.1017 E+0	0.3350 E+0	0.2181 E+1	0.7586 E+1	0.2243 E+2	0.6203 E+2
0.5	-0.9713 E-1	0.3268 E+0	0.2252 E+1	0.8464 E+1	0.2731 E+2	0.8278 E+2
0.6	-0.9290 E-1	0.3191 E+0	0.2321 E+1	0.9371 E+1	0.3273 E+2	0.1077 E+2
0.7	-0.8899 E-1	0.3119 E+0	0.2388 E+1	0.1030 E+2	0.3870 E+2	0.1371 E+3
0.8	-0.8537 E-1	0.3052 E+0	0.2453 E+1	0.1126 E+2	0.4524 E+2	0.1716 E+3
0.9	-0.8202 E-1	0.2988 E+0	0.2517 E+1	0.1225 E+2	0.5235 E+2	0.2116 E+3
1.0	-0.7890 E-1	0.2928 E+0	0.2579 E+1	0.1327 E+2	0.6008 E+2	0.2576 E+3
1.1	-0.7599 E-1	0.2872 E+0	0.2640 E+1	0.1430 E+2	0.6841 E+2	0.3099 E+3
1.2	-0.7328 E-1	0.2818 E+0	0.2699 E+1	0.1537 E+2	0.7737 E+2	0.3693 E+3
1.3	-0.7073 E-1	0.2767 E+0	0.2758 E+1	0.1645 E+2	0.8697 E+2	0.4361 E+3
1.4	-0.6835 E-1	0.2719 E+0	0.2815 E+1	0.1756 E+2	0.9724 E+2	0.5108 E+3
1.5	-0.6611 E-1	0.2673 E+0	0.2872 E+1	0.1870 E+2	0.1081 E+3	0.5941 E+3
1.6	-0.6399 E-1	0.2629 E+0	0.2926 E+1	0.1985 E+2	0.1198 E+3	0.6864 E+3
1.7	-0.6200 E-1	0.2586 E+0	0.2951 E+1	0.2103 E+2	0.1321 E+3	0.7883 E+3
1.8	-0.6012 E-1	0.2548 E+0	0.3034 E+1	0.2223 E+2	0.1451 E+3	0.9003 E+3
1.9	-0.5834 E-1	0.2510 E+0	0.3086 E+1	0.2345 E+2	0.1589 E+3	0.1023 E+4
2.0	-0.5665 E-1	0.2473 E+0	0.3138 E+1	0.2469 E+2	0.1734 E+3	0.1157 E+4

^a Data are presented in the Floating-Point form used in the FORTRAN program language.
For example, 0.1157×10^4 is printed as 0.1157 E+4.

TABLE 2.1.4 FUNCTION $J'_n(x)$

x	n					
	0	1	2	3	4	5
0	0.3750 E+0 ^a	0.8750 E+0	0.2375 E+1	0.4875 E+1	0.8375 E+1	0.1287 E+2
0.1	0.3638 E+0	0.9186 E+0	0.2747 E+1	0.6380 E+1	0.1285 E+2	0.2394 E+2
0.2	0.3534 E+0	0.9605 E+0	0.3135 E+1	0.8114 E+1	0.1862 E+2	0.4019 E+3
0.3	0.3439 E+0	0.1001 E+1	0.3540 E+1	0.1008 E+2	0.2588 E+2	0.6302 E+3
0.4	0.3350 E+0	0.1039 E+1	0.3960 E+1	0.1231 E+2	0.3481 E+2	0.9400 E+3
0.5	0.3268 E+0	0.1077 E+1	0.4395 E+1	0.1478 E+2	0.4562 E+2	0.1349 E+3
0.6	0.3191 E+0	0.1114 E+1	0.4845 E+1	0.1753 E+2	0.5852 E+2	0.1877 E+3
0.7	0.3119 E+0	0.1149 E+1	0.5309 E+1	0.2054 E+2	0.7372 E+2	0.2547 E+3
0.8	0.3052 E+0	0.1184 E+1	0.5786 E+1	0.2385 E+2	0.9146 E+2	0.3383 E+3
0.9	0.2988 E+0	0.1217 E+1	0.6277 E+1	0.2744 E+2	0.1119 E+3	0.4409 E+3
1.0	0.2928 E+0	0.1250 E+1	0.6781 E+1	0.3133 E+2	0.1354 E+3	0.5657 E+3
1.1	0.2872 E+0	0.1282 E+1	0.7297 E+1	0.3552 E+2	0.1621 E+3	0.7156 E+3
1.2	0.2818 E+0	0.1313 E+1	0.7825 E+1	0.4003 E+2	0.1923 E+3	0.8941 E+3
1.3	0.2767 E+0	0.1344 E+1	0.8366 E+1	0.4486 E+2	0.2263 E+3	0.1104 E+4
1.4	0.2719 E+0	0.1376 E+1	0.8919 E+1	0.5003 E+2	0.2642 E+3	0.1351 E+4
1.5	0.2673 E+0	0.1403 E+1	0.9483 E+1	0.5552 E+2	0.3064 E+3	0.1638 E+4
1.6	0.2629 E+0	0.1431 E+1	0.1006 E+2	0.6136 E+2	0.3531 E+3	0.1969 E+4
1.7	0.2588 E+0	0.1459 E+1	0.1064 E+2	0.6754 E+2	0.4046 E+3	0.2350 E+4
1.8	0.2548 E+0	0.1487 E+1	0.1124 E+2	0.7409 E+2	0.4613 E+3	0.2785 E+4
1.9	0.2510 E+0	0.1514 E+1	0.1185 E+2	0.8099 E+2	0.5233 E+3	0.3279 E+4
2.0	0.2473 E+0	0.1540 E+1	0.1247 E+2	0.8826 E+2	0.5909 E+3	0.3838 E+4

^a Data are presented in the Floating-Point form used in the FORTRAN program language.
For example, 0.3838×10^4 is printed as 0.3838 E+4.

arbitrarily, the relationship between the flow disturbances and F_n or G_n [Eqs. (2.1.20)-(2.1.22) or Eqs. (2.1.25)-(2.1.27)] are valid for any R within the linearized supersonic flow theory. As $R \rightarrow \infty$, these relations reduce to the asymptotic linear relations, Eqs. (2.1.11)-(2.1.13), which for $n=0$ correspond to Whitham's asymptotic relation (1952). The second terms in Eqs. (2.1.20)-(2.1.22) and Eqs. (2.1.25)-(2.1.27) represent the corrections of the asymptotic relations in the nearer field.

PROPAGATION OF THE DISTURBANCE

Since the relations, Eqs. (2.1.25)-(2.1.27), are valid where the flow disturbances are weak, we may now write the expressions for flow disturbances at any distance r in terms of corresponding local F function at r ,

$$\left. \begin{aligned} & \frac{1}{\gamma M^2} \frac{\Delta p}{p_\infty} \\ & -u(y) \end{aligned} \right\} = \frac{1}{(2\beta r)^{1/2}} \left[F(y, \theta_0) + \frac{1}{\beta r} \sum_n \cos n \theta_0 \int_0^y F_n(t) K'_n \left(\frac{y-t}{\beta r} \right) dt \right] \quad (2.1.28)$$

$$v(y) = \frac{\beta}{(2\beta r)^{1/2}} \left[F(y, \theta_0) + \frac{1}{\beta r} \sum_n \cos n \theta_0 \int_0^y F_n(t) J'_n \left(\frac{y-t}{\beta r} \right) dt \right] \quad (2.1.29)$$

$$w(y) = \frac{-1}{r(2\beta r)^{1/2}} \left\{ \frac{\partial}{\partial \theta} \left[G(y, \theta) + \frac{1}{\beta r} \sum_n \cos n \theta \int_0^y G_n(t) K'_n \left(\frac{y-t}{\beta r} \right) dt \right] \right\}_{\theta=\theta_0}$$

Based on Whitham's hypothesis on the improvement of the

linear theory (1952), the flow disturbance in steady supersonic two-dimensional flow propagates along an improved two-dimensional characteristic which is at an angle with respect to the flow direction equal to the Mach angle. In three-dimensional flow, the two-dimensional characteristic is replaced by a bi-characteristic direction and a characteristic surface orientation. A bi-characteristic direction is one which is at an angle with respect to the flow direction equal to the Mach angle. A characteristic surface orientation is one for which the angle between the normal and the flow direction is the complement of the Mach angle. A bicharacteristic line is an integral curve for the bicharacteristic direction. A characteristic surface is a surface, the orientation of which is everywhere the characteristic orientation. A general bicharacteristic line through a given point is far from unique; however, a characteristic surface through a given smooth line in space is locally unique. Any envelope of characteristic surface is also a characteristic surface. To a given bicharacteristic direction at a point corresponds a unique characteristic orientation, for which the bicharacteristic direction is tangent to the characteristic surface. Through a given non-singular point in a given characteristic surface passes a unique bicharacteristic line in a characteristic surface (Hayes and Probstein, 1966).

For the present problem of the linearized supersonic flow, the characteristic surfaces are surfaces of revolution with respect to the axis (Ferri, 1954). Through a general point (x, r, θ) on a characteristic surface, the bicharacteristic direction may be found from the tangential direction to the characteristic surface and to the local Mach cone.

$$\frac{\Delta x}{\Delta r} = \frac{(q^2 - v^2)^{1/2} (1+u) \cos \mu - (1+\mu) v \sin \mu}{(q^2 - v^2)^{1/2} v \cos \mu + (q^2 - v^2) \sin \mu},$$

$$\frac{r \Delta \theta}{\Delta r} = w \frac{(q^2 - v^2)^{1/2} \cos \mu - v \sin \mu}{(q^2 - v^2)^{1/2} v \cos \mu + (q^2 - v^2) \sin \mu}$$

with μ and q being the local Mach angle and the local non-dimensional velocity respectively.

By using the definitions of μ and q , and neglecting the second and higher order terms of the flow disturbances, we have the differential equations of the bicharacteristics

$$\frac{\partial x}{\partial r} = \beta + \frac{(\gamma+1)M^4}{2\beta} u - M^2(v + \beta u) \quad (2.1.31)$$

$$\frac{\partial \theta}{\partial r} = \frac{\beta w}{r} \quad (2.1.32)$$

To obtain a set of parametric equations of the bicharacteristics, we may substitute Eqs. (2.1.28)-(2.1.30) into Eqs. (2.1.31) and (2.1.32) and perform the integrations on the line $y = \text{constant}$ and $\theta_0 = \text{constant}$,

$$x = \beta(r - R) + y - k F(y, \theta_0) (r^{1/2} - R^{1/2}) - \int_R^r L(y, \theta_0; r) dr, \quad (2.1.33)$$

and

$$\theta = \theta_0 + \int_R^r M(y, \theta_0; r) dr, \quad (2.1.34)$$

with

$$k = 2^{-1/2} (\gamma+1) M^4 \beta^{-3/2} \quad (2.1.35)$$

$$L(y, \theta_0; r) = \frac{(\gamma+1)M^4}{\beta (2\beta r)^{3/2}} \sum_n \cos n \theta_0 \int_0^y F_n(t) K'_n \left(\frac{y-t}{\beta r} \right) dt + M^2 (v + \beta u) \quad (2.1.36)$$

and

$$M(y, \theta_0; r) = \beta w / r. \quad (2.1.37)$$

Here, y and θ_0 are the coordinates x and θ , respectively, of a point on the cylindrical surface R . $y = \text{constant}$ and $\theta_0 = \text{constant}$ define a bicharacteristic curve from the said point; on this bicharacteristic curve, $F(y, \theta_0) = \text{constant}$. For an axisymmetric flow field ($n=0$), there is no θ -component velocity and θ remains constant; Eqs. (2.1.31) and (2.1.32) reduce to Whitham's characteristic differential equation, and Eq. (2.1.33) reduces to the improved characteristic equation obtained by Pan (1970 a,b).

After knowing $F(y, \theta_0)$ at R , we may integrate Eqs. (2.1.33) and (2.1.34) to obtain $F(x, r, \theta)$ at a cylindrical surface further afield at r . The value of F at a particular point (x, θ) at r is equal to the value of $F(y, \theta_0)$ at a point (y, θ_0) which is on the same bicharacteristic curve as the point (x, θ) at r . Due to the θ -component disturbance the bicharacteristic curve from

(y, θ_0) is generally not lying on the same θ_0 plane (see, Figure 2.1 3a). The bicharacteristics which pass through the straight line $\theta = \text{constant}$ on the surface r originate on the surface at R from the curve $\theta_0 = \theta_0(y)$. Consequently, to determine $F(x, r, \theta)$ on a line $\theta = \text{constant}$ at r , we have to determine the curve $\theta_0 = \theta_0(y)$ at R . On the plane of symmetry $\theta=0$ (or π), where $w=0$, all bicharacteristic curves remain in the same plane; hence $F(x, r, 0)$ is determined only by $F(y, 0)$ at R (see, Figure 3.1.3b).

The shape of the F function obtained at r are generally distorted and different from the original F function at R . The F function on a $\theta = \text{constant}$ line at r is generally a multi-valued function of its argument x . The multi-valued regions are due to the intersection of characteristic surfaces in the physical space where values of physical quantities cease to be unique. This failure of the linear theory as a description of the flow is known to be remedied by the presence of shock surfaces (Courant and Friedrichs, 1948).

It is well known (Courant and Friedrichs, 1948) that the shocks, to a first order in strength, can be determined by a simple geometric property; that is a shock surface bisects the angle between two intersecting characteristic surfaces. As shown by Whitham (1952) the F function, at least in the far field, gives a rough description of the flow pattern, since it shows whether the characteristics are converging in compression, where a shock will appear, or diverging in expansion. The shock

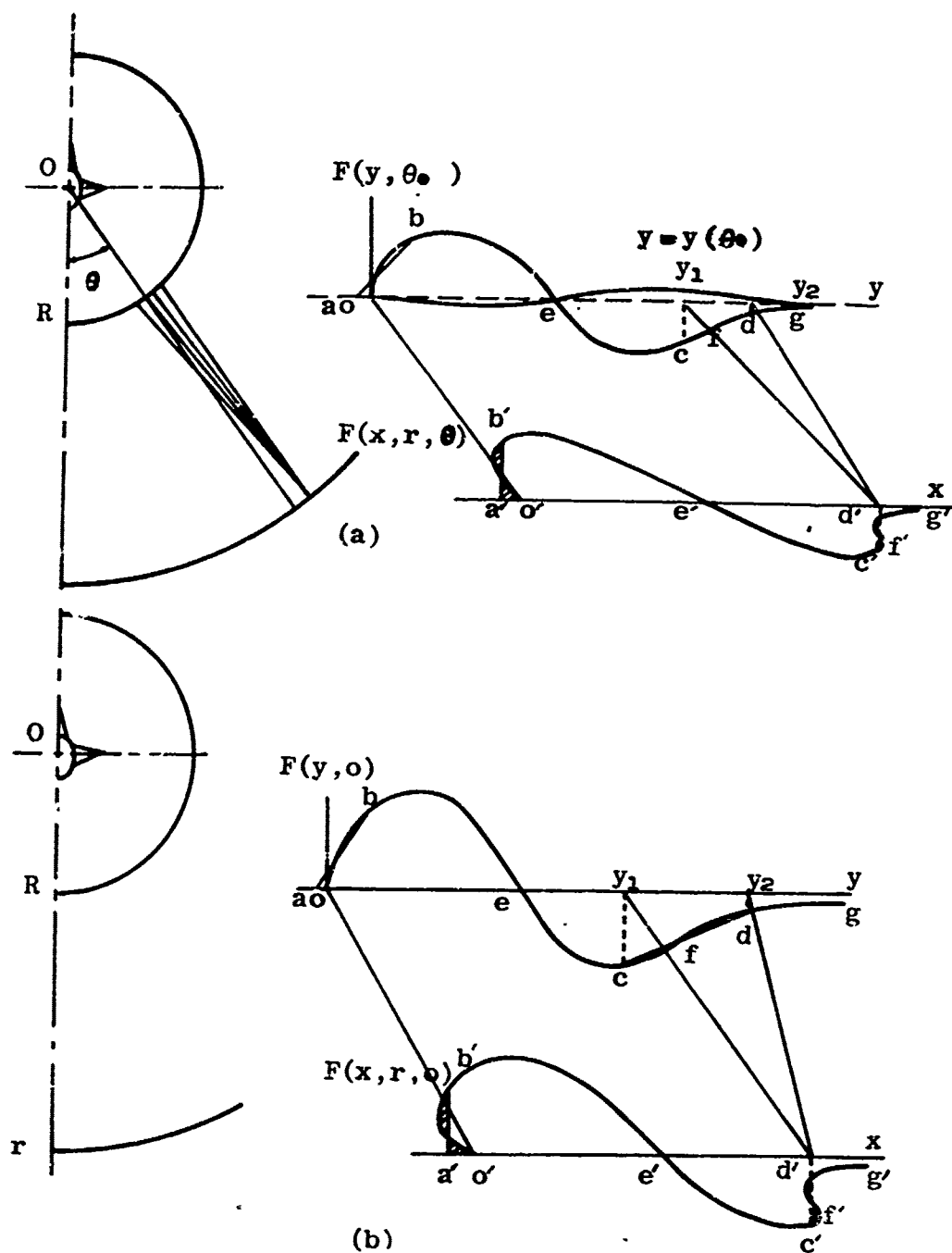


FIGURE 2.1.3 Distortion of the F function (a) $F(y, \theta_0)$,
(b) $F(y, 0)$

position at any distance r may be determined from the F function at R . For an axisymmetric flow, Whitham (1952) obtained a relation called the "area-balance-rule" which states that the lobes cut-off on each side of the F function by a straight segment which determines a shock position must be equal in area. The slope of the straight segment depends on the distance r . In the following, we shall follow Whitham's procedure to obtain general relations for determining shock positions.

Suppose that a general shock intersects $\theta = \text{constant}$ at r at the point,

$$x = \beta(r-R) - G(r, \theta) \quad (2.1.38)$$

and the bicharacteristics, Eq. (2.1.33), specified by y_1 and y_2 ($y_2 > y_1$) on $\theta_0 = \theta_0(y)$ at R intersect the shock at this point (see, points c and d in Figure 2.1.3). The bisection of the angle between the characteristic surfaces by the shock surface requires that

$$\begin{aligned} 2 \frac{\partial G}{\partial r} = \frac{1}{2} k r^{1/2} & \left[F(y_1, \theta_0(y_1)) + F(y_2, \theta_0(y_2)) \right] \\ & + \left[L(y_1, \theta_0(y_1); r) + L(y_2, \theta_0(y_2); r) \right] \end{aligned} \quad (2.1.39)$$

On the other hand, elimination of $x - \beta(r-R)$ from the equations of the shock, Eqs. (2.1.38) and of the bicharacteristic, Eq. (2.1.33), give

$$G(r, \theta) = k F(y_1, \theta_0(y_1)) \left[r^{1/2} - R^{1/2} \right] + \int_R^r L(y_1, \theta_0(y_1); r) dr - y_1, \quad (2.1.40)$$

and

$$G(r, \theta) = k F(y_2, \theta_0(y_2)) \left[r^{1/2} - R^{1/2} \right] + \int_R^r L(y_2, \theta_0(y_2); r) dr - y_2. \quad (2.1.41)$$

G and r as functions of y_1 or y_2 can be solved from Eqs. (2.1.39)-(2.1.41). and then the relation between y_1 and y_2 is obtained.

The relation between r and y_1 (and/or y_2) is obtained by eliminating G from Eqs (2.1.40) and (2.1.41),

$$\frac{F(y_2, \theta_0(y_2)) - F(y_1, \theta_0(y_1))}{y_2 - y_1} = \left\{ k(r^{1/2} - R^{1/2}) + \frac{\int_R^r [L(y_2, \theta_0(y_2); r) - L(y_1, \theta_0(y_1); r)] dr}{F(y_2, \theta_0(y_2)) - F(y_1, \theta_0(y_1))} \right\}^{-1} \quad (2.1.42)$$

For large r , Eq. (2.1.42) may be simplified to a relation obtained by Whitham (1952) for $R=0$,

$$\frac{F(y_2, \theta_0(y_2)) - F(y_1, \theta_0(y_1))}{y_2 - y_1} = \frac{1}{k(r^{1/2} - R^{1/2})} \quad (2.1.43)$$

The geometric interpretation of Eq. (2.1.43) is that the slope of the straight segment cd joining the points y_1 and y_2 of the F function curve at R relates to r only. For an arbitrary r , the slope of the segment cd relates not only to r but to y_1, y_2

and F. For different shocks, the slopes of the segments are different.

To determine the relation between y_1 and y_2 or the position of cd on the F function curve at R, the well known "area-balance-rule",

$$\int_{y_1}^{y_2} F(y_1, \theta_0(y)) dy = \frac{1}{2} (y_2 - y_1) \left[F(y_1, \theta_0(y_1)) + F(y_2, \theta_0(y_2)) \right], \quad (2.1.44)$$

is found to be replaced by the following relation,

$$\begin{aligned} \int_{y_1}^{y_2} f(y, \theta_0(y)) dy &= \frac{1}{2} (y_2 - y_1) \left[F(y_1, \theta_0(y_1)) - F(y_2, \theta_0(y_2)) \right] \\ &+ \frac{1}{2} \left[F(y_1, \theta_0(y_1)) \right] \int_R^r \left[L(y_1, \theta_0(y_1); r) - L(y_2, \theta_0(y_2); r) \right] dr \\ &+ \int_{y_1}^{y_2} F(y_1, \theta_0(y)) dy \left[\frac{\partial}{\partial y} \int_R^r L(y, \theta_0(y); r) dr \right] \end{aligned} \quad (2.1.45)$$

Now Eq. (2.1.45) together with Eq. (2.1.42) determines the positions of y_1 and y_2 on $F(y_1, \theta_0(y))$ for fixed r . These relations may be used to determine the positions of other shocks. For example, the position of the front shock ab (Figure 2.1.3) may be determined by setting $F(y_1, \theta_0(y_1)) = 0$ at the point a on the F function curve. We may note here that Eqs. (2.1.42) and (2.1.45) are so complex that no explicit solution for $r(y_1, y_2)$

possible. Results may only be obtained by a numerical iterative procedure by using Eqs. (2.1.43) and (2.1.44) as a first approximation.

After having determined the positions of shock waves, the local F function at r becomes a single valued function except with a finite number of discontinuities. Then the corresponding flow disturbances may be determined from the local F function and its Fourier components by Eqs. (2.1.28)-(2.1.30) or the relations (2.1.25)-(2.1.27) by replacing R by r .

2.1.3 WIND TUNNEL TESTING METHOD BASED ON LARGE MODELS

As discussed in the subsection 2.1.1, in experimental investigations of sonic boom in wind tunnels it is usually necessary to use very small models in order to obtain direct measurements of the far field pressure signature in the vicinity of a wind tunnel wall. The present new method is based on large models in wind tunnels, where only the near or the mid-field is simulated. By measuring the pressure distribution at the vicinity of wind tunnel wall it is possible to determine the signature of sonic boom at large distances in the far-field. In this subsection, we shall present a theoretical study of the new wind tunnel testing method.

GENERAL CONSIDERATION

A three-dimensional model is tested in a circular cylindrical supersonic wind tunnel with radius R (Figure 2.1.4a). The flow

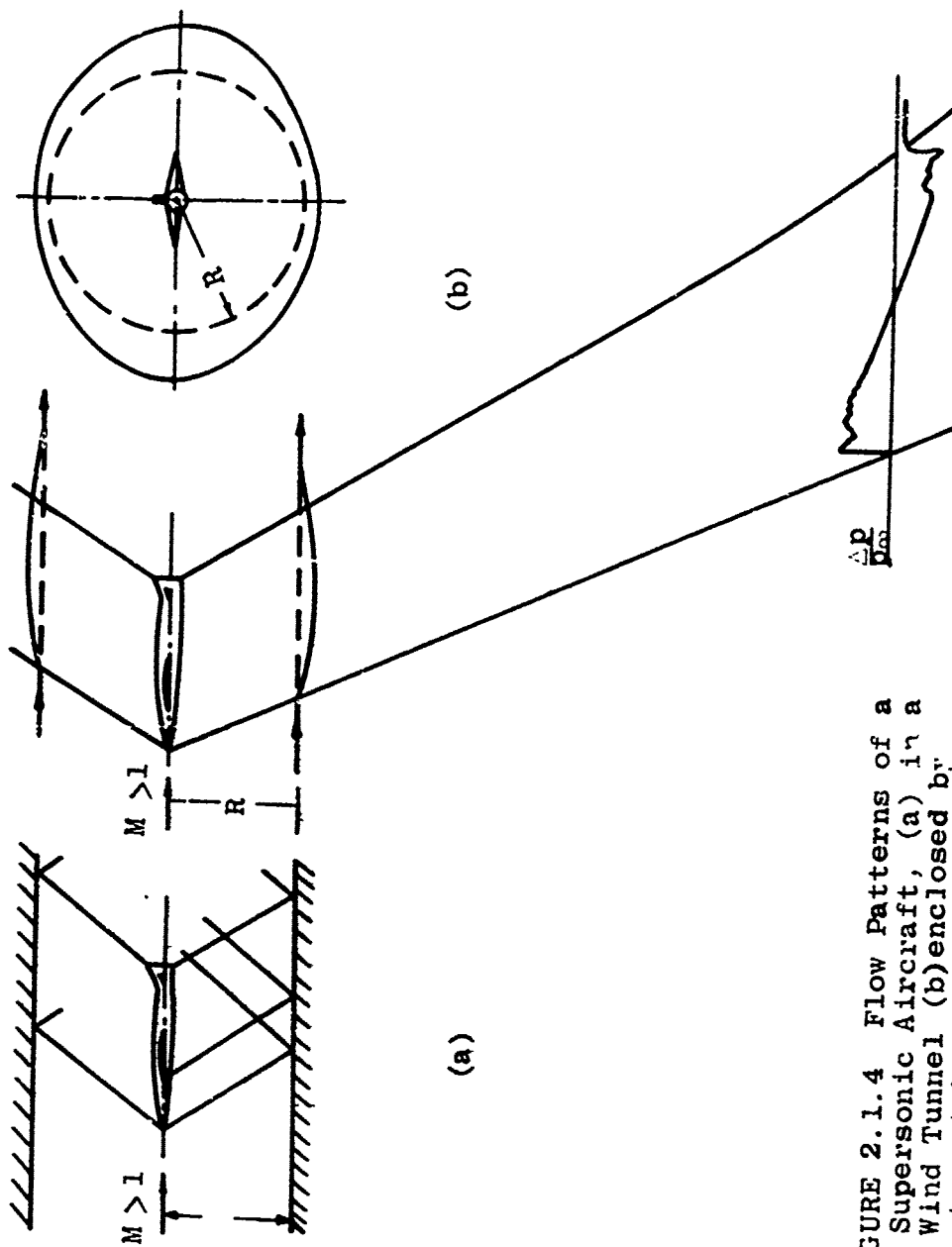


FIGURE 2.1.4 Flow Patterns of a Supersonic Aircraft, (a) in a Wind Tunnel (b) enclosed by streamtube in free flight.

is assumed to be steady, homogeneous, irrotational and inviscid. It is well known that the disturbance emitted from the model is reflected at the wind tunnel wall, in order that the streamlines adjacent to the wall may be always tangent to the wall. Hence, the three-dimensional reflected pressure disturbance can be measured at the wind tunnel wall. If the flow field over the test model inside the wind tunnel can be described by the linearized supersonic flow theory and if the cumulative nonlinear effects can be neglected within the wind tunnel, the flow field near the wall may also be described by the linearized supersonic flow equations. It is possible to relate the incident disturbance with the reflected disturbance at the wall by specifying proper boundary conditions on the wall (Pan, 1970c, 1971).

In free flight, however, streamlines over the model may be distorted freely according to the emitted disturbance. Any circular cross-sectional streamtube in the free stream may be distorted into a quasi-circular cylindrical shape. The quantity of flow in the wind tunnel of radius R is equal to the quantity of flow confined in a streamtube of the same upstream radius R enclosing this model in free flight (see, Figure 2.1.4b). Based on the linearized supersonic flow theory, the actual flow disturbance at the distance R in free flight equals to the incident disturbance on the wind tunnel wall with the same radius R .

After knowing the actual pressure disturbance at a streamtube with upstream radius R enclosing the model, we may now

apply the extended theory developed in the preceding subsection to extrapolate this known disturbance to any distance in further afield.

WIND TUNNEL WALL REFLECTION

In this subsection, we shall obtain the relation between the actual free flight(incident) pressure disturbance and the measured (reflected) pressure disturbance both on the cylindrical wind tunnel wall. We assume that the flow field may be described by the linearized supersonic flow theory. The pressure (Mach) waves generated by the model propagated outward and downstream and are reflected at the wind tunnel wall; the reflected wave will not interact with the model. Unlike the reflection of a plane wave at a rigid plane surface which gives a constant reflection factor 2.0, the reflection of a curved wave from a cylindrical rigid surface may not be described by a simple constant reflection factor. Since the flow field behind a curved wave is generally not uniform, the flow field behind a curved reflected wave depends on both the incident curved wave and the distance from the wave front.

Referring to Figure 2.1.4a with the coordinates described in Figure 2.1.2, the disturbance velocity potential ϕ in the wind tunnel satisfies Eq.(2.1.1). Equation (2.1.1) together with the uniform free stream boundary conditions may be solved by a technique of Laplace transform, i.e.,

$$\bar{\Phi}(s, r, \theta) = \frac{1}{\beta R} \int_0^{\infty} \Phi(x, r, \theta) e^{-sx/\beta R} dx. \quad (2.1.46)$$

The general solution to the transformed governing equation Eq.(2.1.1) is given by (Ward, 1955).

$$\bar{\Phi}(s, r, \theta) = \sum_n \cos n \theta \left[A_n K_n \left(\frac{sr}{R} \right) + B_n I_n \left(\frac{sr}{R} \right) \right], \quad (2.1.47)$$

where K_n and I_n are modified Bessel functions, and A_n and B_n are functions of s only. [Readers should not be confused by the modified Bessel functions K_n used here with the functions K_n defined by the Eqs (2.1.23)].

In Eq.(2.1.47) the terms in K_n which represent waves traveling outward from the model and downstream are the incident waves with respect to the wall, while the terms in I_n which represent waves traveling in both directions are related to the waves reflected from the wall. The relation between A_n and B_n may be determined by the boundary condition on the wall, (i.e., $\partial\Phi/\partial r = 0$ at $r = R$),

$$B_n = -A_n K'_n(s)/I'_n(s). \quad (2.1.48)$$

The function A_n may be determined from the boundary conditions on the model surface; we, however, shall leave it as an arbitrary function.

Now the general solution in (s, r, θ) reduced to

$$\bar{\Phi}(s, r, \theta) = \sum_n \cos n \theta A_n K_n \left(\frac{sr}{R} \right) \left[1 - \frac{K'_n(s) I_n \left(\frac{sr}{R} \right)}{I'_n(s) K_n \left(\frac{sr}{R} \right)} \right]. \quad (2.1.49)$$

The transformed disturbance pressure \bar{P} is, by Eqs. (2.1.7) and (2.1.46),

$$\bar{P}(s, r, \theta) = - \frac{s}{\beta R} \bar{\Phi}(s, r, \theta) \quad (2.1.50)$$

On the wind tunnel wall ($r = R$), the disturbance pressure $\bar{P}(s, R, \theta)$ is the measured (reflected) pressure, denoted by \bar{P}_R ,

$$\bar{P}_K = \sum_n \cos n \theta \bar{P}_{Rn}(s, R) \quad (2.1.51)$$

with \bar{P}_{Rn} being the Fourier components of \bar{P}_R , and from Eqs. (2.1.49) and (2.1.50),

$$\bar{P}_{Rn}(s, R) = - \frac{s}{\beta R} A_n K_n(s) \left[1 - \frac{K'_n(s) I_n(s)}{I'_n(s) K_n(s)} \right]. \quad (2.1.52)$$

On the other hand, it is easy to show that the Fourier components of the free flight (incident) disturbance pressure on the wall is

$$\bar{P}_{I_n}(s, R) = - \frac{s}{\beta R} A_n K_n(s). \quad (2.1.53)$$

Hence, we may relate the measured pressure with the free flight pressure on the wind tunnel wall,

$$\bar{P}_{R_n}(s, R) = \bar{P}_{I_n}(s, R) \left[1 - \frac{K'_n(s) I_n(s)}{I'_n(s) K_n(s)} \right]. \quad (2.1.54)$$

We may also express the free flight pressure in terms of the measured pressure and use the well known Bessel function relations (Watson, 1966),

$$\bar{P}_{I_n}(s, R) = \frac{1}{2} \bar{P}_{R_n}(s, R) s K_n(s) \left[I_{n+1}(s) + I_{n-1}(s) \right] \quad (2.1.55)$$

Now the relations between $P_{I_n}(x, R)$ and $P_{R_n}(x, R)$ may be obtained by performing the inverse Laplace transform,

$$P_{I_n}(x, R) = \frac{1}{2} \left[P_{R_n}(x, R) - \frac{1}{2} \int_0^x P_{R_n}(y, R) R_n\left(\frac{x-y}{\beta R}\right) dy \right], \quad x > 0$$

$$= 0 \quad x < 0 \quad (2.1.56)$$

Here, $R_n(x)$ the reflection functions, are the inverse Laplace transform of the $\bar{R}_n(s)$,

$$\bar{R}_n(s) = 1 - s K_n(s) \left[I_{n+1}(s) + I_{n-1}(s) \right]. \quad (2.1.57)$$

Since the Laplace inversing of $\bar{R}_n(s)$ is not known at the present, exact values of $R_n(x)$ for all n and x cannot be obtained.

However, for most practical cases, the argument of $R_n(x)$ is usually small, and we may obtain an asymptotic expression of $R_n(x)$ for small x by inverting the asymptotic expression of $\bar{R}_n(s)$ for large s . The result is

$$R_n(x) = \sum_{m=1}^{\infty} C_{nm} x^{m-1} / 8^m (m-1)! \quad (2.1.58)$$

where

$$C_{nm} = \sum_{\substack{i=0 \\ i+j=m}}^m (-1)^j a_{ni} b_{nj},$$

with

$$a_{ni} = \prod_{j=1}^i \left[\frac{4n^2 - (2j-1)^2}{j} \right],$$

$$b_{ni} = \frac{1}{2} \left[\prod_{j=1}^i \left[\frac{4(n+1)^2 - (2j-1)^2}{j} \right] + \prod_{j=1}^i \left[\frac{4(n-1)^2 - (2j-1)^2}{j} \right] \right],$$

and $a_{n0} = b_{n0} = 1$. Values of $R_n(x)$ are plotted in Figure 2.1.5 for $n=0$ to 5 and $0 \leq x \leq 1.7$. After having obtained $P_{In}(x, R)$, we may calculate the free flight disturbance pressure distribution $P_I(x, R, \theta)$ on the wind tunnel wall,

$$P_I(x, R, \theta) = \sum_n \cos n\theta P_{In}(x, R) \quad (2.1.59)$$

PROCEDURE OF THE EXTRAPOLATION OF MEASURED DISTURBANCE

After obtaining the incident pressure disturbance at the wind tunnel wall, we may follow the extended theory developed in the subsection 2.1.2 to find the sonic boom signature in the far-field. In the following, we shall outline the procedures

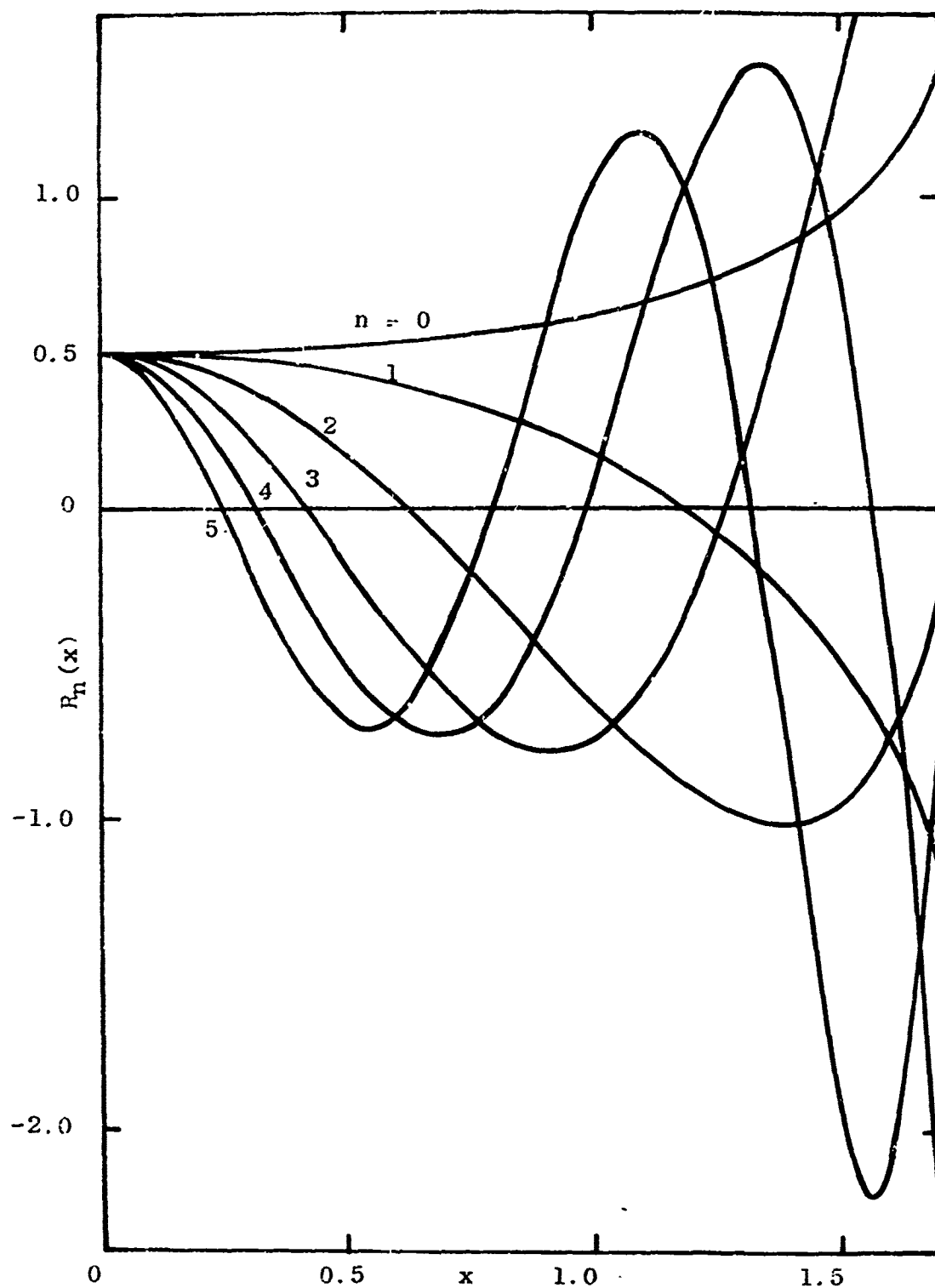


FIGURE 2.1.5 Reflection Functions $R_n(x)$

of the extrapolation method and list the relevant formulas in each procedure.

A three-dimensional pressure distribution, $P_R(x, \theta, R)$ is measured at a circular cylindrical wind tunnel of radius R (for example, by using a scanning system suggested by R. C. Bauer of ARO, Inc. to this author, 1971). This three-dimensional signature is expanded in Fourier series in θ ,

$$P_R(x, \theta, R) = \sum_n P_{Rn}(x, R) \cos n \theta;$$

the Fourier coefficients P_{Rn} of P_R can be obtained.

The corresponding Fourier coefficients $P_{In}(x, R)$ of the incident pressure disturbance $P_I(x, \theta, R)$ and $P_I(x, \theta, R)$ itself can be found, from Eq. (2.1.56),

$$P_{In}(x, R) = \frac{1}{2} \left[P_{Rn}(x, R) - \frac{1}{\beta r} \int_0^x P_{Rn}(t, R) R_n \left(\frac{x-t}{\beta R} \right) dt \right],$$

and from Eq. (2.1.59),

$$P_I(x, R, \theta) = \sum_n P_{In}(x, R) \cos n \theta.$$

$P_I(x, R, \theta)$ is a three-dimensional pressure disturbance on a streamtube with upstream radius R , which corresponds to the wind tunnel.

By using the pressure disturbance $P_I(x, R, \theta)$ or $P_{In}(x, R)$, we can calculate the local F function of this streamtube; from Eq. (2.3.20),

$$F_n(y, R) = (2\beta R)^{1/2} \left[P_{In}(y) - \frac{1}{\beta R} \int_0^y P_{In}(t) S_n\left(\frac{y-t}{\beta R}\right) dt \right],$$

and from Eq. (2.1.15),

$$F(y, \theta_0, R) = \sum_n F_n(y, R) \cos n \theta_0.$$

$F(y, \theta_0, R)$, representing the disturbance generated by the stream-tube with upstream radius R or by the tested model in free flight at R , propagates to further afield r along bicharacteristics given by Eq. (2.1.33),

$$x = \beta(r-R) + y - k F(y, \theta_0) (r^{1/2} - R^{1/2}) - \int_R^r L(y, \theta_0; r) dr$$

and Eq. (2.1.34),

$$\theta = \theta_0 + \int_R^r M(y, \theta_0; r) dr.$$

After shock positions were fixed on the F function by Eqs. (2.1.42) and (2.1.45), the new single valued $F(x, r, \theta)$ is obtained at r . This new F function is then expanded in Fourier series.

$$F(x, r, \theta) = \sum_n F_n(x, r) \cos n \theta.$$

Corresponding to the Fourier components, $F_n(x, r)$, the Fourier components of the pressure disturbance, $P_n(s, r)$, are found from

Eq. (2.1.25).

$$P_n(x,r) = \frac{1}{(2\beta r)^{1/2}} \left[F_n(x,r) + \frac{1}{\beta r} \int_0^x F_n(t,r) K_n\left(\frac{x-t}{\beta r}\right) dt \right]$$

Finally, the three-dimensional pressure disturbance $P(x,r,\theta)$ at r is obtained by summing up all Fourier components,

$$P(x,r,\theta) = \sum_n P_n(x,r) \cos n\theta.$$

2.1.4 EXAMPLES AND DISCUSSIONS

Several numerical calculations* of near-field pressure signatures were performed to compare the results based on the present analysis with those based on the current sonic boom calculation and with some available wind tunnel measurements. Typical examples are presented and discussed in the following.

Figure 2.1.6 shows a comparison of the shifts of characteristics at different r for different points x on the axis of a 6.46° half-angle cone-cylinder body. The length, l , of the cone portion of this body is taken to be 1.0 and the free stream Mach number is 1.41. In this figure, y_w is the shift of the asymptotic characteristic curve based on Whitham's theory (1952) from the linear characteristic curve; y_1 , is the shift of the characteristic curve based on the present analysis (Pan, 1970a).

*This author, Dr. Y. S. Pan, wishes to acknowledge Misters K. T. Wang and M. O. Varner, Research Assistants, for their valuable assistance in the numerical computations.

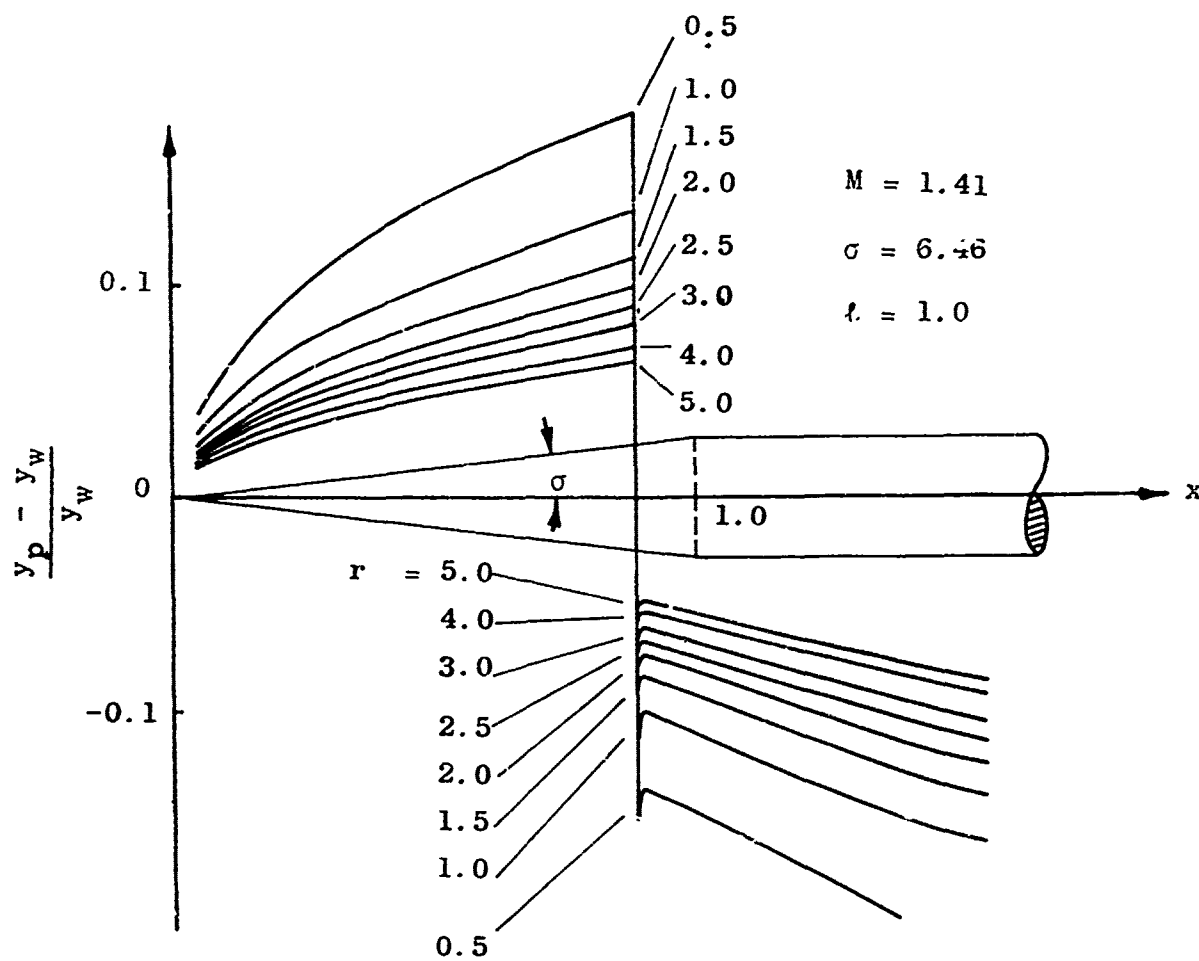


FIGURE 2.1.6 Cone-cylinder body and shifts of characteristics at different r

For this example, the present characteristics are located generally ahead of the asymptotic characteristics. At $r = 0.5$, the differences of the shifts are as large as 20 percent of Whitham's values. As r increases, the percentage of the difference decreases.

Figures 2.1.7a - 2.1.7b show the near-field pressure signatures at $r/\ell = 0.5, 1.0, 1.5, 2.0, 2.5, 3.0, 4.0$ and 5.0 from the axis of the cone-cylinder body described in the preceding section. Comparisons show the differences between the signatures of the present analysis and of the current sonic boom theory. The differences are due to the present correction of the linear asymptotic relations between the flow disturbances and the local F function and due to the shift of the characteristic curves. The peak pressures predicted by the present analysis are generally lower than, and located ahead of, those predicted by the current sonic boom theory. This prediction is qualitatively consistent with some of the near-field experimental observations (for example, Morris, Lamb and Carlson, 1970).

In Figures 2.1.7b - 2.1.7h, numerical pressure data are also presented. These data were obtained by Kutler (1971)* using a shock-capturing finite-difference approach (Kutler and Lomax, 1971). The present signatures are generally in excellent agreement with the numerical data except at the neighborhood of

* Numerical data generously provided by Dr. Paul Kutler of NASA Ames Research Center are gratefully acknowledged.

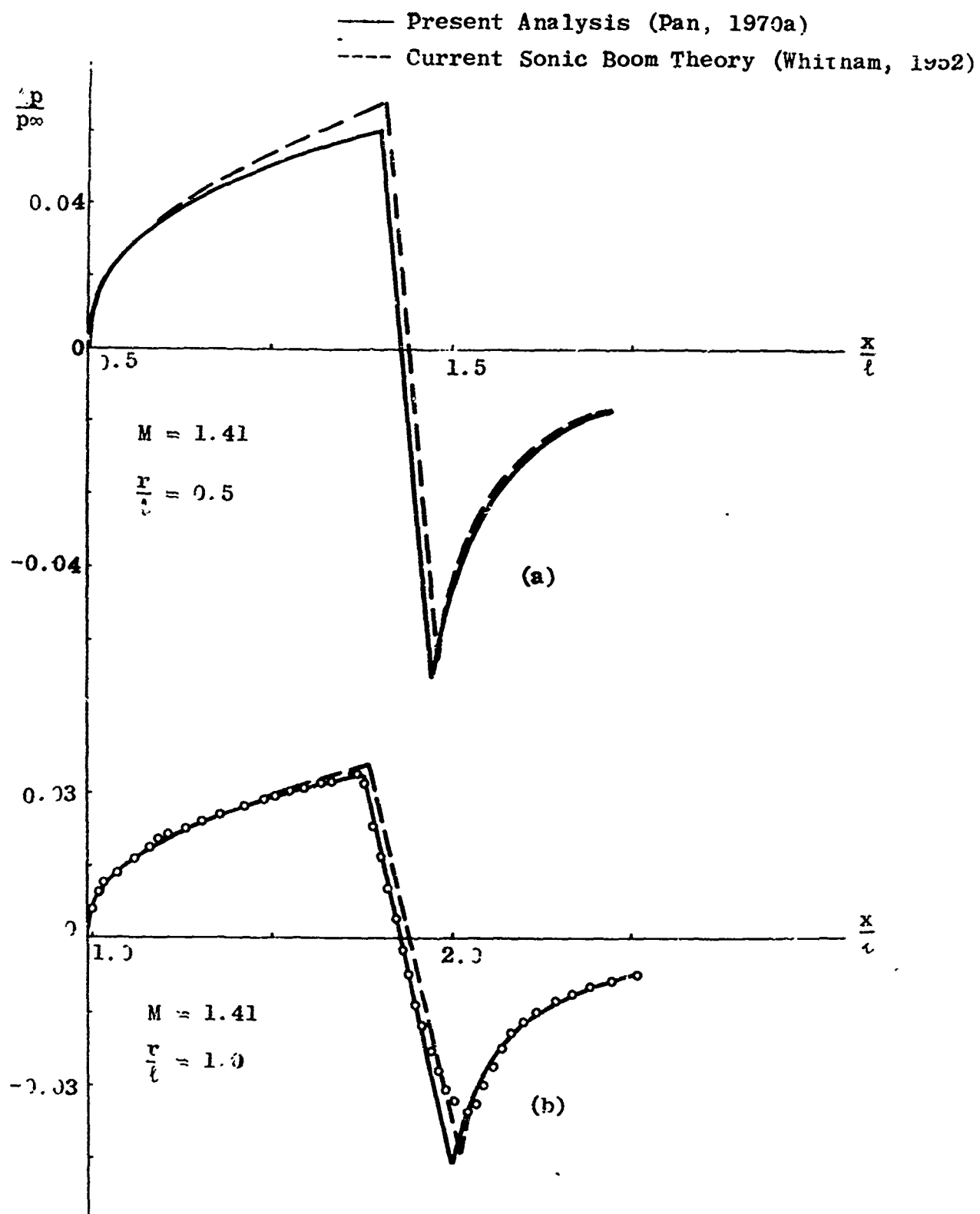


FIGURE 2.1.7 Near-field pressure signatures

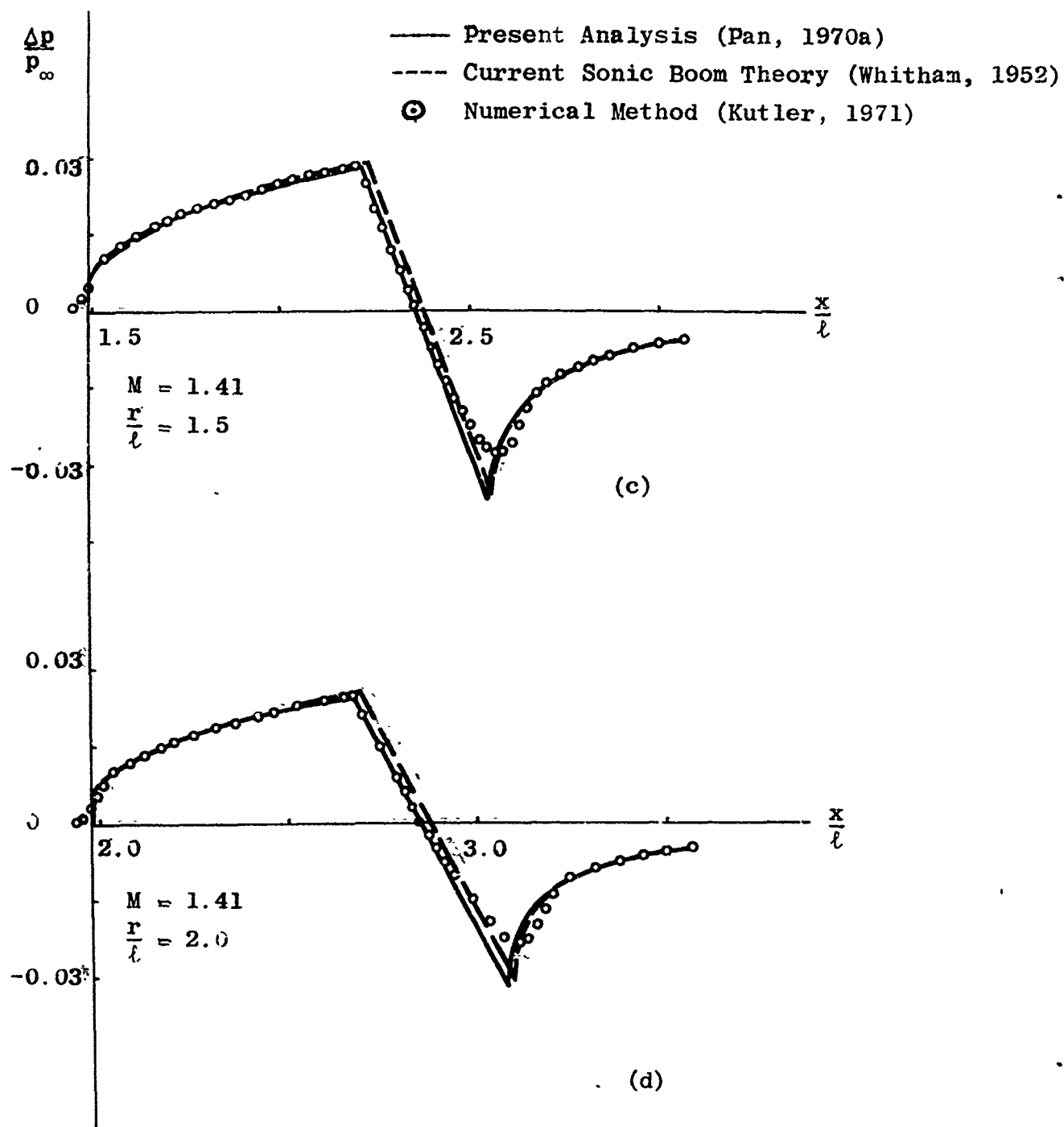


FIGURE 2.1.7 Near-field pressure signatures

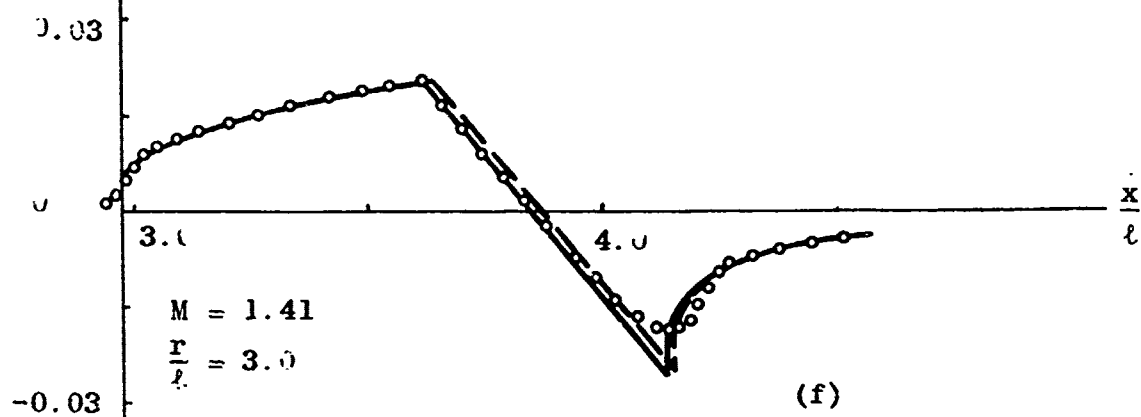
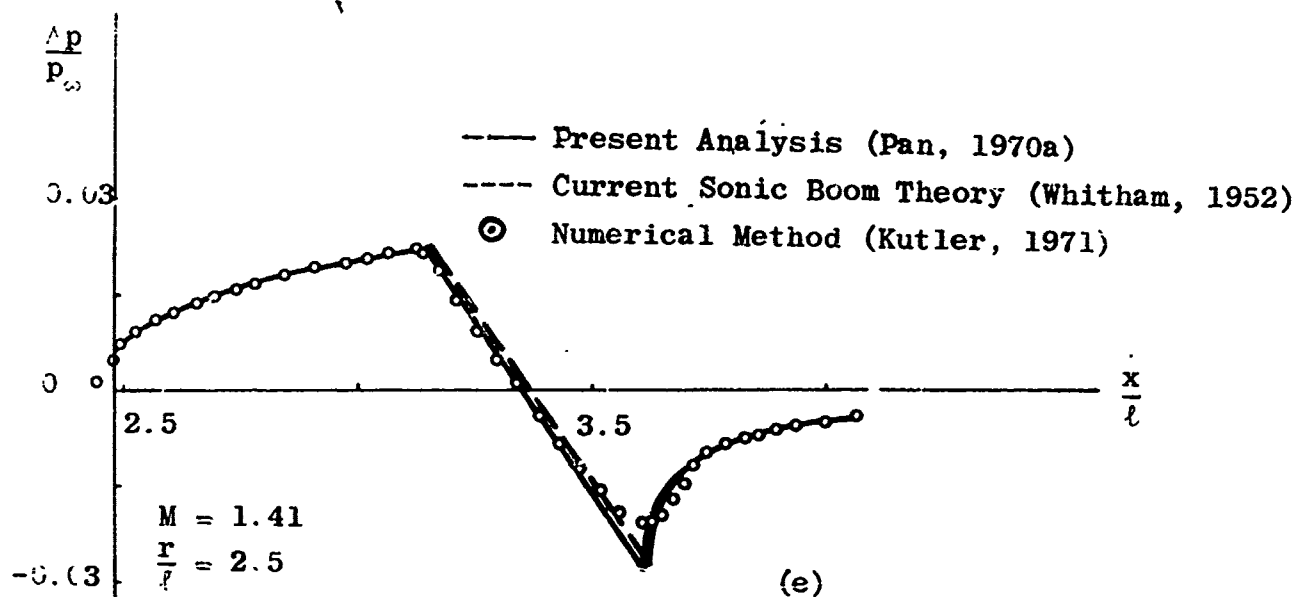


FIGURE 2.1.7 Near-field pressure signatures

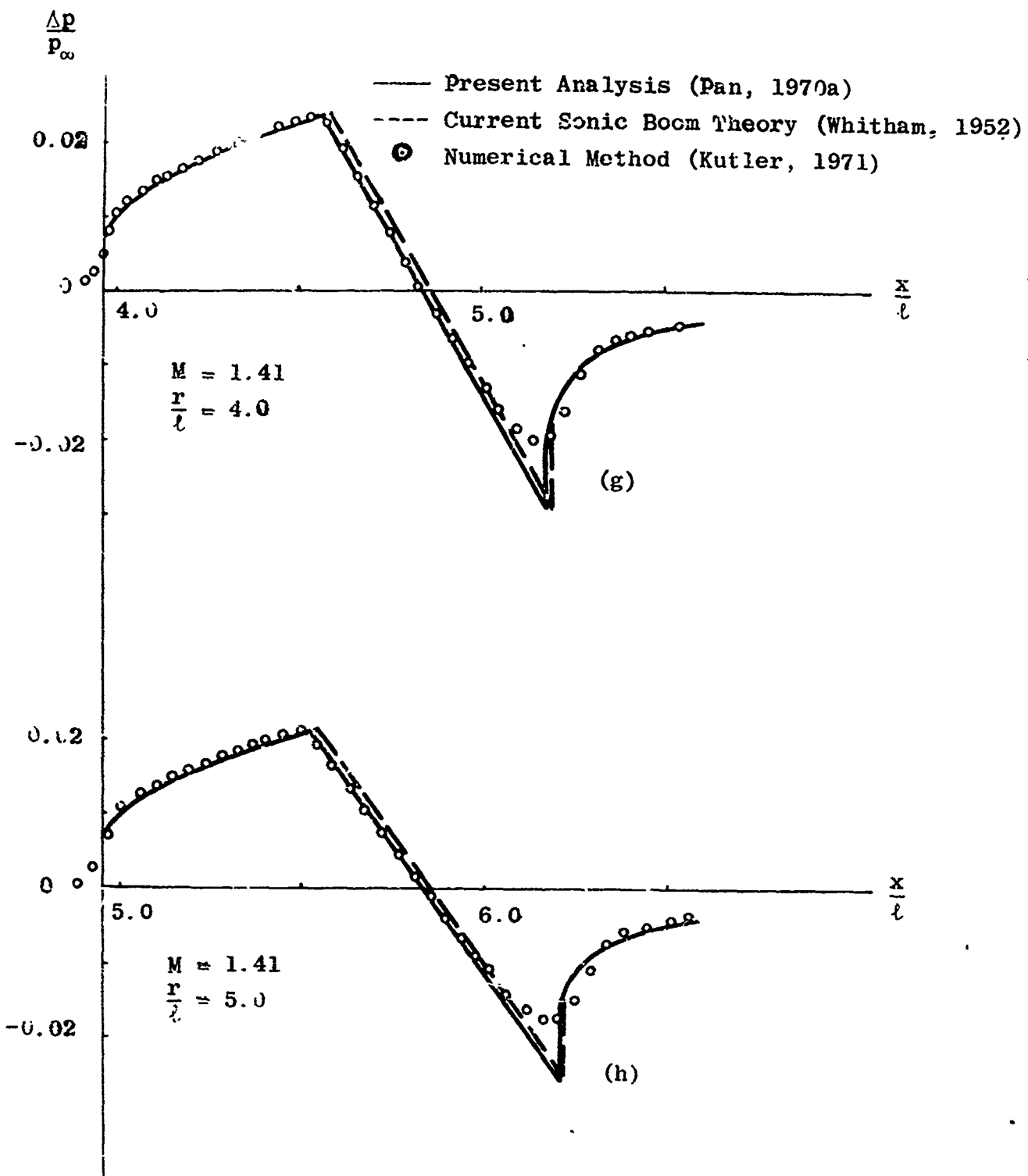


FIGURE 2.1.7 Near-field pressure signatures

the shock waves. The difference near the shock waves is due to the fact that, in the shock-capturing finite-difference approach, the shock waves which occur are spread over a few mesh intervals. Therefore the exact positions of the shock waves cannot be exactly predicted by this numerical method.

Figure 2.1.8 shows the shifts of characteristics at $r = 1.0$ from the same cone-cylinder body at Mach numbers 1.2, 1.41, 2.0 and 3.0. Generally, the shift of characteristics increases with increasing Mach number except at the cone portion. In this region, the F function is positive and the shift decreases with increasing large Mach number. Figure 2.1.9a - 2.1.9d show the comparison of pressure signatures, based on two different analyses, at $r/l = 1.0$ of the same cone-cylinder body at several different Mach numbers. Because of the larger shifts of characteristics at larger Mach numbers, larger shifts of pressure signatures appear at larger Mach numbers. The difference of the pressure strengths decreases as the Mach number increases.

Figure 2.1.10 and 2.1.11 demonstrate the extrapolation of an axisymmetric pressure signature. From Kutler's numerical data (1971) at $r/l = 1.5$, a corresponding F function is obtained and is shown in Figure 2.1.10 (the dotted data represents the F function based on Whitham's asymptotic relation). This F function is propagated to $r/l = 2.0, 2.5, 3.0, 4.0$, and 5.0 . The corresponding pressure signatures at different r/l are obtained from different local F functions and are shown in Figures 2.1.11a-2.1.11e. Comparisons of the extrapolated pressure signatures

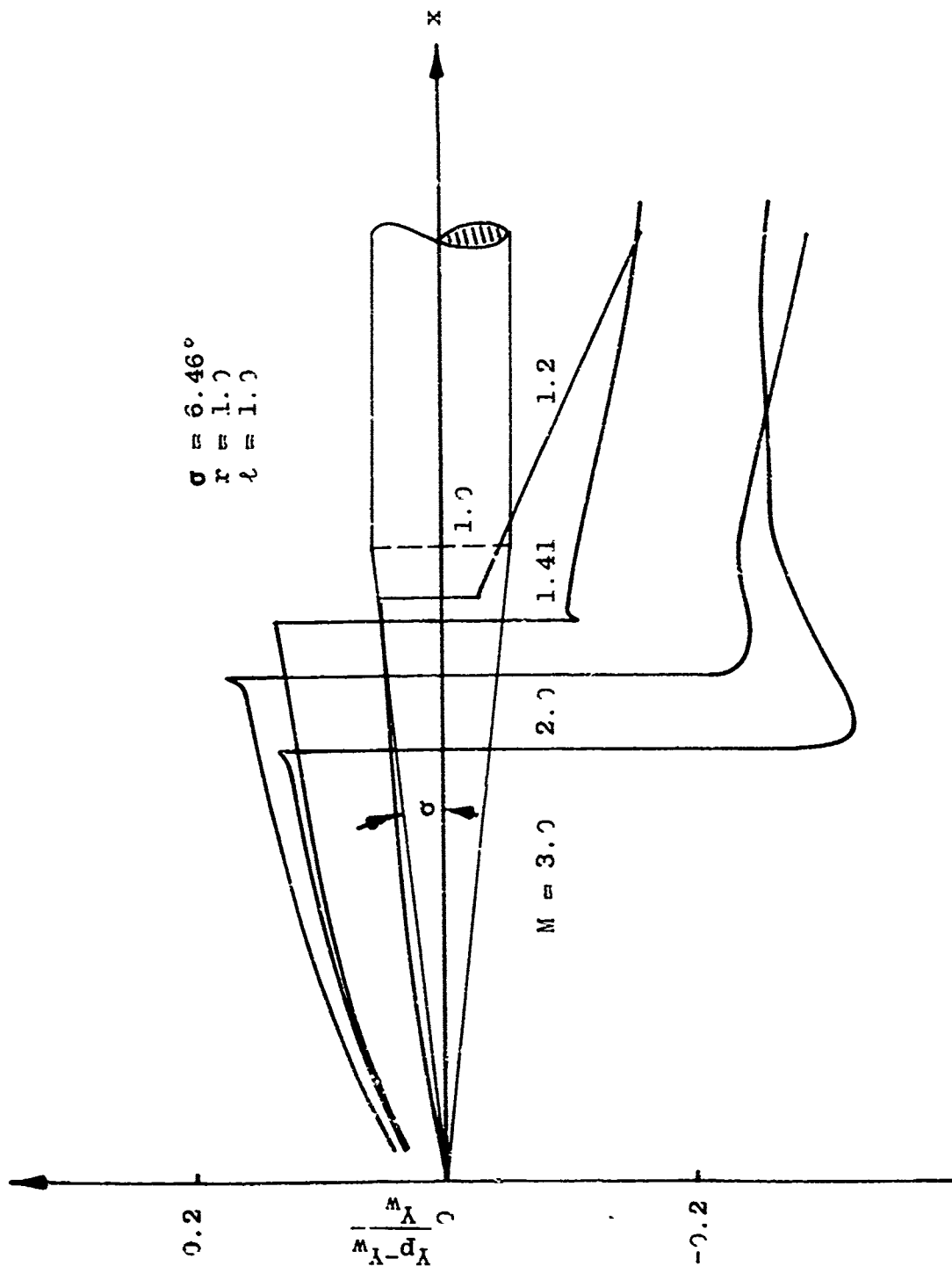


FIGURE 2.1.8 Cone-cylinder body and shifts of characteristics at different M .

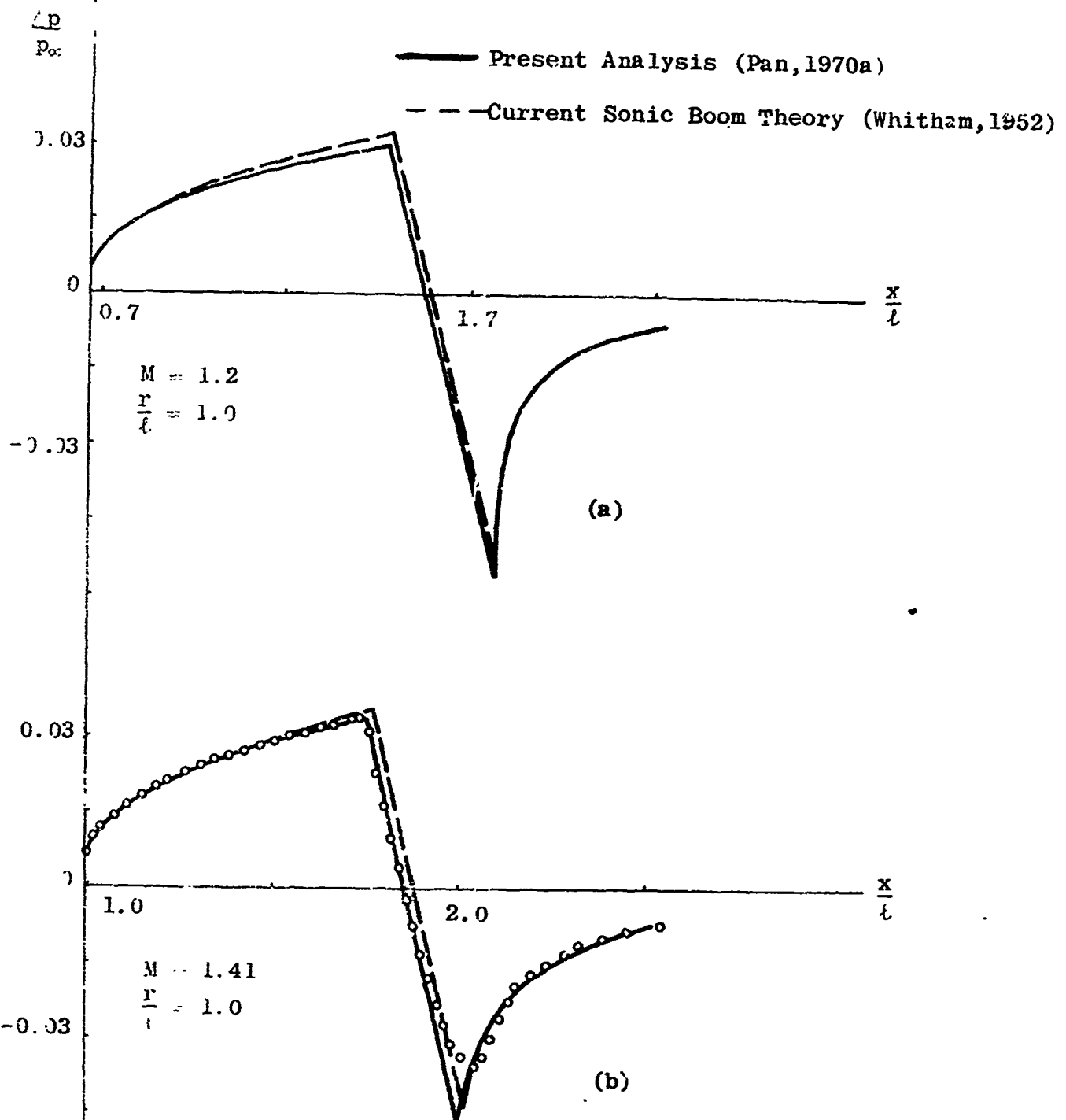


FIGURE 2.1.9 Near-field pressure signatures

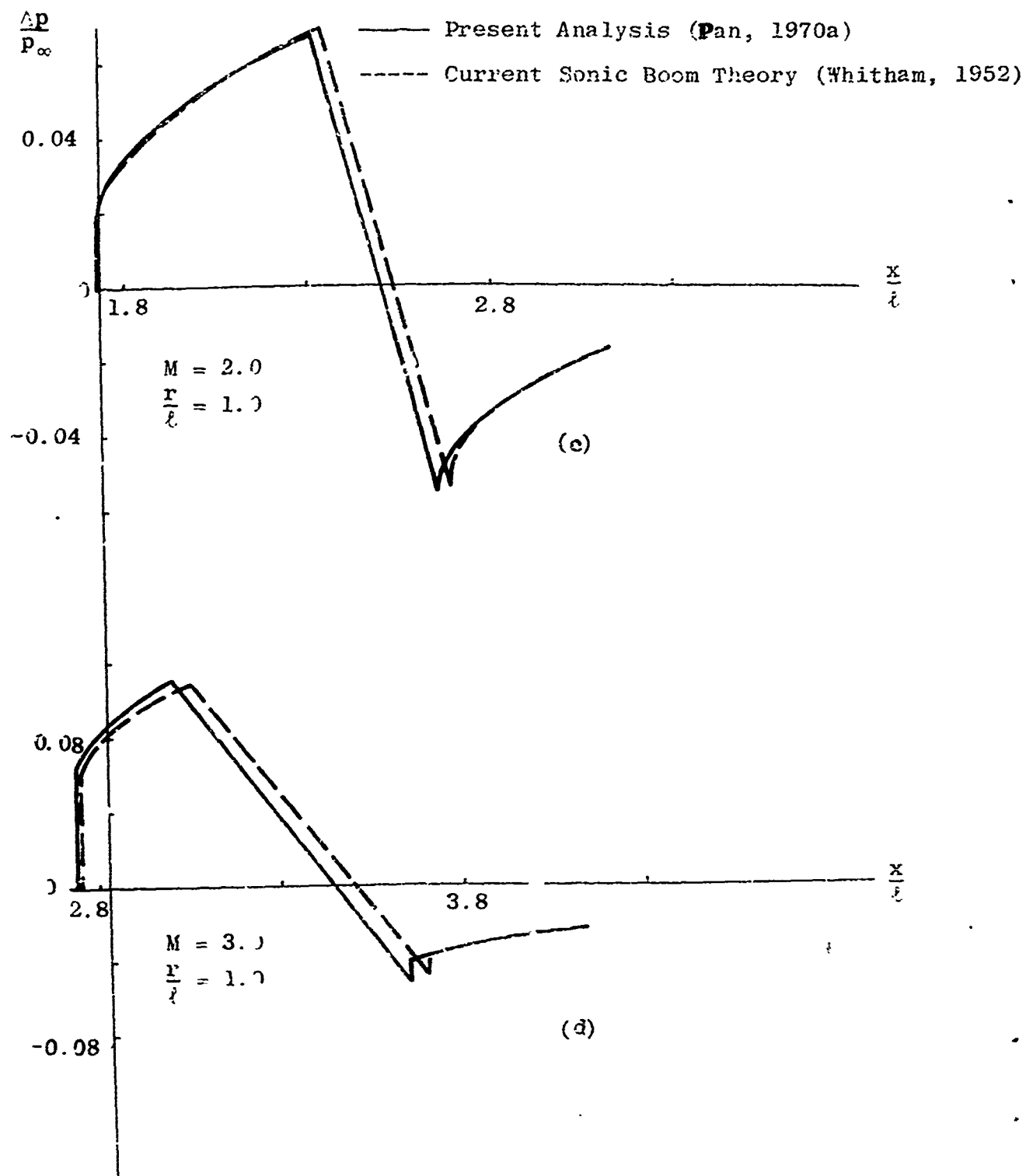


FIGURE 2.1.9 Near-field pressure signatures

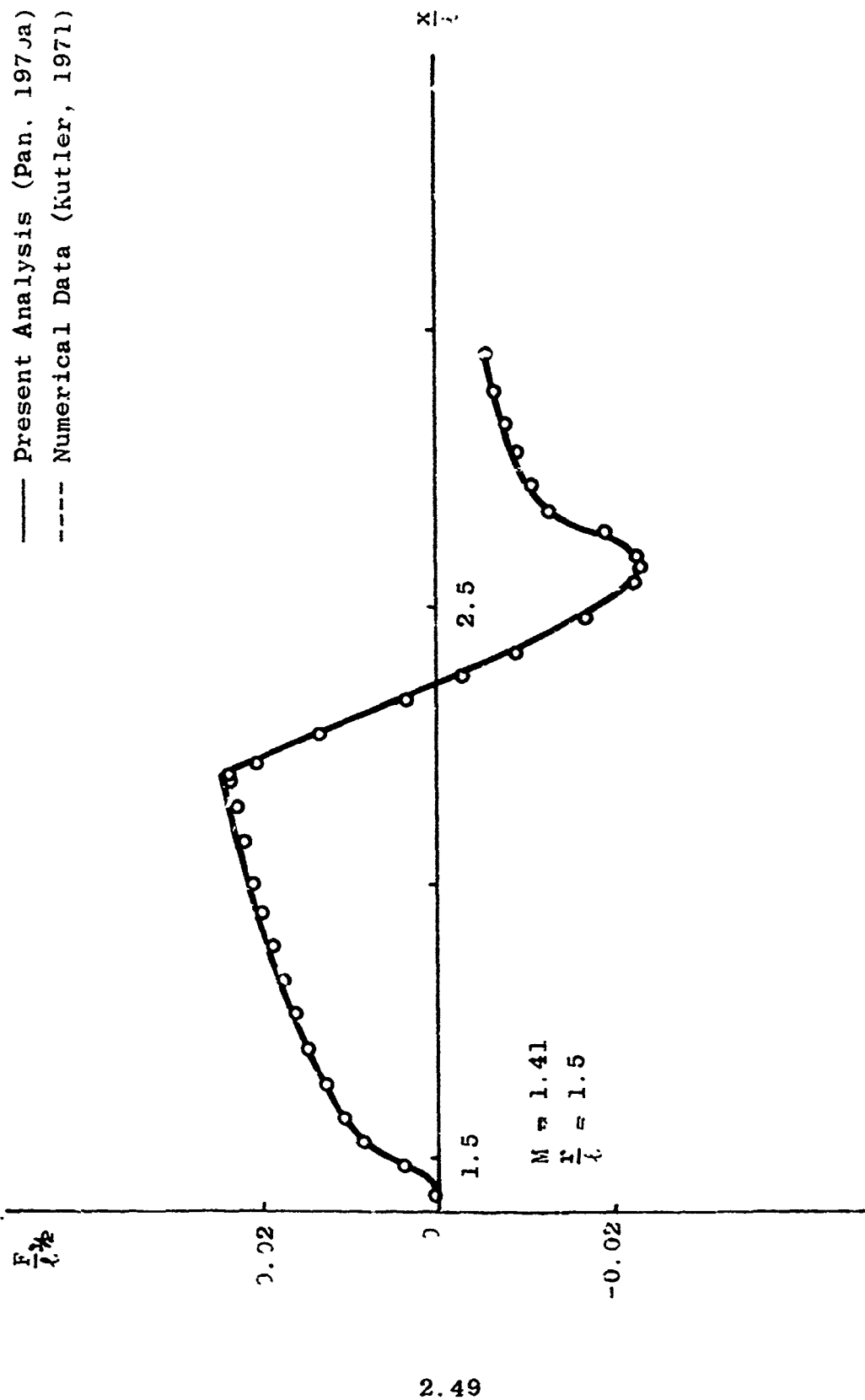


FIGURE 2.1.10 F function calculated from near-field pressure signature

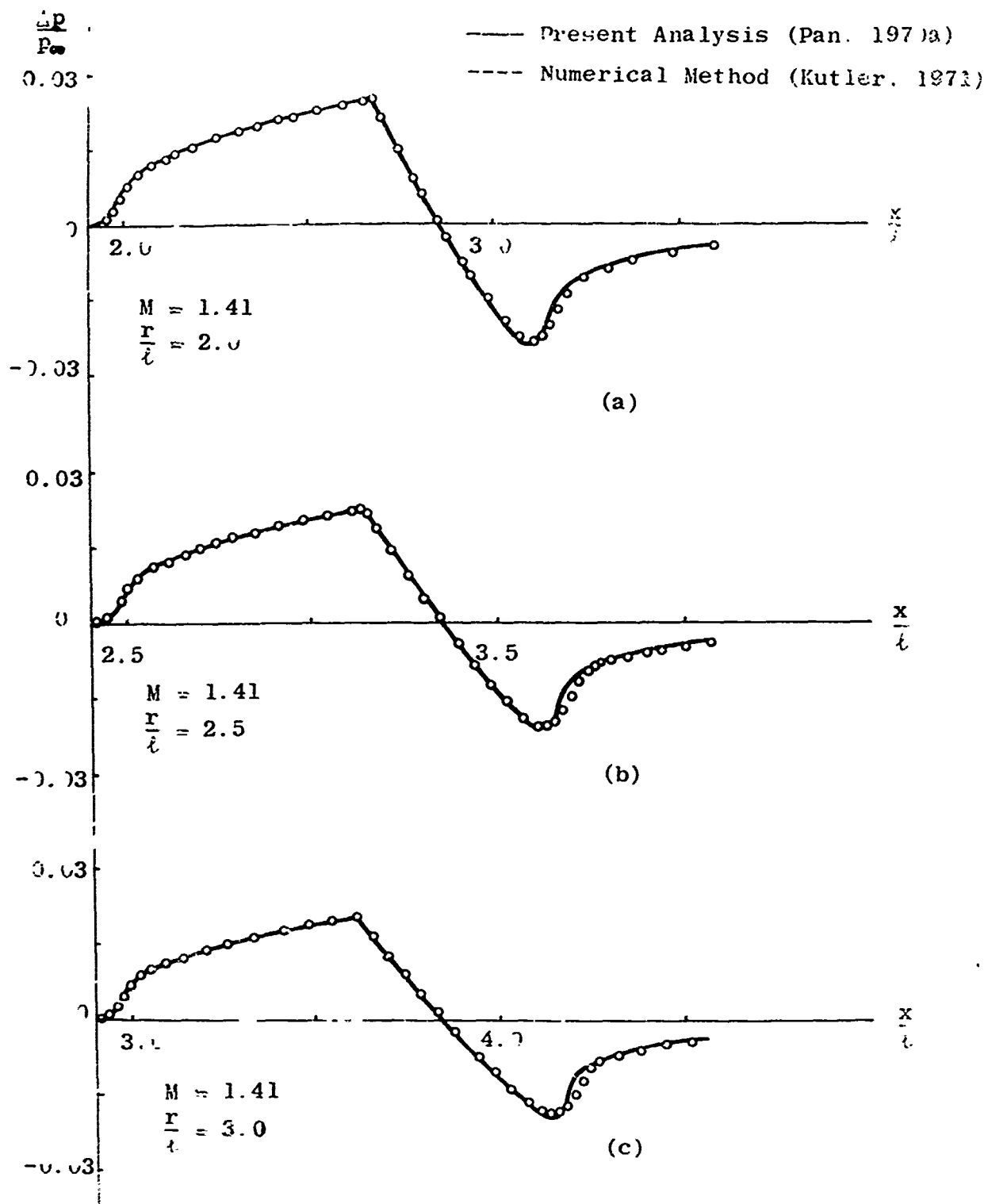


FIGURE 2.1.11 Extrapolation of pressure signatures

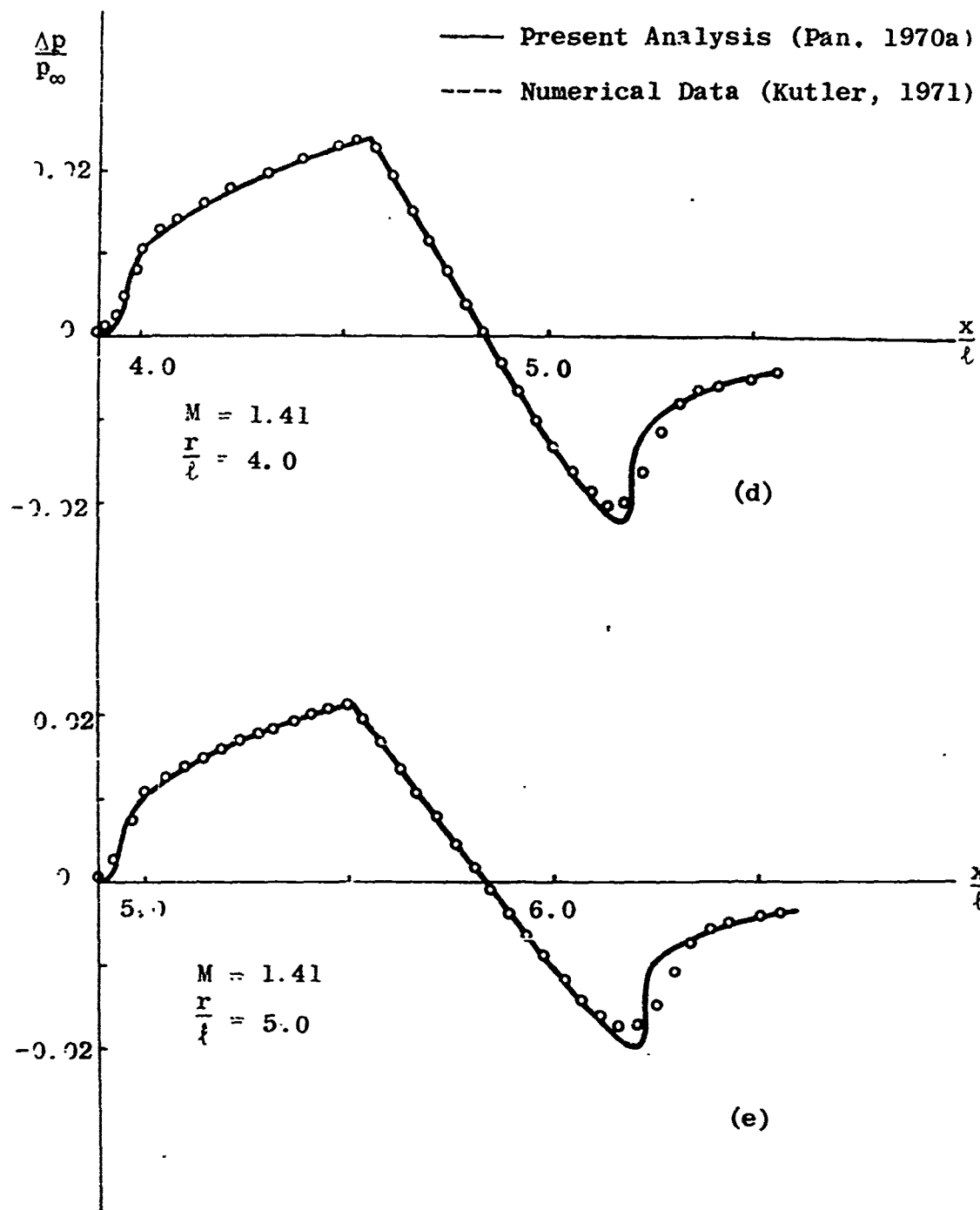


FIGURE 2.1.11 Extrapolation of pressure signatures

with Kutler's numerical data are again in good agreement except at the neighborhoods of the shock waves.

Figure 2.1.12) shows the pressure signatures of a slender body of revolution at $r/l = 4.2$ and $M = 1.2$. Experimental data (Barger, 1968) are compared with the results of the two different theoretical calculations. The difference between the two theoretical curves is obvious. By observation, one cannot tell which curve is in better agreement with the experimental data, because the streamwise positions of the experimental data with respect to the body are usually not specified. Based on Whitham's theory, Barger (1968) developed a procedure to design a body of revolution from a specified signature. Pan and Varner (1971) performed a similar calculation by using the present analysis. Examples indicate the different body radii obtained from the two different analyses. The differences are most apparent at the rearward portion of the bodies.

Figure 2.1.13-2.1.18 demonstrate an extrapolation of a measured three-dimensional pressure signature. A three-dimensional measured pressure signature is assumed in a form, $P_R = P_{R0} + P_{R1} \cos \theta$, and is shown Figure 2.1.13. A free stream Mach number of $M = 2.0$ and a wind tunnel wall radius of $R = 0.5$ are assumed. The magnitude of the assumed pressure disturbance has been exaggerated to apply the usual linearized approaches. Following the procedures described in Subsection 2.1.3, the corresponding incident (free flight) pressure disturbance is calculated ($n = 0$ and 1) and is shown in Figure 2.1.14.

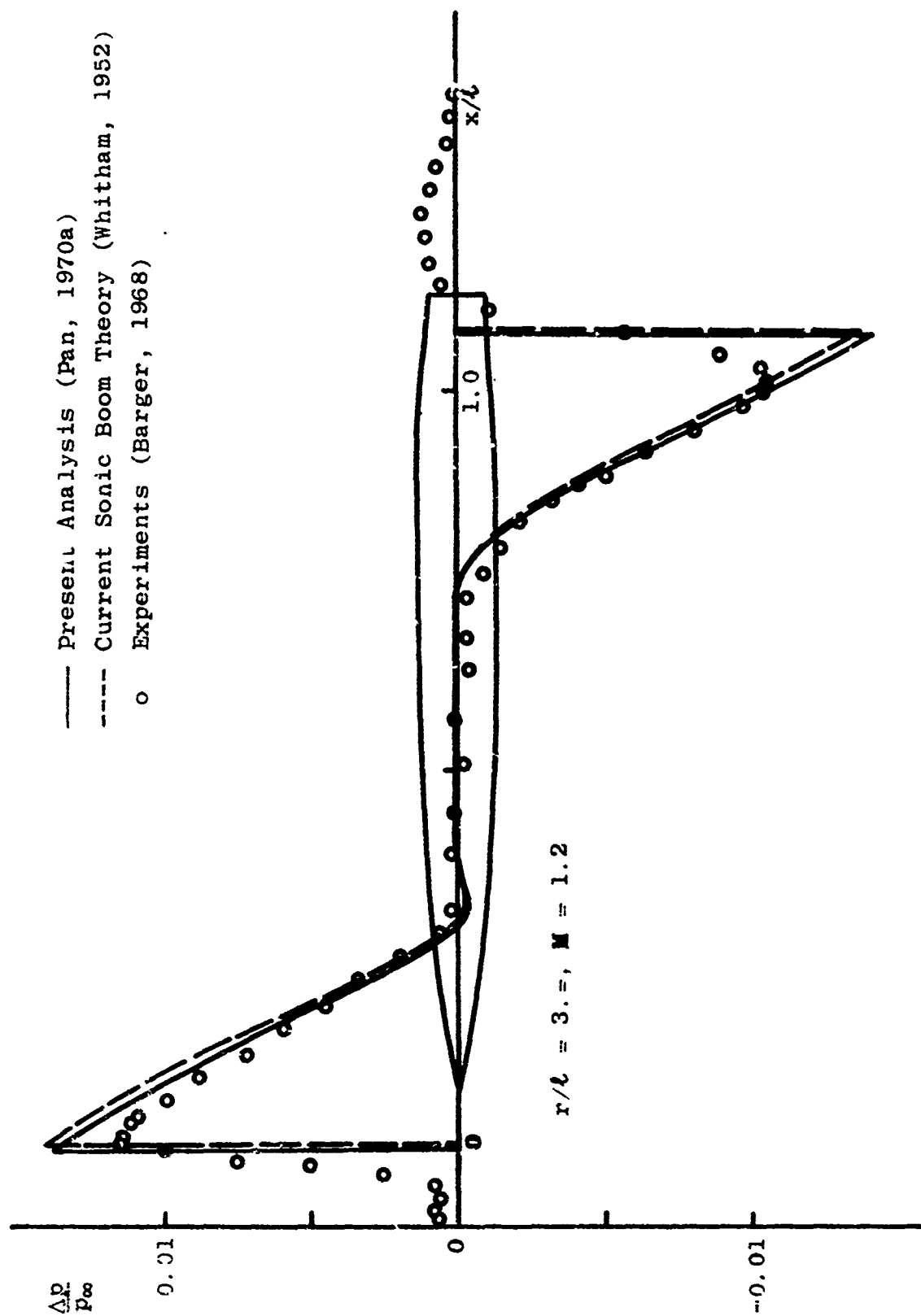


FIGURE 2.1.12 Calculated and measured pressure signatures

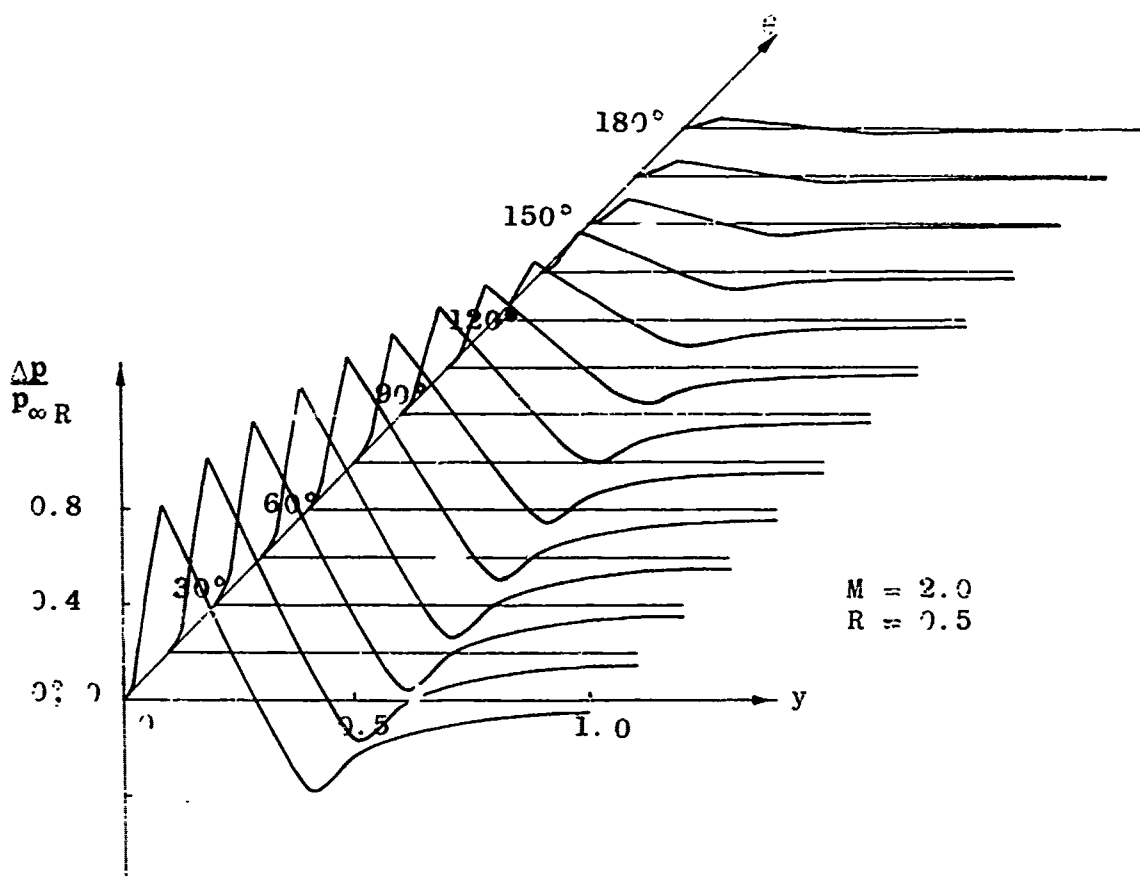


FIGURE 2.1.13 Three-dimensional reflected pressure disturbances

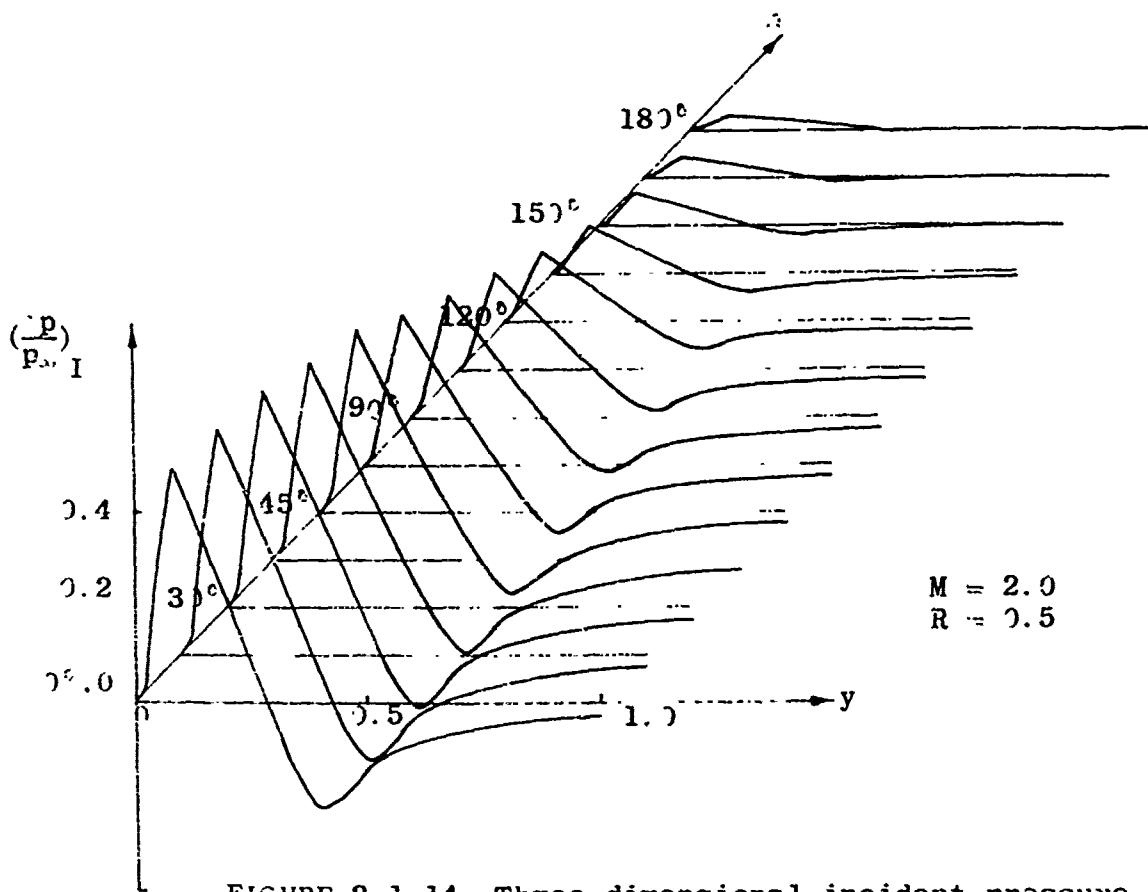


FIGURE 2.1.14 Three-dimensional incident pressure disturbances

From the incident pressure disturbance of its Fourier components ($n = 0, 1$) the Fourier components of the corresponding F function are first calculated. By summing up the Fourier components ($n = 0, 1$), the local F function is obtained and is shown in Figure 2.1.15. Since the kernel functions S_0 and S_1 in the formula for calculating F_n and F_n are of different signs but with the same order of magnitude, the near-field effects of the F function are almost negligible in this example. For more complicated signatures where more Fourier component terms are required, the near-field effects on the function may be important.

The disturbance represented by the F function is extrapolated to the downstream at $r = 10.0$. The local single valued F function at $r = 10.0$ is obtained by following the procedures described in Subsection 2.1.3 and is shown in Figure 2.1.16. The F function at $r = 10.0$ is then expanded in a six-term Fourier series in θ ($n = 0$ to 5). This six-term Fourier series is generally a good representation of the F function except at certain positions (e.g. shock waves) where the F function is discontinuous in θ . From each Fourier component of the F function, six Fourier components of the corresponding pressure disturbance are obtained. By summing up the six Fourier components, the corresponding three-dimensional pressure signature is obtained and is shown in Figure 2.1.17. In this figure, the pressure signatures near the leading shock wave are fixed approximately from the six-term Fourier representation of the pressure signatures which, for $\theta = 0^\circ$, 90° and 180° , are shown by dashed lines in the same figure.

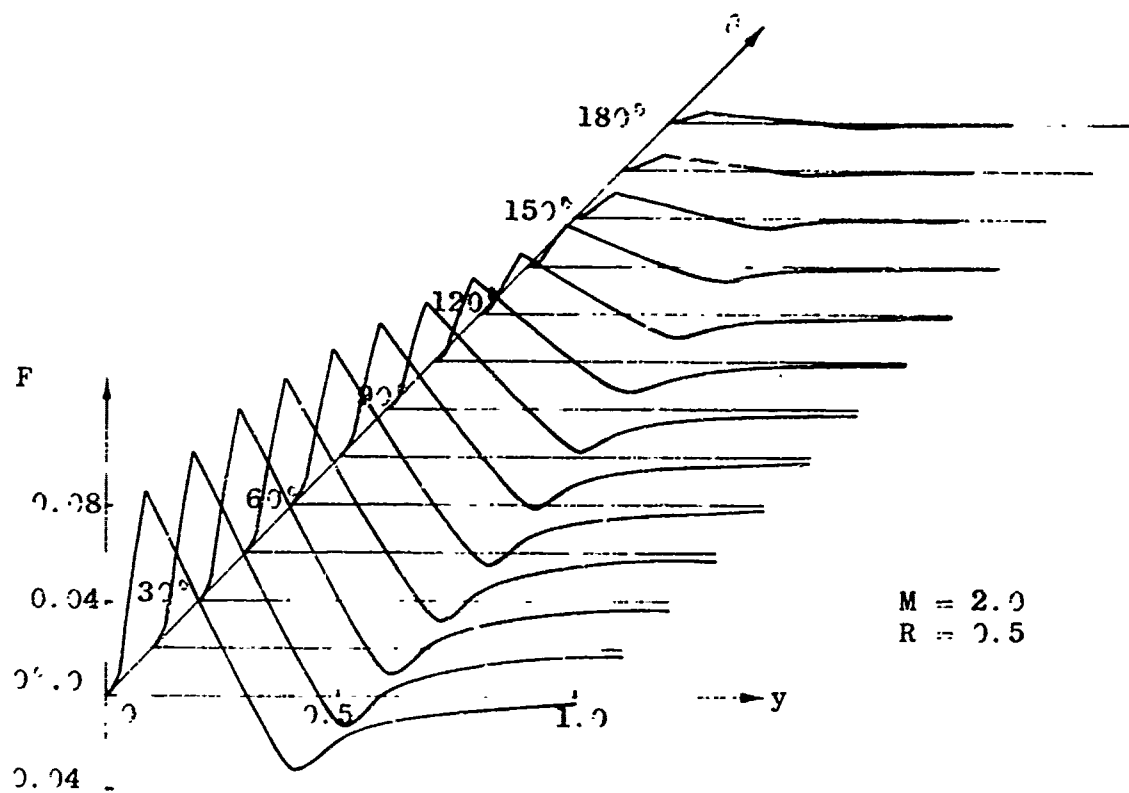


FIGURE 2.1.15 Three-dimensional F function

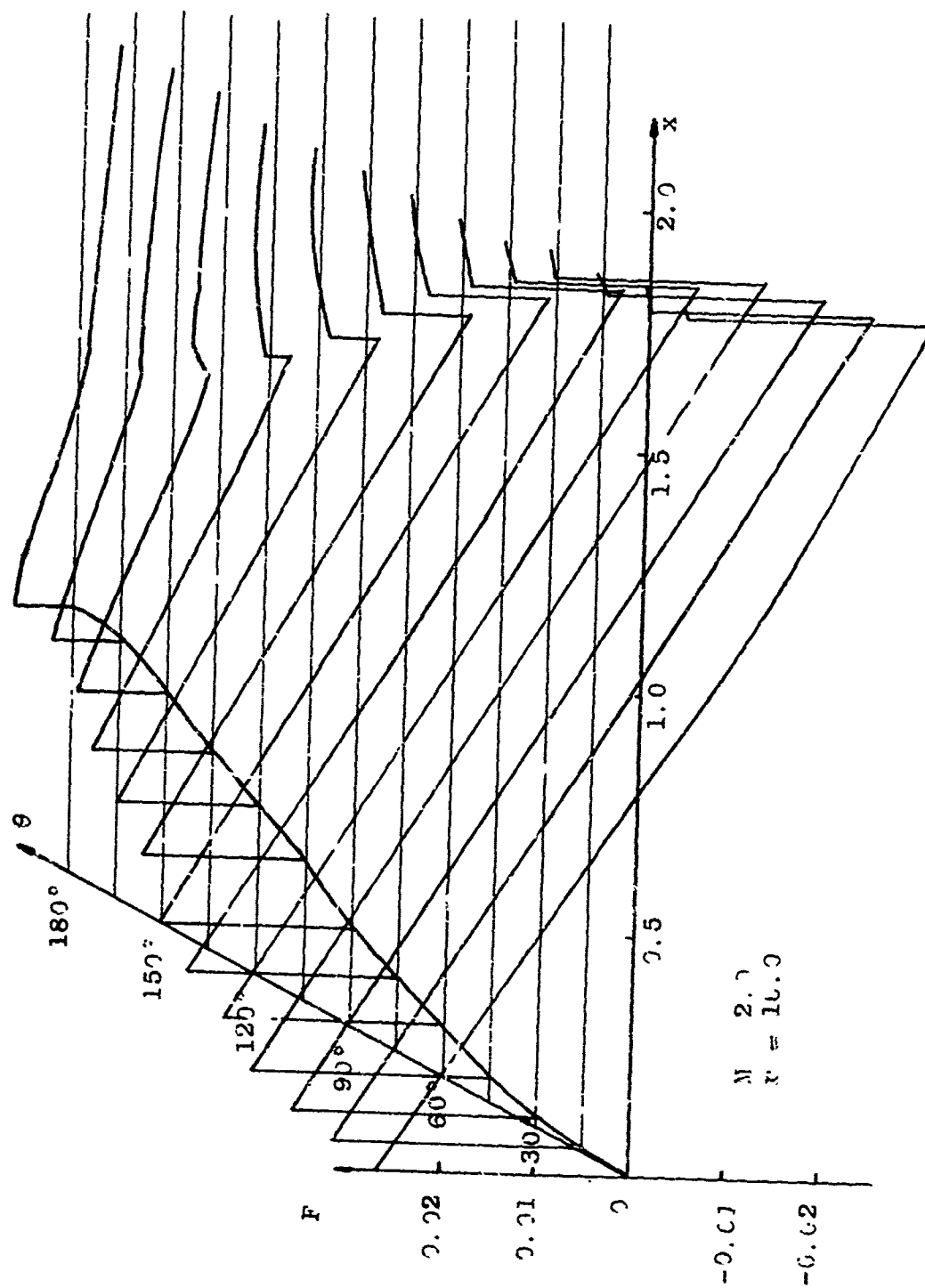


FIGURE 2.1.16. Three-dimensional F-function at $r = 10.0$

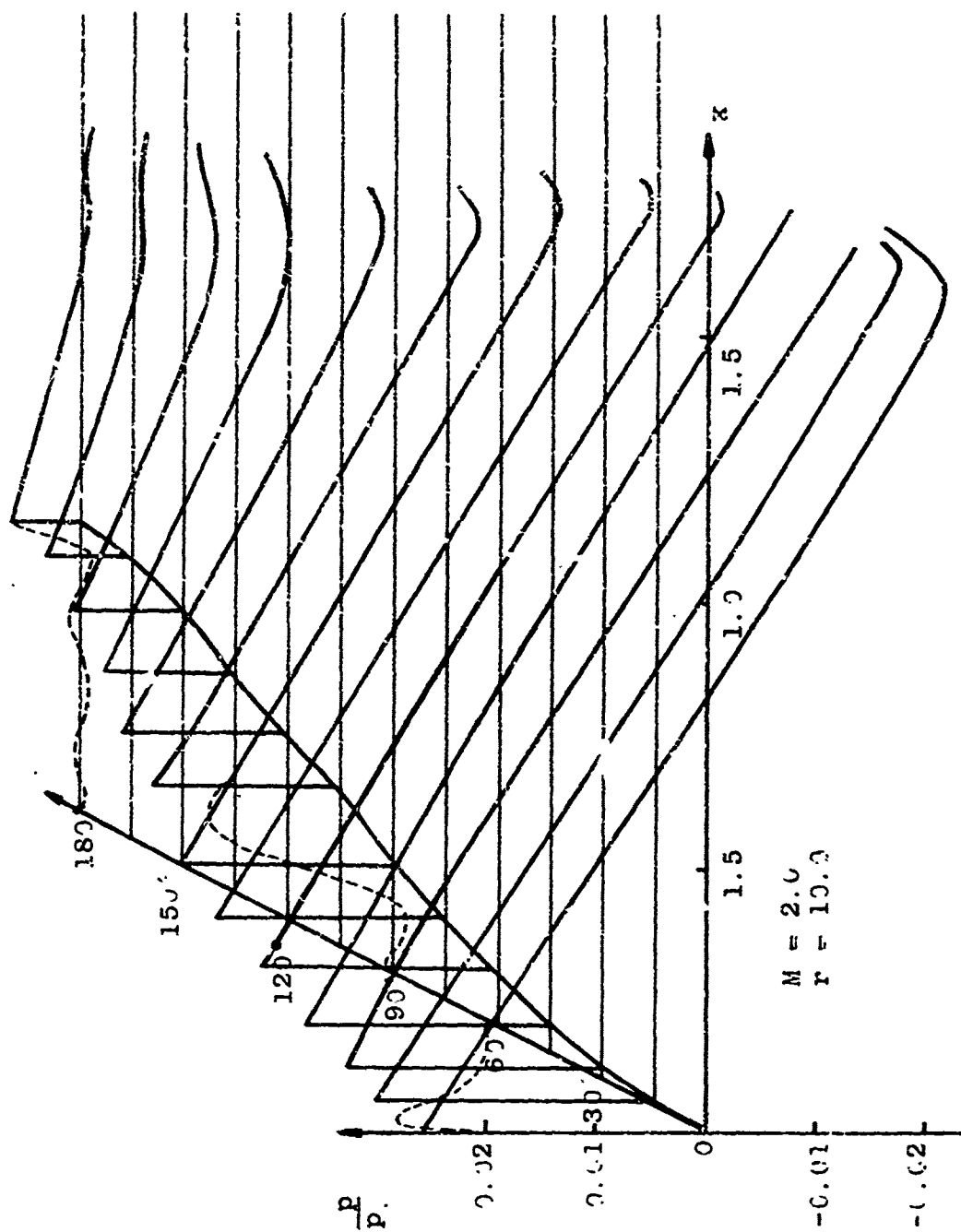


FIGURE 2.1.17 Three-dimensional pressure disturbance at $x = 10.0$

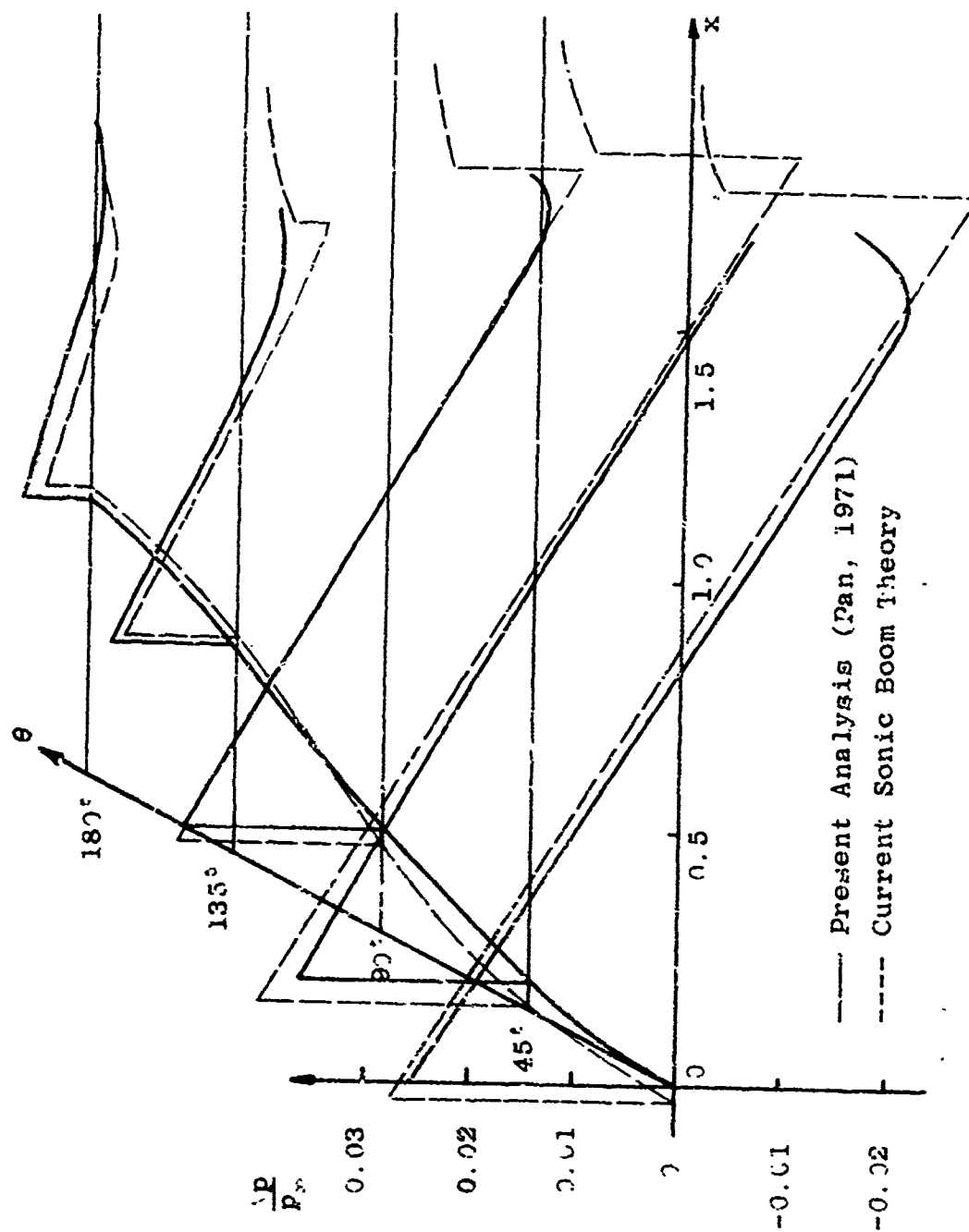


FIGURE 2.1.18 Comparisons of pressure signatures

If we take more terms in the Fourier series in the F function, and consequently in the pressure disturbance, the actual signature will approach the signature indicated by the solid lines.

In Figure 2.1.18, the pressure signatures at $\theta = 0^\circ$, 45° , 90° , 135° and 180° obtained previously are compared with those obtained directly from the current sonic boom theory. In this example, the current sonic boom theory over-estimates the peak pressures for $0^\circ \leq \theta \leq 90^\circ$ as much as 20 percent but under-estimates the peak pressures for $90^\circ < \theta \leq 180^\circ$ as much as 50 percent. Although no general quantitative conclusion on the importance of the near-field effects can be obtained from this single example, this example does show that the near-field effects may be important for extrapolating complicated near-field three-dimensional signatures.

2.1.5 CONCLUSIONS

The current sonic boom theory, which is based on the well known "Supersonic Area Rule" and Whitham's "supersonic projectile theory", has been extended to take into account the three-dimensional near-field effects. The present extended theory permits us to calculate the flow disturbances in the almost entire flow field of a steady supersonic flow over a three-dimensional configuration.

Based on the present theory, a new wind tunnel testing method based on large models is developed. This new method permits us to use the models of usual size in wind tunnels to determine the sonic boom on the ground by measuring the pressure

signature at the wind tunnel wall. This method has great significance in making wind tunnel tests more reliable by avoiding the use of extremely small models as is usually done today.

2.1.6 RECOMMENDATIONS

THEORETICAL WORKS

It is recommended to compute a more complete set of the kernel functions S_n, T_n, K'_n and J'_n which are required for the application of the present theory to the practical sonic boom calculations and to the extrapolation of pressure signatures measured in the wind tunnels. Only part of these kernel functions have been computed and presented in this report.

It is recommended, based on the present theory, to develop a FORTRAN computer program. More three-dimensional calculations are required to compare with experimental data and/or with the calculations based on the current sonic boom theory.

It is recommended to develop a sonic boom theory valid at large Mach numbers. . . . the range of applicability of the present quasi-linear approach is quite limited, a theory which takes into account non-linear effects at large Mach numbers should be developed and should be of great importance in the near future.

EXPERIMENTAL WORKS

It is recommended, based on the present method, to develop wind tunnel test procedures to produce suitable three-dimensional pressure signatures for extrapolation to the far field that is

for determining the sonic boom on the ground.

It is also recommended that an experimental check of the reliability of the present theory and the wind tunnel method be made.

2.2. FUNDAMENTAL THEORIES, APPLICABILITY AND EXTENSIONS

2.2.1. The Near-Field Flow Pattern of an Inclined Slender Body of Revolution by Dr. S. N. Chaudhuri, and UTSI student Sarat Praharaj

Summary

In the present paper Whitham's far-field theory of supersonic flow pattern has been generalized for the near-field points of an inclined body of revolution. Using the correct expression for the characteristics (as far as the first-order theory is concerned) it is shown that the new F-function which describes the near-field flow pattern is dependent on the following besides the body geometry: the distance from the axis of the body, the Mach number, the angle of attack and the azimuthal plane angle. We have obtained closed form results for the new F-function for any smooth body of revolution. The recurrence formulas given are convenient for computer programming. The pressure signatures for near-field positions have also been calculated. They can, of course, no longer be related to the new F-functions by simple formulas. The routine method given to calculate the fundamental F-function and the pressure signature at near-field points of non-axisymmetric bodies will be useful in the preliminary design study of equivalent bodies of revolution.

LIST OF SYMBOLS

α	=	Angle of attack
β	=	$(M^2 - 1)^{1/2}$
Φ	=	Velocity potential
ϕ	=	Perturbation velocity potential
ϕ_0	=	Axial-flow perturbation velocity potential (First Order)
ϕ_1	=	Cross-flow perturbation velocity potential (First Order)
$F(y)$	=	Whitham's function for the points, where $\beta r/x - \beta r$ is large
$\bar{F}\{y, r, M, R(y), \alpha, \theta\}$	=	Whitham's function at any point
$f(t)$	=	Strength of source (singularity) distribution
$g(t)$	=	Strength of doublet (singularity) distribution
M	=	Free stream Mach number
p_0	=	Free stream static pressure
Δp	=	Pressure in excess of undisturbed (free stream) static pressure
q	=	total velocity
$q_{(x)}$	=	total axial velocity component
$q_{(r)}$	=	total radial velocity component
$q_{(\theta)}$	=	total azimuthal velocity component
r	=	Distance of a point on the characteristic from the axis of the body
$R(y)$	=	Radius of the body of revolution at y
U	=	Free stream speed
x	=	Distance of any point measured from the nose
y	=	Distance of any point from the nose, where the characteristic produced meets the axis.

Introduction

For an axisymmetrical flow past a slender body of revolution Whitham (1952) developed an elegant modified theory which essentially retains the simplicity of the linearized theory as given by Lighthill (1952) and others but remedies the failure of the linear theory as a description of the flow pattern. The fundamental hypothesis of Whitham is that the linearized theory gives valid first approximation to the flow everywhere provided that in it the approximate characteristics are replaced by a sufficiently good approximation to the exact ones. This hypothesis has been amply substantiated by checks detailed in Whitham's paper (Whitham, 1952).

The following are some of the important assumptions made in Whitham's theory (Whitham, 1952):

- (i) The body is slender and pointed at the nose, with the front shock attached. (It may be remarked here that even if these conditions are not satisfied, Whitham's theory can still be used to deduce the behaviour of the flow at large distances from the axis of the body).
- (ii) Whitham's discussions of the flow pattern is limited strictly to the behaviour at large distances from the axis of the body. In particular, the Whitham function $F(y)$ which is fundamental to the whole theory and is the most important function associated

with flow past a body of revolution is obtained only for far-field positions. The condition is also valid for front shocks at any distance. This simplifies the mathematical analysis considerably and makes the F-function dependent only on y , the distance of any point from the nose where the characteristic produced meets the axis.

- (iii) Apparently a third restrictive condition in Whitham's theory is that of axial symmetry. However, Ward (1949) has shown[†] that the flow becomes axisymmetrical when $\beta r/(x-\beta r)$ is large (See Fig. 2.2.1) Here $\beta = (M^2 - 1)^{1/2}$ with M as the free-stream Mach number and r is the distance of a point on the characteristic from the axis of the body. The quantity $(x-\beta r)$ is the linearized form of the characteristic variable and measures the distance from the nose at which the characteristic starts. This Ward's condition is clearly satisfied at large distances, but it is also true at points on the front shocks because the appropriate characteristic surfaces arise so very close to the nose. Hence the results for the front shock and all the Whitham theory at large distances apply unchanged to non-axisymmetrical slender body. From this Whitham concludes (Whitham, 1952) that it is reasonable to expect that his results

[†] This also follows from the result established in the present paper as will be shown later.

for large distances apply to the supersonic flow past any finite body. Mathematically this leads to the interesting result that even for non-axisymmetrical bodies the simplified Whitham F-function can be used for far-field points.

We shall now examine the above assumptions critically with a view to its application to the calculation of near-field flow pattern of an inclined slender body of revolution.

The first assumption is essential to our theory because the first-order potential equations are used. Strictly we do not use the entire linearized equation in our analysis as it would be had the x-axis been aligned with the free-stream direction. This was first noted by Lighthill (1948). The consequences of this distinction has been considered in detail by Van Dyke (1952) and we will discuss it later.

The second assumption is, in general, obviously invalid for near-fields. It is, however, still true for the front shock system originating very close to the nose but not for other points of the body. Whitham (1952) replaces the approximate straight characteristics $x - \beta r$ by a better approximation, $y(x, r)$ given by equation (10)* in (Whitham, 1952).

Whitham justifiably simplifies the "extremely complicated" expression (10) for his far-field theory and obtains the

*Incidentally, there is an error in equation (10). The second integral on the right-hand-side of the equation should be multiplied by $(-M^2)$ and not by $(-2M^2)$. This, however, does not affect Whitham's results as he has not used equation (10) in his paper.

well-known results for the equation of the characteristics[†]
 [equations (12) and (13) of Whitham's paper (1952)]

$$x = \beta r - k F(y) r^{1/2} + y$$

where

$$F(y) = \int_0^y \frac{f'(t) dt}{(y-t)^{1/2}}$$

and

$$k = 2^{-1/2} (\gamma + 1) M^4 \beta^{-3/2}$$

Whitham notes, however, that expression (10) of his paper (Whitham, 1952) still provides the correct approximation to the characteristic curves near the body and should be used for near- and mid-field calculations.

Using the correct expression for $y(x, r)$ as given in equation (10) of the above reference it will be observed that the new F -function will be dependent on y, r, M and $R(y)$ (see list of symbols) for axisymmetrical flows. We have denoted this function by $\bar{F}_S\{y, r, M, R(y)\}$. For inclined flows there are two more variables on which \bar{F} -function will depend, namely, the angle of attack α and the azimuthal plane angle θ .

We have obtained closed form results for the new \bar{F} -function for any smooth body of revolution. The recurrence formulas given are convenient to use for computer programming.

[†]In Whitham's paper $\alpha = (M^2 - 1)^{1/2}$, which we have replaced here by β in order to use the Greek letter α for angle of attack.

It is shown that if the shape of the meridian curve is expressible as a polynomial, all the integrals are related by simple recurrence formulas and ultimately depend on one standard form. It is a fortunate fact that any function, which is continuous in a closed interval, can be uniformly approximated within any prescribed tolerance, over that interval, by some polynomial. This follows from the well-known theorem, which states that for a continuous function $y(x)$ in an interval (a,b) there will be a polynomial $f(x)$ such that $|f(x) - y(x)| \leq \epsilon$ in (a,b) for an arbitrary positive ϵ .

Once our polynomial $f(x)$ has been determined so that it satisfactorily approximates the given meridian curve $R(x)$ over a certain interval (a,b) it is easy to see that integration, being essentially a smoothing process, will involve lesser error than the derivations in $f(x)$ and $R(x)$ (Hildebrand, 1956). It is of importance to emphasize here the fact that the integrands representing the \bar{F} -functions are of the type $G(x) f(x)$, where $G(x)$ are given functions and $f(x)$ is the approximated polynomial. Therefore the closed form solutions obtained will introduce even smaller error than by using mechanical quadratures.

The third restrictive condition in Whitham's theory is that of axial symmetry. As mentioned earlier the far-field flow pattern is not significantly affected by removing this assumption of axial symmetry. But it is obvious that we have to consider the effects of cross-flow for bodies at an

angle of attack in the calculation of the flow pattern at near-field points. This has been done by a distribution of doublets with their axes perpendicular to the body center-line. The strength of the doublets per unit length is found to be proportional to the cross section-area if we replace the exact tangency condition by an approximate one. This approximation is exactly similar to the first order axial flow problem.

To illustrate the type of \bar{F} -curve that results from the present theory we have calculated the new function \bar{F} for two bodies. Their shapes are given by

$$(a) \quad R(x) = 0.1 x(1-x), \quad 0 \leq x \leq 1 \\ = 0, \quad x > 1$$

$$(b) \quad R(x) = 0.1 \{1 - (1-x)^3\}, \quad 0 \leq x \leq 1 \\ = 0.1, \quad x > 1$$

A comparison of the near- and mid field \bar{F} -function with the far field F -functions bring out the following important facts:

- (i) As expected \bar{F} -function very nearly coincides with the F -function for points close to the nose.
- (ii) At other stations there are significant differences with changes in r , especially the peaks and troughs of \bar{F} -function.

- (iii) For axisymmetric flows \bar{F} -function is a weak function of M upto about 3. This again is to be expected from the slender body theory.
- (iv) For inclined flows the effect of Mach number is more pronounced.

Improved First-Order Theory for Supersonic Flow Past Inclined Body of Revolution

Consider uniform supersonic flow past a body of revolution inclined at an angle of attack α [see Fig. 2.2.1]. The boundary condition at the body is simplified by choosing a cylindrical coordinate system (x, r, θ) aligned with the body axis. We resolve the free-stream velocity into axial and cross-flow components, as shown in Fig. 2.2.2. The shape of the body is defined by its continuous meridian curve $r = R(x)$.

For moderate supersonic Mach numbers the flow is assumed to be isentropic and irrotational throughout so that there exists a velocity potential $\phi(x, r, \theta)$. The equation of motion is then

$$\begin{aligned} (a^2 - \phi_x^2) \phi_{xx} + (a^2 - \phi_r^2) \phi_{rr} + (a^2 - \frac{1}{r^2} \phi_\theta^2) \frac{1}{r^2} \phi_{\theta\theta} + (a^2 + \frac{\phi_\theta^2}{r^2}) \frac{1}{r} \phi_r \\ - \frac{2}{r} \phi_r \phi_\theta \phi_{r\theta} - \frac{2}{r} \phi_x \phi_\theta \phi_{\theta x} - 2 \phi_x \phi_r \phi_{xr} = 0 \end{aligned} \quad (2.2.1a)$$

where the speed of sound a is related to its free stream value a_0 by

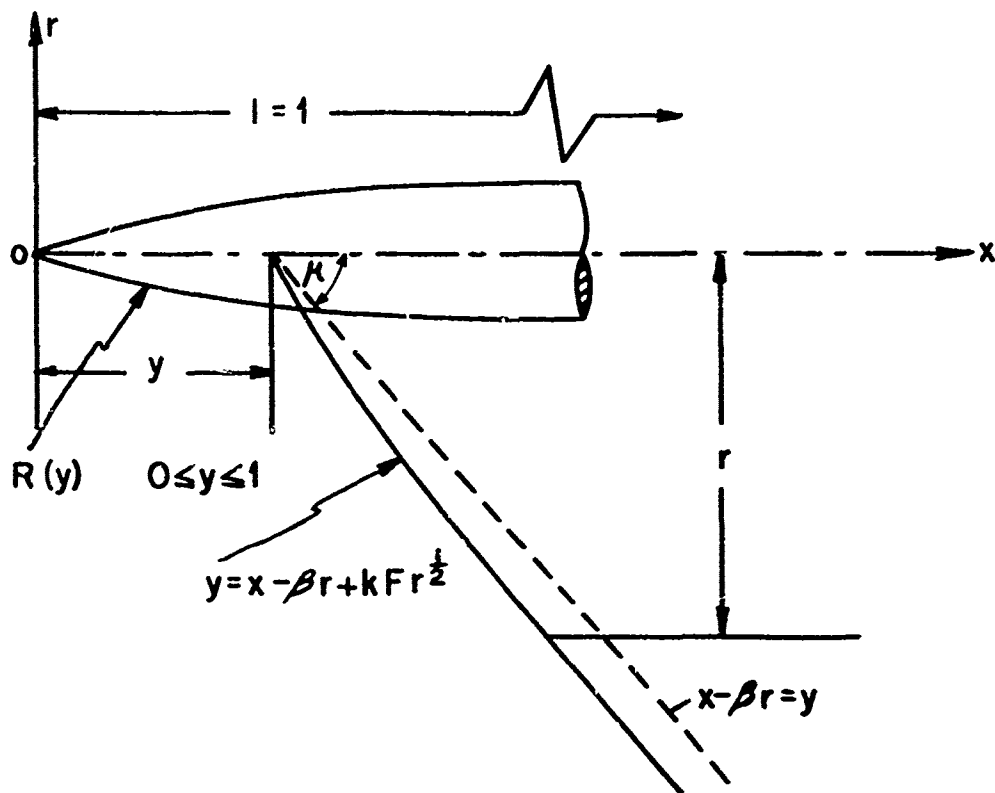


Figure 2.2.1: Nomenclature

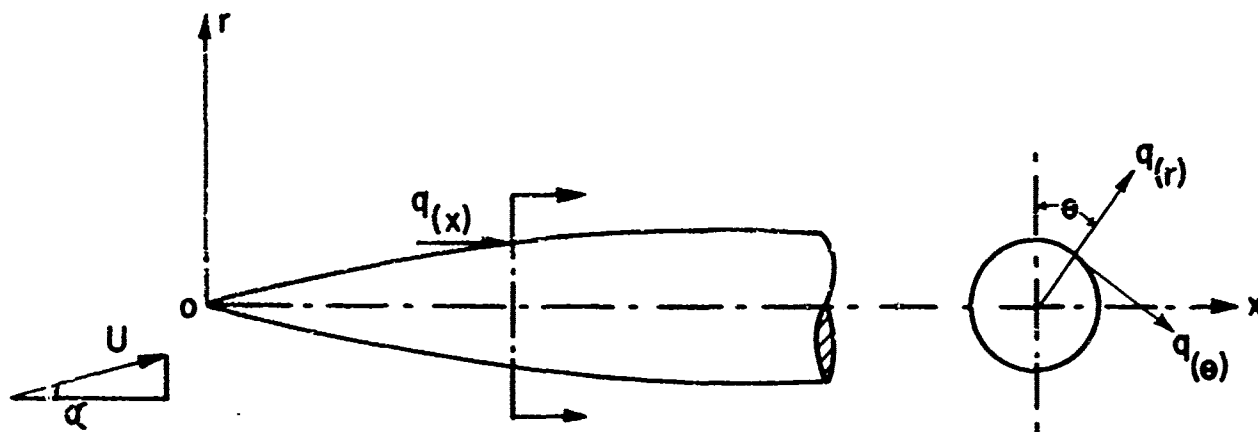


Figure 2.2.2: Nomenclature

$$a^2 = a_o^2 - \frac{\gamma-1}{2} (\phi_x^2 + \phi_r^2 + \frac{1}{r^2} \phi_\theta^2 - U^2) \quad (2.2.1b)$$

The suffixes have been used to denote partial differentiations.

Introducing a perturbation potential $\phi(x, r, \theta)$ we write

$$\phi(x, r, \theta) = U[x \cos \alpha + r \sin \alpha \cos \theta + \phi(x, r, \theta)] \quad (2.2.2a)$$

The total axial, radial and azimuthal velocity components are then given by

$$\begin{aligned} q_{(x)} &= \phi_x = U(\cos \alpha + \phi_x), \\ q_{(r)} &= \phi_r = U(\sin \alpha \cos \theta + \phi_r), \\ q_{(\theta)} &= \frac{1}{r} \phi_\theta = U(-\sin \alpha \sin \theta + \frac{1}{r} \phi_\theta) \end{aligned} \quad (2.2.2b)$$

Substituting eq. (2.2.2a) into equations (2.2.1) gives the exact equation in the perturbation velocity potential. We need not write the full equation for our purpose. However, in order to bring out the distinction between first-order and linearized equation for this inclined flow problem we reproduce the perturbation equation partially retaining only terms linear in ϕ :

$$\begin{aligned} \phi_{rr} + \frac{1}{r} \phi_r + \frac{1}{r^2} \phi_{\theta\theta} - \beta^2 \phi_{xx} &= -\phi_{xx} \sin^2 \alpha + \phi_{rr} \sin^2 \alpha \cos^2 \theta \\ &+ \left(\frac{1}{r} \phi_{\theta\theta} - \frac{1}{r} \phi_x \right) \sin^2 \alpha \sin^2 \theta + \phi_{xr} \sin 2\alpha \cos \theta \\ &- \frac{1}{r} \phi_{x\theta} \sin 2\alpha \sin \theta - \frac{1}{2r} \phi_{r\theta} \sin 2\alpha \sin 2\theta \end{aligned}$$

$$+ \frac{2}{r} \phi_r \sin^2 \alpha \sin^2 \theta + \frac{1}{r^2} \phi_\theta \sin^2 \alpha \sin 2\theta$$

+ the nonlinear terms in ϕ (2.2.3a)

To this we add the following boundary conditions:

- (i) All perturbations should vanish upstream of the body so that

$$\phi(0, r, \theta) = \phi_x(0, r, \theta) = 0 \quad (2.2.3b)$$

- (ii) The flow should be tangential to the surface of the body so that

$$\phi_r(x, R, \theta) + \sin \alpha \cos \theta = R' [\cos \alpha + \phi_x(x, R, \theta)], \quad (2.2.3c)$$

where

$$R' = \frac{dR(x)}{dx}.$$

Actually, the first upstream conditions should be supplemented by the shock condition along the bow wave. However, this refinement is not necessary for the order of accuracy sought here.

The First-Order Problem and Its Justification

The complete perturbation equation (2.2.3a) including the non-linear terms is equivalent to the original non-linear equation of motion, Eqs. (2.2.1). Consequently, simplifying assumptions must be made in order to solve it. The well known

theory of Kármán and Moore (1932) or axially symmetric flow and of Tsien (1938) or inclined flow is based upon the assumption that the entire right-hand side of Eq. (2.2.3a) can be neglected leaving the wave equation. Its solution will be termed the first-order potential (Van Dyke, 1951) and is denoted by $\varphi(x, r, \theta)$.

It is clear from Eq. (2.2.3a) that the first-order and linearized problems are the same where the free stream is aligned to the x-axis, i.e., where $\alpha = 0$. But, as mentioned earlier, Lighthill (1948) first noted that when $\alpha \neq 0$ the linearized problem is not the same as the first-order solution because we are neglecting the linear terms in φ in Eq. (2.2.3a). The justification advanced for this approximation for inclined flows follows from the slender-body theory in which the following are some of the important assumptions generally made: (i) approximate pressure relation; (ii) approximate tangency condition; and (iii) small angle of attack. Hence, Lighthill (1948) and Laitone (1947) conclude that the exact solution of the first order equation is fruitless and that first-order theory is incapable of yielding results more exact than those of slender body theory.

The first-order problem is, therefore,

$$\varphi_{rr} + (\varphi_r/r) + (\varphi_{\theta\theta}/r^2) - \beta^2 \varphi_{xx} = 0 \quad (2.2.4a)$$

$$\varphi(0, r, \theta) = \varphi_x(0, r, \theta) = 0 \quad (2.2.4b)$$

$$\varphi_r(x, R, \theta) + \sin \alpha \cos \theta = R' [\cos \alpha + \varphi_x(x, R, \theta)]. \quad (2.2.4c)$$

The first-order problem is satisfied exactly by setting

$$\varphi(x, r, \theta) = \varphi_0(x, r) \cos \alpha + \varphi_1(x, r) \sin \alpha \cos \theta \quad (2.2.5)$$

The first term corresponds to the axial component of free stream velocity and the second, to the cross-flow component (Fig. 2.2.2). We shall assume that α is small so that $\cos \alpha \simeq 1$ and $\sin \alpha \simeq \alpha$.

The first-order problem is thus separated into two completely independent problems. For the axial flow,

$$\varphi_{orr} + (\varphi_{or}/r) - \beta^2 \varphi_{oxx} = 0 \quad (2.2.6a)$$

$$\varphi_o(o, r) = \varphi_{ox}(o, r) = 0 \quad (2.2.6b)$$

$$\varphi_{or}(x, R) = R' [1 + \varphi_{ox}(x, R)] \quad (2.2.6c)$$

and for the cross-flow,

$$\varphi_{1rr} + (\varphi_{1r}/r) - (\varphi_1/r^2) - \beta^2 \varphi_{1xx} = 0 \quad (2.2.7a)$$

$$\varphi_1(o, r) = \varphi_{1x}(o, r) = 0 \quad (2.2.7b)$$

$$1 + \varphi_{1r}(x, R) = R' \varphi_{1x}(x, R) \quad (2.2.7c)$$

The general solutions of Eqs. (2.2.6a) and (2.2.7a) satisfying upstream conditions (2.2.6b) and (2.2.7b) are given in (Von Karman, 1932) and (Tsien, 1938).

$$\varphi_0(x, r) = - \int_0^{x-\beta r} X(t, \beta r) f(t) dt, \quad (2.2.8a)$$

$$\varphi_1(x, r) = \frac{1}{\beta r} \int_0^{x-\beta r} (x-t) X(t, \beta r) g(t) dt, \quad (2.2.8b)$$

where

$$X(t, \beta r) = \{ (x-t)^2 - \beta^2 r^2 \}^{-1/2} \quad (2.2.8c)$$

The corresponding first derivatives are

$$\varphi_{0x} = - \int_0^{x-\beta r} X(t, \beta r) f'(t) dt, \quad (2.2.9a)$$

$$\varphi_{0r} = \frac{1}{r} \int_0^{x-\beta r} (x-t) X(t, \beta r) f'(t) dt, \quad (2.2.9b)$$

$$\varphi_{1x} = \frac{1}{\beta r} \int_0^{x-\beta r} (x-t) X(t, \beta r) g'(t) dt, \quad (2.2.9c)$$

$$\varphi_{1r} = - \frac{1}{\beta r^2} \int_0^{x-\beta r} (x-t)^2 X(t, \beta r) g'(t) dt \quad (2.2.9d)$$

The functions f and g are strictly determined from the tangency conditions, Eqs. (2.2.6c) and (2.2.7c) which leads to Volterra integral equations, which can, in general, only be solved numerically. For our order of accuracy as used by Whitham (1952) we may, neglect the term φ_x compared with $\cos \alpha$ in the exact tangency condition of Eq. (2.2.3c) and arrive at the linearized boundary condition at the body surface:

$$\phi_r(x, R, \theta) + \alpha \cos \theta = R' \quad (2.2.10)$$

where we have taken α to be small.

For first-order axial and cross-flow problems, Eqs. (2.2.6c) and (2.2.7c) they take the form

$$\phi_{0r}(x, R) = R'(x) \quad (2.2.11a)$$

$$\phi_{1r}(x, R) = -1 \quad (2.2.11b)$$

As remarked by Van Dyke (1951) these approximations have the advantage that the resulting first-order solutions satisfy the supersonic similarity law (the supersonic counterpart of the Goethert rule), which is not true if the exact tangency condition is used. Except possibly for extremely thick bodies, the resulting error in using the approximate tangency conditions, Eqs. (2.2.11) must be small at all Mach numbers (Van Dyke, 1951).

The linearized boundary conditions (2.2.11a) and (2.2.11b) lead to the following values for the arbitrary functions $f(x)$ and $g(x)$ (Von Karman, 1932) (Tsien, 1938):

$$f(x) = R(x) R'(x) + \frac{1}{2\pi} \frac{dS(x)}{dx}, \quad (2.2.12a)$$

and

$$g(x) = 2R(x) R'(x) + \frac{dS(x)}{\pi dx}, \quad (2.2.12b)$$

where $S(x) = \pi R^2(x)$ is the cross-sectional area of the body at x .

Denoting the axial, radial and azimuthal perturbation velocity components by u, v and w in this first-order solution, we obtain

$$u = \varphi_{0x} + \alpha \varphi_{1x} \cos \theta, \quad (2.2.13a)$$

$$v = \varphi_{0r} + \alpha \varphi_{1r} \cos \theta, \quad (2.2.13b)$$

$$w = -\frac{\alpha}{r} \varphi_1 \sin \theta \quad (2.2.13c)$$

where φ_0, φ_1 and their derivatives are given by equations (2.2.8) and (2.2.9) with $f(t)$ and $g(t)$ from Eqs. (2.2.12).

We now replace the straight downstream characteristics $x-\beta r$ by $y(x, r)$ as in Whitham's theory (1952). With this modification u, v and w become

$$u = - \int_0^y \frac{f'(t)}{Y(y, t, \beta r)} dt + \frac{\alpha \cos \theta}{\beta r} \int_0^y \frac{(y-t+\beta r)g'(t)}{Y(y, t, \beta r)} dt \quad (2.2.14a)$$

$$v = \frac{1}{r} \int_0^y \frac{(y-t+\beta r)f'(t)}{Y(y, t, \beta r)} dt - \frac{\alpha \cos \theta}{\beta r^2} \int_0^y \frac{(y-t+\beta r)^2 g'(t)}{Y(y, t, \beta r)} dt, \quad (2.2.14b)$$

$$w = -\frac{\alpha \sin \theta}{\beta r^2} \int_0^y \frac{(y-t+\beta r)g(t)}{Y(y, t, \beta r)} dt, \quad (2.2.14c)$$

where

$$Y(y, t, \beta r) = \{ (y-t)(y-t+2\beta r) \}^{1/2} \quad (2.2.15c)$$

y is now determined from the condition that $y(x, r) = \text{constant}$ is a characteristic curve, that is, along it

$$\frac{dx}{dr} = \cot(\mu + \delta), \quad (2.2.16)$$

where μ is the local Mach angle and δ is the local flow direction. The value of y on a characteristic has not been defined uniquely, although on the body it must be approximately equal to $x - \beta r$ (which it replaces in linearized theory). It is now made quite definite by taking it equal to the value of $x - \beta r$ at the point where the characteristic produced meets the body axis.

On expressing $\cot(\mu + \delta)$ in terms of u, v and w by means of Bernoulli's equation and neglecting terms $O(u^2 + v^2 + w^2)$, the integration of eq. (2.2.16) with respect to r yields

$$x = \beta r - c(y, r) + y \quad (2.2.17)$$

where

$$\begin{aligned} c(y, r) = & \frac{(\gamma+1)M^4}{2\beta^2} \int_0^y \frac{N(r) - N(R)}{(y-t)^{1/2}} f'(t) dt \\ & + M^2 \int_0^y \ln \left\{ \frac{N(r) - (y-t)^{1/2}}{N(r) + (y-t)^{1/2}} \cdot \frac{N(R) + (y-t)^{1/2}}{N(R) - (y-t)^{1/2}} \right\} f'(t) dt \\ & - \frac{(\gamma+1)M^4}{2\beta^2} \alpha \cos \theta \int_0^y \frac{N(r) - N(R)}{(y-t)^{1/2}} g'(t) dt \\ & - \left\{ \frac{(\gamma+1)M^4 - 2M^2\beta^2}{2\beta^2} \right\} \alpha \cos \theta \int_0^y \ln \left\{ \frac{N(r) - (y-t)^{1/2}}{N(r) + (y-t)^{1/2}} \cdot \frac{N(R) + (y-t)^{1/2}}{N(R) - (y-t)^{1/2}} \right\} g'(t) dt \\ & + \frac{M^2}{\beta r} \alpha \cos \theta \int_0^y N(r) (y-t) g'(t) dt - \frac{M^2 \alpha \cos \theta}{\beta R} \int_0^y N(R) (y-t) g'(t) dt \end{aligned}$$

$$\begin{aligned}
& - 2M^2 \alpha \cos \theta \int_0^y \ln \left\{ \frac{N(r) - (y-t)^{1/2}}{N(R) - (y-t)^{1/2}} \right\} g'(t) dt \\
& - 2M^2 \alpha \cos \theta \int_0^y \ln \left\{ \frac{R(y)}{r} \right\}^{1/2} g'(t) dt,
\end{aligned} \tag{2.2.18}$$

where

$$N(r) \equiv N(y, t, 2\beta r) = (y-t+2\beta r)^{1/2}, \tag{2.2.19a}$$

$$N(R) = N(y, t, 2\beta R(y)) = \{y-t+2\beta R(y)\}^{1/2} \tag{2.2.19b}$$

and $R \equiv R(y)$.

Writing

$$c(y, r) = k \bar{F}\{y, r, R(y), M, \alpha, \theta\} r^{1/2} \tag{2.2.20}$$

where

$$k = 2^{-1/2} (\gamma+1) M^4 \beta^{-3/2} \tag{2.2.21}$$

and changing the variable of integration by substituting

$$(y-t)^{1/2} = \xi, \tag{2.2.22}$$

the \bar{F} -function may be written as (see Appendix 2.2.1).

$$\begin{aligned}
\bar{F}\{y, r, R(y), M, \alpha, \theta\} &= \frac{2}{\sqrt{2\beta r}} [I_1(r) - I_1\{R(y)\}] \\
&\quad - \frac{4\beta^2}{(\gamma+1)M^2 \sqrt{2\beta r}} [I_2(r) - I_2\{R(y)\}] \\
&\quad - \frac{2\alpha \cos \theta}{\sqrt{2\beta r}} [\bar{I}_1(r) - \bar{I}_1\{R(y)\}] + \frac{2\alpha \cos \theta}{\sqrt{2\beta r}} [\bar{I}_2(r) - \bar{I}_2\{R(y)\}]
\end{aligned}$$

$$+ \frac{4\alpha\beta \cos \theta}{(\gamma+1)M^2 r \sqrt{2\beta r}} \bar{I}_3(r) - \frac{4\alpha\beta \cos \theta}{(\gamma+1)M^2 R(y) \sqrt{2\beta r}} \bar{I}_3\{R(y)\} \quad (2.2.23)$$

where

$$I_1(r) = \int_0^{y^{1/2}} (\xi^2 + 2\beta r)^{1/2} f'(y - \xi^2) d\xi, \quad (2.2.24a)$$

$$I_2(r) = \int_0^{y^{1/2}} (\xi^2 + 2\beta r)^{-1/2} f(y - \xi^2) d\xi, \quad (2.2.24b)$$

$$\bar{I}_1(r) = \int_0^{y^{1/2}} (\xi^2 + 2\beta r)^{1/2} g'(y - \xi^2) d\xi, \quad (2.2.24c)$$

$$\bar{I}_2(r) = \int_0^{y^{1/2}} (\xi^2 + 2\beta r)^{-1/2} g(y - \xi^2) d\xi, \quad (2.2.24d)$$

$$\bar{I}_3(r) = \int_0^{y^{1/2}} \xi^3 (\xi^2 + 2\beta r)^{1/2} g'(y - \xi^2) d\xi. \quad (2.2.24e)$$

and $I_1(R), I_2(R), \bar{I}_1(R), \bar{I}_2(R)$ and $\bar{I}_3(R)$ are obtained from Eqs. (2.2.24) by replacing r by $R(y)$.

Then the characteristics obtained by the improved linearized theory are given by

$$x = \beta r - k \bar{F}\{y, r, R(y), M, \alpha, \theta\} r^{1/2} + y \quad (2.2.25)$$

where k is given by eq. (2.2.21).

If we now assume axisymmetric flow, that is, $\alpha = 0$ the \bar{F} -function becomes independent of the azimuthal angle θ , and we obtain

$$\bar{F}_S\{y, r, R(y), M\} = \frac{2}{2\beta r} [I_1(r) - I_1(R)] - \frac{4\beta^2}{(\gamma+1)M^2} \frac{1}{2\beta r} [I_2(r) - I_2(R)] \quad (2.2.26)$$

where the expressions for I_1 and I_2 are given by (2.2.24a) and (2.2.24b).

If we assume $\beta r/y \gg 1$, we obtain Whitham's simplified F-function which depends only on y :

$$F(y) = 2 \int_0^{\sqrt{y}} f'(y-\xi^2) d\xi \quad (2.2.27)$$

Making use of the substitution (22), we can write this in the form given by Whitham (Whitham, 1952):

$$F(y) = \int_0^y \frac{f'(t)}{(y-t)^{1/2}} dt \quad (2.2.28)$$

F-Function

The \bar{F} -function is given by Eq. (2.2.23) in which the I-integrals of Eqs.(2.2.24) can be rewritten after substitution of the values of $f(x)$ and $g(x)$ from Eqs. (2.2.12)

$$I_1(r) = \frac{1}{2\pi} \int_0^{y^{1/2}} (\xi^2 + 2\beta r)^{1/2} S''(y-\xi^2) d\xi, \quad (2.2.29a)$$

$$I_2(r) = \frac{1}{2\pi} \int_0^{y^{1/2}} (\xi^2 + 2\beta r)^{-1/2} S'(y-\xi^2) d\xi, \quad (2.2.29b)$$

$$\bar{I}_1(r) = \frac{\beta}{\pi} \int_0^{y^{1/2}} (\xi^2 + 2\beta r)^{1/2} S''(y-\xi^2) d\xi = 2\beta I_1(r), \quad (2.2.29c)$$

$$\bar{I}_2(r) = \frac{\beta}{\pi} \int_0^{y^{1/2}} (\xi^2 + 2\beta r)^{-1/2} S'(y-\xi^2) d\xi = 2\beta I_2(r), \quad (2.2.29d)$$

$$\bar{I}_3(r) = \frac{1}{\pi} \int_0^{y^{1/2}} \xi^3 (\xi^2 + 2rx)^{1/2} S''(y - \xi^2) d\xi$$

where primes indicate differentiation with respect to the argument $(y - \xi^2)$.

The $I_1(R)$, $I_2(R)$ etc. are obtained from above by replacing r by $R(y)$.

If $f(x)$ and $g(x)$, which are proportional to $S'(x)$, are given as polynomials we proceed with the integration as given below.

If, however, the value of $S'(x)$, which is assumed to be continuous, is known for at least $(n+1)$ values of x , say

x_0, x_1, \dots, x_n , the simplest and most often used process consists in selecting an approximate function $y_n(x)$ which takes on the same values as does $S'(x)$ for each of those $(n+1)$ values of x . Here again the choice of polynomials, called the collocation polynomials, is convenient. For, whereas in the general case there may be no function, or there may be several, the existence and uniqueness theorem states that there is one and only one polynomial of degree n or less which takes on the prescribed values at each of the $(n+1)$ points. The basic interpolation formula was given by Lagrange which expresses the approximate polynomial in terms of only the ordinates given. It is, however, often convenient to use Newton's interpolation polynomial with divided differences or Aitken's iterated interpolation polynomials. These latter formulas are especially suitable for the detection and propagation of error at each stage.

For details reference (Hildebrand, 1956) may be consulted. When the values as well as the derivatives upto a certain order of a function are given at specified arguments, we can use Hermite's interpolation polynomials (also called osculating polynomials) to approximate the given meridian curve.

We, therefore, write

$$S'(y-\xi^2) = S'\{(y+2\beta r) - (\xi^2 + 2\beta r)\} = \sum_{n=0}^N A_n(y, \beta r) (\xi^2 + 2\beta r)^n \quad (2.2.30)$$

Substituting this or its derivative in the expressions (2.2.29) it is readily seen that all the integrals of $I_1(r)$, $I_2(r)$, $\bar{I}_1(r)$ and $\bar{I}_2(r)$ reduce to the following form:

$$T_{p/2}(r) = \int_0^{y^{1/2}} (\xi^2 + 2\beta r)^{p/2} d\xi, \quad p = -1, 0, 1, 2, \dots, N \quad (2.2.31)$$

The recurrence formula for the $T_{p/2}$ - integrals is easily established as

$$T_{p/2}(r) = \frac{y^{1/2}(y+2\beta r)^{p/2}}{p+1} + \frac{2\beta r p}{p+1} T_{\frac{p-2}{2}} \quad (2.2.32)$$

and since

$$T_{-1/2}(r) = \int_0^{y^{1/2}} (\xi^2 + 2\beta r)^{-1/2} d\xi = \ln \frac{y^{1/2} + (y+2\beta r)^{1/2}}{(2\beta r)^{1/2}} \quad (2.2.32)$$

all the integrals of $I_1(r)$, $I_2(r)$, $\bar{I}_1(r)$ and $\bar{I}_2(r)$ can be written in closed form.

The integrals of $\bar{I}_3(r)$ will be of the form

$$Q_{p/2} = \int_0^{y^{1/2}} \xi^3 (\xi^2 + 2\beta r)^{p/2} d\xi \quad (2.2.34)$$

which is readily integrable as it can be reduced to a standard form.

$$Q_{p/2} = \frac{(p+2)y - 4\beta r}{(p+2)(p+4)} (y + 2\beta r)^{\frac{p}{2} + 1} + \frac{2(2\beta r)^{\frac{p}{2} + 2}}{(p+2)(p+4)} \quad (2.2.35)$$

The \bar{F} -function of Eq. (2.2.23) can, therefore be determined in all cases where the body is smooth, in closed form.

The \bar{F} -curve gives immediately a rough description of the flow pattern since it shows whether the characteristics are converging in compression ($\partial\bar{F}/\partial y > 0$) then a shock will appear or diverging in expansion ($\partial\bar{F}/\partial y < 0$). The method of area balancing given by Whitham (1952) can be used to build up the details of the flow pattern.

The Pressure Signature

From Bernoulli's equation, which is approximately true since the small entropy changes at a shock contribute a term of smaller order,

$$\frac{\Delta p}{p_0} = \left[\left\{ 1 + \frac{\gamma-1}{2} M^2 \left(1 - \frac{q^2}{u^2} \right) \right\}^{\frac{\gamma}{\gamma-1}} - 1 \right] \quad (2.2.36)$$

where Δp is the pressure in excess of the undisturbed pressure.

Now

$$\frac{\Delta p}{p_0} = \frac{(2\beta)^{1/4} \gamma r^{-3/4}}{(1+\gamma)^{1/2}} \left\{ \int_0^{y_0} F(y) dy \right\}^{1/2} (1 - 2 \alpha \beta \cos \theta) \quad (2.2.39)$$

where y_0 is the first zero of $F(y)$, the Whitham function for far-field points. In between the shocks equation (2.2.38) holds. The two integrals of Eq. (2.2.38) may be evaluated in closed form using the T-integrals of Eqs. (2.2.32) and (2.2.33).

Examples

In order to compare the near-field \bar{F} -curve with the far-field Whitham function, we have calculated these functions and the pressure signatures for two examples of body of revolution.

(a) The shape of the first body is given by

$$\begin{aligned} R(x) &= 0.1 (x - x^2), \quad 0 \leq x \leq 1 \\ &= 0, \quad x > 1 \end{aligned} \quad (2.2.40)$$

The Whitham F-function is easily calculated analytically and is given by

$$F(y) = 0.02 [(1 - 6y + 6y^2) y^{1/2} + 2(1 - 2y)y^{3/2} + 1.2 y^{5/2}] \quad (2.2.41)$$

The \bar{F} -function, as given by Eq. (2.2.23) has been expressed in terms of the I_1 , I_2 and I_3 integrals which are in turn expressible by means of the T and Q integrals of Eqs. (2.2.32) and (2.2.34). For this example, if we put

$$a_r = y + 2\beta r \quad \text{and} \quad a_R = y + 2\beta R(y) \quad (2.2.42)$$

$$\begin{aligned} \frac{q^2}{U^2} &= (1 + \varphi_{ox} + \alpha \varphi_{1x} \cos \theta)^2 + (\alpha \cos \theta + \varphi_{or} + \varphi_{ir} \alpha \cos \theta)^2 \\ &\quad + (\alpha \sin \theta + \frac{1}{r} \varphi_1 \alpha \sin \theta)^2 \\ &= 1 + 2(\varphi_{ox} + \alpha \varphi_{1x} \cos \theta + \alpha \varphi_{or} \cos \theta) + \text{higher order terms} \end{aligned}$$

and

$$1 - \frac{q^2}{U^2} \approx -2 [\varphi_{ox} + \alpha \varphi_{1x} \cos \theta + \alpha \varphi_{or} \cos \theta]$$

neglecting higher order terms.

Hence, within the order of accuracy employed in the first-order theory equation (2.2.36) may be approximated by

$$\frac{\Delta p}{p_o} = -\gamma M^2 [\varphi_{ox} + (\varphi_{1x} + \varphi_{or}) \alpha \cos \theta] \quad (2.2.37)$$

Substituting the values of the derivatives of φ_o and φ_1 from Eq (2.2.9) and making use of (2.2.12) and (2.2.22), Eq. (2.2.37) may be rewritten as

$$\frac{\Delta p}{p_o} = \frac{\gamma M^2}{\pi} \left[\int_0^y \frac{S''(y-\xi^2)}{(\xi^2 + 2\beta r)^{1/2}} d\xi - \frac{3\alpha \cos \theta}{\beta r} \int_0^y \frac{(\xi^2 + \beta r) S''(y-\xi^2)}{(\xi^2 + 2\beta r)^{1/2}} d\xi \right] \quad (2.2.38)$$

Since the points of a front shock are "effectively at large distances", Whitham's approximate treatment (1952) is valid on the shock and we reproduce his result with minor alteration for the inclined body. Hence for the front shock, when r is large

For the near field, if we put

$$A_r = 1 - a_r, \quad A_R = 1 - a_R \quad (2.2.47)$$

where a_r and a_R are given by eq. (2.2.42) the analytical expression for the integrals required for the calculation of the \bar{F} -curve are as follows,

$$I_1(r) = 0.01 [A_r(15A_r^3 - 6)T_{1/2}(r) + (60A_r^3 - 6)T_{3/2}(r) + 90A_r^2T_{5/2}(r) + 60A_rT_{7/2}(r) + 15T_{9/2}(r)], \quad (2.2.47a)$$

$$I_2(r) = 0.01 [3A_r^2(1 - A_r^3)T_{-1/2}(r) + 3A_r(2 - 5A_r^3)T_{1/2}(r) + 3(1 - 10A_r^2)T_{3/2}(r) - 30A_r^2T_{5/2}(r) - 15A_rT_{7/2}(r) - 3T_{9/2}(r)] \quad (2.2.47b)$$

$$I_3(r) = 0.01 [A_r(15A_r^3 - 6)Q_{1/2}(r) + (60A_r^3 - 6)Q_{3/2}(r) + 90A_r^2Q_{5/2}(r) + 60A_rQ_{7/2}(r) + 15Q_{9/2}(r)] \quad (2.2.47c)$$

Again the values of $I_1\{R(y)\}$, $I_2\{R(y)\}$ and $I_3\{R(y)\}$ are obtained from (2.2.47) by replacing r by $R(y)$.

The pressure signature in between the shocks can be expressed in terms of the known integrals given above yielding

$$I_1(r) = 0.01 [(1 - 6a_r + 6a_r^2)T_{1/2}(r) + (6 - 12a_r)T_{3/2}(r) + 6T_{5/2}(r)], \quad (2.2.43a)$$

$$I_2(r) = 0.01 [(a_r - 3a_r^2 + 2a_r^3)T_{-1/2}(r) - (1 - 6a_r + 6a_r^2)T_{1/2}(r) - (3 - 6a_r)T_{3/2}(r) - 2T_{5/2}(r)], \quad (2.2.43b)$$

$$I_3(r) = 0.01 [(1 - 6a_r + 6a_r^2)Q_{1/2}(r) + 6(1 - a_r)Q_{3/2}(r) + 6Q_{5/2}(r)] \quad (2.2.43c)$$

The $I_1\{R(y)\}$, $I_2\{R(y)\}$ and $I_3\{R(y)\}$ are obtained from (2.2.43) by replacing r by $R(y)$.

The pressure signature in between the shocks is given by

$$\frac{\Delta p}{p_0} = 0.02 \gamma M^2 \{ [1 + (3\beta) \alpha \cos \theta] \{ (1 - 6a_r + 6a_r^2) T_{-1/2}(r) + (6 - 12a_r)T_{1/2}(r) + 6T_{3/2}(r) \} - \frac{3}{r} \alpha \cos \theta I_1(r) \} \quad (2.2.44)$$

For the front shock the jump in pressure can be calculated from eq. (2.2.39).

(b) The shape of the second body considered is given by

$$R(x) = 0.1 [1 - (1-x)^3], \quad 0 \leq x \leq 1 \quad (2.2.45)$$

$$= 0.1, \quad x > 1$$

The Whitham F-function for the far-field points is given by

$$F(y) = [0.3(1-y)^4 - 0.12(1-y)]y^{1/2} + [0.4(1-y)^3 - 0.04]y^{3/2} + 0.36(1-y)^2y^{5/2} + 0.171(1-y)y^{7/2} + \frac{1}{30}y^{9/2} \quad (2.2.46)$$

The pressure signature in between the shocks is given by

$$\begin{aligned} \frac{\Delta p}{p_0} = 0.02 \gamma M^2 & \left[\{ 1 + (3\beta) \alpha \cos \theta \} \{ (15a_r^4 - 60a_r^3 + 90a_r^2 - 54a_r + 9) T_{-1/2}(r) \right. \\ & - (60a_r^3 - 180a_r^2 + 180a_r + 54) T_{1/2}(r) \\ & + (90a_r^2 - 180a_r + 90) T_{3/2}(r) + 60(1-a_r) T_{5/2}(r) \} \\ & \left. - \frac{3}{r} \alpha \cos \theta I_1(r) \right] \end{aligned} \quad (2.2.48)$$

Conclusions

The worked examples, given in the paper, show a significant difference between \bar{F} -function in near and far field points. It is quite clear from the plots that for $\theta = 180^\circ$ at a certain angle of attack, the peak pressures for near fields are higher than those at zero angle of attack. From the plot of \bar{F} -function and also from the pressure plots, it is seen that the expansion is stronger than the case of zero angle of attack. This is even otherwise obvious from the physical point of view. For $\theta = 0^\circ$, the reverse is true, i.e., the pressure peaks become smaller and expansion becomes weaker with angle of attack. Thus we observe that with an angle of attack we have a shock-expansion system, in which the strength varies as the azimuthal angle is varied around the body of revolution.

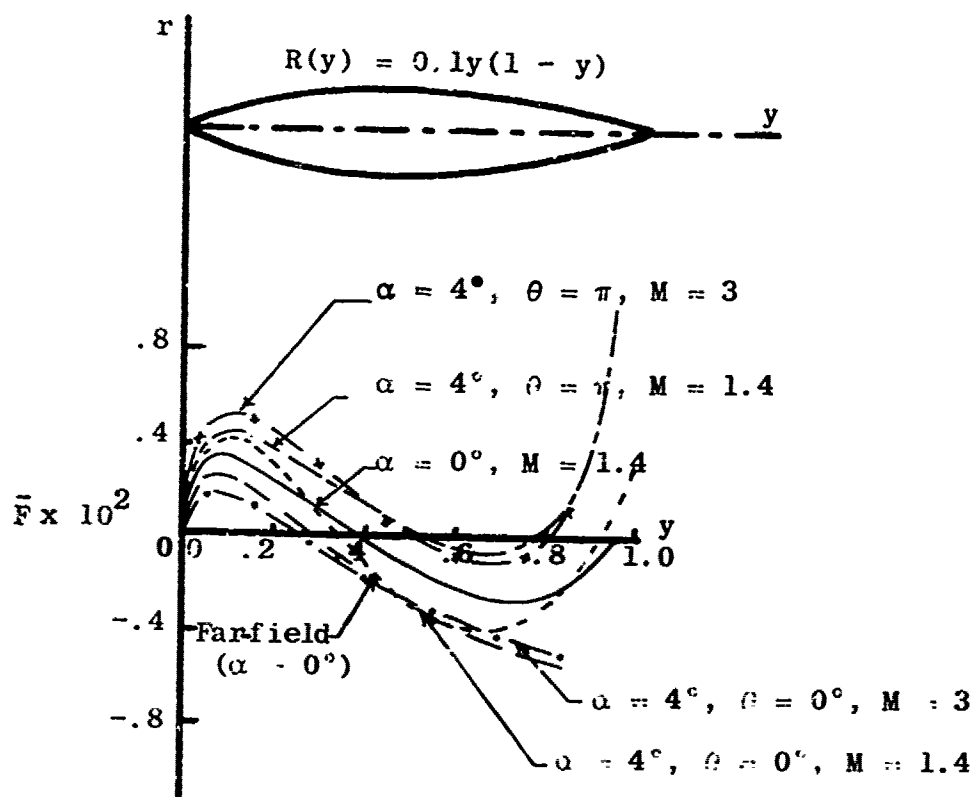


Figure 2.2.3: Plot of F-function at $r = .125$ for various cases for the body $R(y) = 0.1 y(1-y)$.

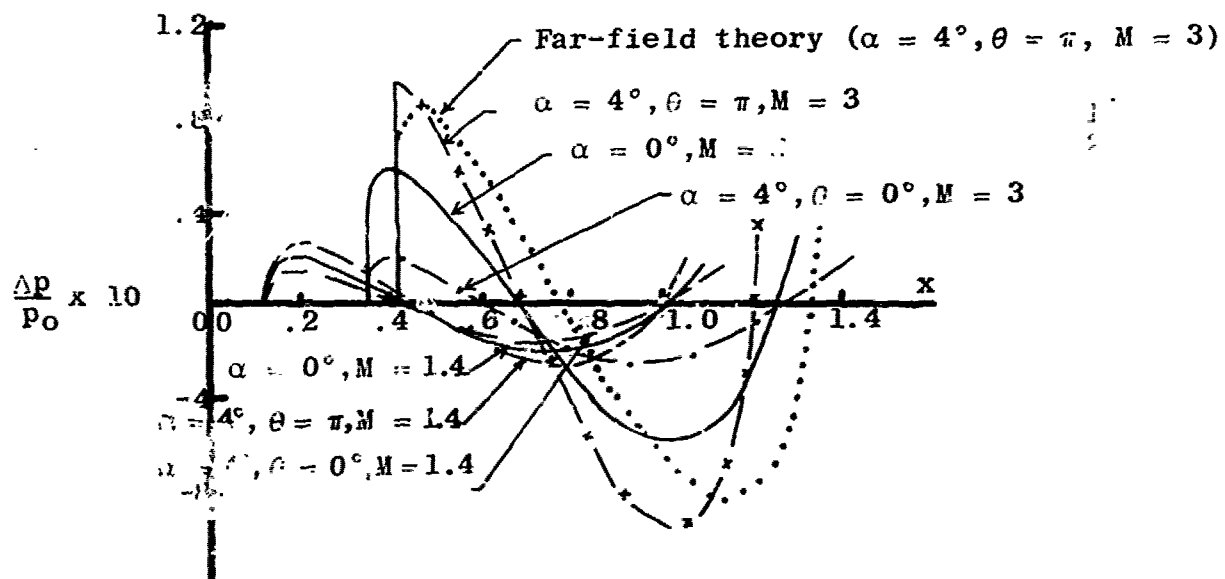


figure 2.2.4: Pressure signature for the body $R(y) = 0.1 y(1-y)$ with and without angle of attack ($r = 0.125$ for all cases).

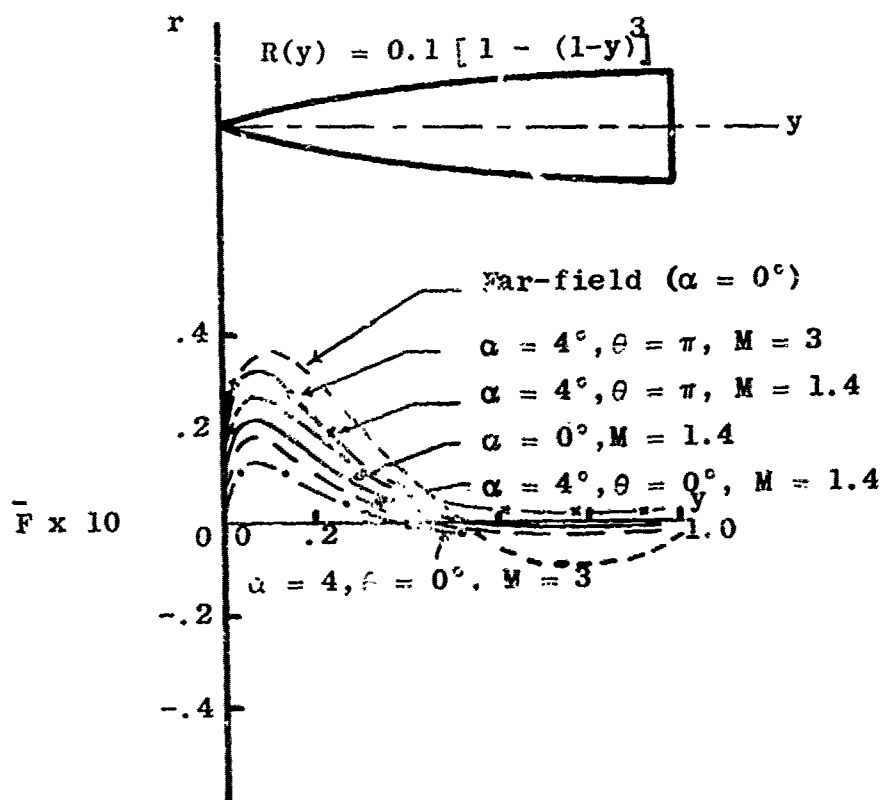


Figure 2.2.5: Plot of F-function at $r = 0.125$ for various cases for the body $R(y) = 0.1[1 - (1-y)^3]$.

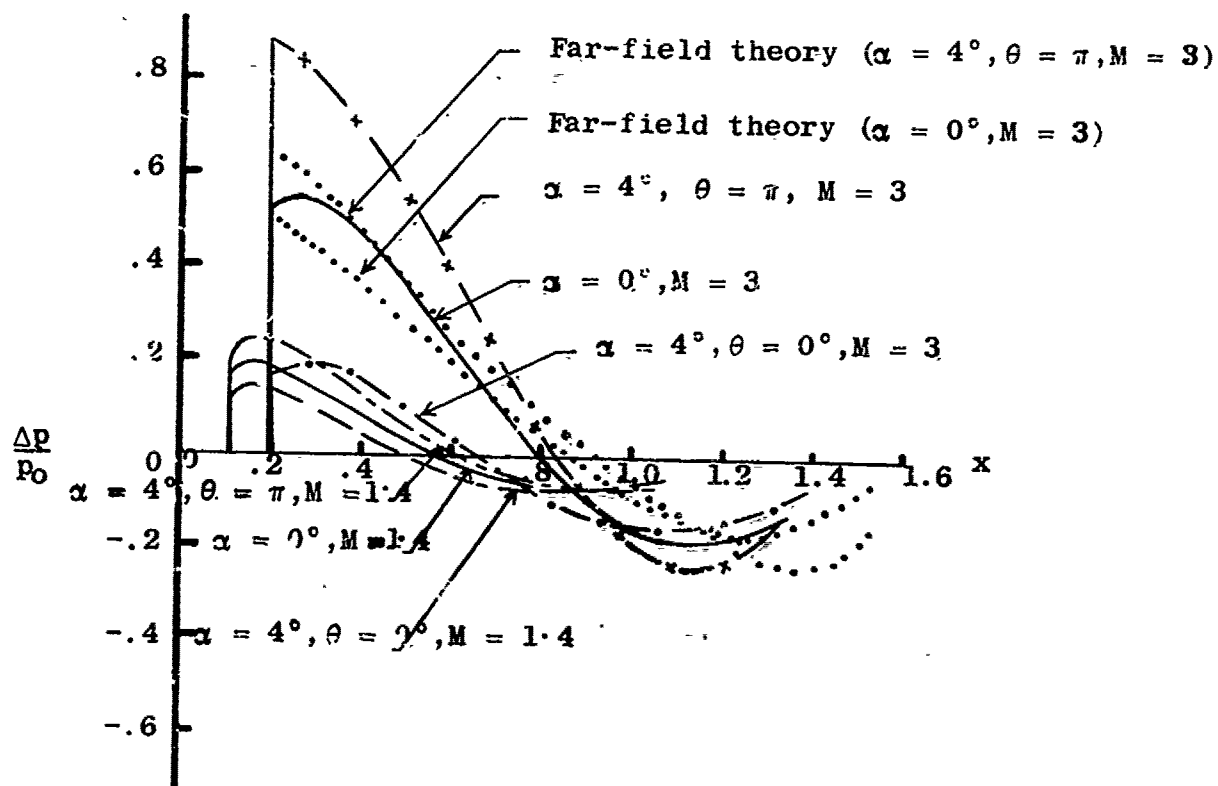


Figure 2.2.6: Pressure signature for the body $R(y) = 0.1[1-(1-y)^3]$ with and without angle of attack ($r = 0.125$ for all cases).

2.2.2 DETERMINATION OF A BODY OF REVOLUTION FOR A SPECIFIED PRESSURE SIGNATURE AT ANY FIELD

Summary

Design of bodies of revolution to produce specified sonic-boom signatures at a given Mach number and lateral spacing from the body uses the far-field theory of Whitham and a procedure has been put forward by Barger (1968) for calculating the shape of the bodies of revolution. Since the above theory does not strictly apply to near-field region, the present work gives a mathematical procedure for determining the bodies of revolution for specified signatures at any field. However, it should be pointed out here that the near- and far-field theorems merge at a certain spacing from the body and beyond this field the far-field theory due to Barger could be used for its mathematical simplification.

Introduction

The Whitham Theory (Whitham, 1952) has been shown to predict accurately far-field signatures produced by a body of revolution. This theory, however, is not very accurate in the near and mid-field points and Sec. 2.2.1 points out the limitations and applicability of Whitham's far-field theory. The far-field theory applicable to the inverse problem for determining the shape of a body of revolution that will produce a specified pressure signature at a given Mach number and certain field away from the body, has been given by Barger (1968). This theory does not strictly apply to near- and mid-field points. The present work employs near- and mid-field theory in order to determine a body of revolution for a specified, physically obtainable pressure signature at the near-field region. Although variations in the shape of a generating body do not normally prevent its signature from developing into the well-known N-shaped wave at large distances, there are some signatures that do not attain the classical N-wave form in the far-field. One such example is given in the reference (Barger, 1968) where the specified near-field pressure signature has a form with its positive and negative parts separated by a section of zero overpressure. Moreover, even if the signature does approach an N-wave, it may develop so gradually that it does not attain its final asymptotic form within the distance corresponding to objectionable overpressures (McLean, 1965), or even if N-wave is formed at the given distance the overpressures are of less magnitude than annoying levels.

There is a need for analytical methods that are capable of accurately predicting the near flow field pressures about arbitrary aircraft configurations for design optimizations in connection with sonic boom as well as the performance of the vehicle (Hunton, 1968). Near-field pressure signatures are also of interest in connection with certain sonic-boom studies such as wind-tunnel investigations and signature measurements using a probe aircraft. Available theories are either too cumbersome mathematically for ease of handling on the computer (e.g., method of characteristics) or are limited in range of application (e.g., Whitham, 1952) because of some mathematical simplification such as the linear theory concept. As a result, problems of analysis do occur in the flow regions very near the aircraft in connection with the design and arrangement of configuration components. Various wing-body combinations have to be examined to come up with various desired configurations. Whitham's theory is easily applied to the bodies of revolution but can not be applied to wings to determine the flow fields at the near-field points. For these fields a wing can not be replaced by an equivalent body of revolution and thus new prediction techniques wherein a wing is represented by some sort of spatial distribution of singularities over the entire wing surface, have to be developed. This phase of the sonic boom research is now under progress. Thus the present work is a preliminary study towards the overall optimization of the aircraft in connection with sonic boom.

The purpose of the present paper is to describe a procedure for designing bodies of revolution corresponding to specified pressure signatures at any field.

Formulation of the Problem

Let the steady stream have velocity U in the x -direction, and at a general point (x, r) let the velocity be $(U + Uu, Uv)$. Assuming the flow to be irrotational the perturbation velocities u and v may be deduced from a potential ϕ which, on the linearized axisymmetric theory satisfies the equation

$$\phi_{rr} + \frac{1}{r} \phi_r - \beta^2 \phi_{xx} = 0 \quad (2.2.49)$$

where $\beta^2 = (M^2 - 1)$ and suffixes denote partial differentiation. The solution of Eq. (2.2.49) which represents a disturbance propagated downstream from a body is

$$\phi = - \int_0^{x-\beta r} \frac{f(t) dt}{\{(x-t)^2 - \beta^2 r^2\}^{1/2}} \quad (2.2.50)$$

giving

$$u = - \int_0^{x-\beta r} \frac{f'(t) dt}{\{(x-t)^2 - \beta^2 r^2\}^{1/2}}, \quad (2.2.51)$$

$$v = \frac{1}{r} \int_0^{x-\beta r} \frac{(x-t) f'(t) dt}{\{(x-t)^2 - \beta^2 r^2\}^{1/2}} \quad (2.2.52)$$

The downstream approximate characteristics of the equation are $x - \beta r = \text{constant}$. We now replace $x - \beta r$ by $y(x, r)$, a better approximation to the exact characteristic. Carrying out the modification, u and v become

$$u = - \int_0^y \frac{f'(t) dt}{[(y-t)(y-t+2\beta r)]^{1/2}}, \quad (2.2.53)$$

$$v = \frac{1}{r} \int_0^y \frac{(y-t+\beta r)f'(t) dt}{[(y-t)(y-t+2\beta r)]^{1/2}} \quad (2.2.54)$$

y is now determined from the condition that $y(x,r) = \text{constant}$ is a characteristic curve, that is, along it $dx/dr = \cot(\mu+\theta)$, where μ is the local Mach angle and θ is the local direction of flow. Proceeding as detailed in Whitham's paper (Whitham, 1952) and assuming $\beta r/y \gg 1$, u, v and the equation of the characteristic are given by

$$u = - \frac{F(y)}{(2\beta)^{1/2}} r^{-1/2}; \quad v = \beta u, \quad (2.2.55)$$

$$x = \beta r - k F(y) r^{1/2} + y, \quad (2.2.56)$$

where

$$F(y) = \int_0^y \frac{f'(t) dt}{(y-t)^{1/2}} \quad (2.2.57)$$

and

$$k = 2^{-1/2} (\gamma+1) M^4 \beta^{-3/2} \quad (2.2.58)$$

From Bernoulli's equation, which is approximately true since

the small entropy changes at a shock contribute a term of smaller order, we have by neglecting terms $O(u^2 + v^2)$,

$$\frac{\Delta p}{p_0} = -\gamma M^2 u \quad (2.2.59)$$

where $\Delta p = p - p_0$ is the pressure in excess of the undisturbed pressure p_0 .

Then the problem is to solve the singular integral equation (2.2.53) when $u(y)$ is given by (2.2.59).

To Find a Body of Revolution for a Given Near- or Mid-Field Pressure Signature

Solution of the Integral Equation

Method 1 - Analytical - Numerical Method:

The integral equation now to be solved is

$$-u(y) = \int_0^y \frac{f'(t) dt}{(y-t+2\beta r)^{1/2} (y-t)^{1/2}} \quad (2.2.60)$$

where $u(y)$ is known from Eq. (2.2.59) and $f'(y)$ is the unknown function.

Putting $\psi(t) = -f'(t)$ for convenience, Eq. (2.2.60) may be rewritten as

$$u(y) = \int_0^y K(y,t) \psi(t) dt, \quad (2.2.61)$$

in which the kernel has the form

$$K(y, t) = \frac{G(y, t)}{(y-t)^{1/2}}, \quad (2.2.62)$$

where

$$G(y, t) = (y-t + 2\beta r)^{-1/2} \quad (2.2.63)$$

is continuous in $T(0 \leq t \leq y \leq b(\text{say}))$.

Precisely as in the case of Abel's equation, of which Eq. (2.2.61) is an immediate generalization, we see that Eq. (2.2.61) cannot have a continuous solution unless $u(y)$ is continuous in $I(0 \leq y \leq b)$ and $u(0) = 0$. We will assume that these conditions are satisfied by $u(y)$.

Multiply Eq. (2.2.61) by $(z-y)^{1/2}$, where

$$0 \leq z \leq b,$$

and integrate the resulting equation with respect to y from 0 to z , obtaining

$$\int_0^z \frac{u(y) dy}{(z-y)^{1/2}} = \int_0^z \frac{1}{(z-y)^{1/2}} \int_0^y \frac{G(y, t)}{(y-t)^{1/2}} \psi(t) dt dy. \quad (2.2.64)$$

The right-hand side of this formula reduces by Dirichlet's extended formula (Tricomi, 1957) to

$$\int_0^z \psi(t) \int_t^z \frac{G(y, t)}{(z-y)^{1/2} (y-t)^{1/2}} dy dt.$$

If we then write

$$F(z) = \int_0^z \frac{u(y)}{(z-y)^{1/2}} dy, \quad (2.2.65a)$$

$$L(x, t) = \int_t^z \frac{G(y, t)}{(z-y)^{1/2} (y-t)^{1/2}} dy \quad (z > t) \quad (2.2.65b)$$

equation (2.2.64) takes the form

$$F(z) = \int_0^z L(z, t) \psi(t) dt \quad (2.2.66)$$

We will now show that the kernel L of this equation is continuous in T , except possibly on the line $z=t$ where it is not yet defined. For this purpose introduce ξ as the variable of integration in place of t by means of the formula

$$\xi = \frac{y-t}{z-t}. \quad (2.2.67)$$

We thus get when $z > t$

$$L(z, t) = \int_0^1 \frac{G[(z-t)\xi+t, t]}{(1-\xi)^{1/2} \xi^{1/2}} d\xi. \quad (2.2.68)$$

Since this integral remains convergent when we replace G by the upper limit of its absolute value, it follows that it is uniformly convergent in T , and since G is continuous, L is also continuous wherever it is defined.

In order next to see whether L approaches a limit as the point (z, t) approaches a point (c, c) on the hypotenuse of T , we apply the mean value theorem for integrals to the original

definition of L given in Eq. (2.2.65b), getting

$$L(z, t) = G(x, t) \int_0^z \frac{dy}{(z-y)^{1/2} (y-t)^{1/2}} = \frac{\pi}{\sin \pi/2} G(s, t), (t < s < z). \quad (2.2.69)$$

Consequently

$$\lim_{\substack{z \rightarrow c \\ t \rightarrow c}} L(z, t) = \pi G(c, c) = \frac{\pi}{(2\beta r)^{1/2}} \quad (2.2.70)$$

from equation (2.2.63).

We see then that L is continuous throughout T , and that if we have $G(y, y) \neq 0$ at any point of I , it follows that $L(y, y) \neq 0$ in I .

In order that the equation (2.2.63) be a Volterra integral equation of the first kind with finite kernel, G should be such that $L(z, t)$ have a partial derivative with respect to z finite in $D[0 \leq z \leq b, 0 \leq t \leq b]$ and whose discontinuities, if any, are regularly distributed.

Let

$$G_1(z, t) = \frac{\partial G}{\partial z} = -\frac{1}{2} (z-t + 2\beta r)^{-3/2} \quad (2.2.71)$$

which is obviously continuous in T . If we now differentiate Eq. (2.2.68) with respect to z under the integral sign, we get

$$\int_0^1 \frac{\xi}{1-\xi}^{1/2} G_1[(z-t) \xi + t, t] d\xi. \quad (2.2.72)$$

Since this integral is obviously uniformly convergent, we see, by the ordinary test for differentiating an infinite integral under the sign of integration, that

$$L_1(z, t) = \frac{\partial L}{\partial z} = \int_0^1 \left(\frac{\xi}{1-\xi} \right)^{1/2} G_1[(z-t)\xi + t, t] d\xi,$$

or

$$L_1(z, t) = -\frac{1}{2} \int_0^1 \left(\frac{\xi}{1-\xi} \right)^{1/2} \frac{d\xi}{\{(z-t)\xi + 2\beta r\}^{3/2}}$$

which is valid throughout T.

It can now be shown that the continuous solution of Eq. (2.2.66) satisfies Eq. (2.2.61) and that it is unique (Bocher, 1909).

We shall now reduce equation (2.2.61) to Volterra's integral equation of the second kind which is more readily solved by Picard's method or numerically.

Differentiating Eq. (2.2.66) with respect to z, we have

$$F'(z) = L(z, z) \Psi(z) + \int_0^z L_1(z, t) \Psi(t) dt \quad (2.2.74)$$

But by Eq. (2.2.70)

$$L(z, z) = \frac{\pi}{(2\beta r)^{1/2}} \neq 0 \quad (2.2.75a)$$

It can be easily shown that (Hadamard, 1928)

$$\int_0^y \frac{F(t)}{(y-t)^{3/2}} dt = \int_0^y \frac{F(t) - F(y)}{(y-t)^{3/2}} dt + F(y) \int_0^y \frac{dt}{(y-t)^{3/2}}$$

Using the above formula we get,

$$\begin{aligned} F'(z) &= \frac{\partial}{\partial z} \int_0^z \frac{u(y)}{(z-y)^{1/2}} dy = -\frac{1}{2} \int_0^z \frac{u(y)}{(z-y)^{3/2}} dy \\ &= -\frac{1}{2} \int_0^z \frac{u(y) - u(z)}{(z-y)^{3/2}} dy + \frac{u(z)}{z^{1/2}} \end{aligned} \quad (2.2.75b)$$

Hence Eq. (2.2.74) becomes.

$$F'(z) = \frac{\pi}{(2\beta r)^{1/2}} \Psi(z) + \int_0^z L_1(z, t) \Psi(t) dt \quad (2.2.76)$$

where $F'(z)$, the known function is given by Eq. (2.2.75b) and the kernel $L_1(s, t)$ by Eq. (2.2.73)

The Kernel Function $L_1(z, t)$

$$L_1(z, t) = -\frac{1}{2} \int_0^1 \frac{\xi^{1/2} d\xi}{(1-\xi)^{1/2} \{(z-t)\xi + 2\beta r\}^{3/2}} \quad (2.2.77)$$

Substituting $\xi = \sin^2 \theta$ and simplifying, we have for $z > t$ (see Appendix 2.2.2)

$$L_1(z, t) = \frac{2\beta r}{(z-t)(z-t+2\beta r)^{1/2}} E(\kappa) - \frac{1}{(z-t)(z-t+2\beta r)^{1/2}} K(\kappa) \quad (2.2.78)$$

where

$$\kappa = \left(\frac{z-t}{z-t+2\beta r} \right)^{1/2} \quad (2.2.72)$$

and $K(\kappa)$ and $E(\kappa)$ are complete elliptic integral of the first and the second kind.

It remains to find the value of $L_1(z, t)$ for $z = t$. We have from Eq. (2.2.73)

$$[L_1(z, t)]_{z=t} = - \frac{1}{2} \frac{1}{(2\beta r)^{3/2}} \int_0^1 \left(\frac{\xi}{1-\xi} \right)^{1/2} d\xi = - \frac{\pi}{4(2\beta r)^{3/2}} \quad (2.2.80)$$

Method 2 - Direct Numerical Method of Solution (Collocation Method)

It is, however, possible to solve the integral equation by application of the collocation method without reduction to the second kind.

The integral equation to be solved is

$$\int_0^y \frac{f'(t) dt}{(y-t+2\beta r)^{1/2} (y-t)^{1/2}} = - u(y) \quad (2.2.81)$$

where $u(y)$ is assumed to be a known continuous function in $I(0 \leq y \leq b(\text{say}))$ and $u(0) = 0$.

In the general case we can assume that $f'(t)$ can be expressed in the form

$$f'(t) = \sum_{n=0}^N a_n t^{\frac{n}{2}} \quad (2.2.82)$$

which includes polynomials as special cases. We proceed to determine the unknown coefficients, a_n by introducing expression Eq. (2.2.82) into Eq. (2.2.53), giving

$$\sum_{n=0}^N a_n \int_0^y \frac{t^{\frac{n}{2}} dt}{(y-t+2\beta r)^{1/2} (y-t)^{1/2}} = -u(y). \quad (2.2.83)$$

The following two types of integrals occur in Eq. (2.2.83) according as $n=2m$, an even positive integer or $n=2m+1$, an odd positive integer,

$$I_1(y) = \int_0^y \frac{t^m dt}{(y-t+2\beta r)^{1/2} (y-t)^{1/2}}, \quad (2.2.84a)$$

$$I_2(y) = \int_0^y \frac{t^{\frac{2m+1}{2}} dt}{(y-t+2\beta r)^{1/2} (y-t)^{1/2}}. \quad (2.2.84b)$$

In Appendix 2.2.3, it is shown that

$$I_1(y) = 2[Y^m T_0 - \binom{m}{1} Y^{m-1} T_1 + \dots + (-1)^r \binom{m}{r} Y^{m-r} T_r \dots + (-1)^m T_m] \quad (2.2.85)$$

where

$$T_0 = \ln \left(\frac{y^{1/2} + Y^{1/2}}{(2\beta r)^{1/2}} \right), \quad (2.2.86a)$$

and the recurrence formula for the evaluation of T_m is

$$T_m = \frac{y^{1/2} Y^{\frac{2m-1}{2}}}{2m} + \frac{(2m-1)}{2m} 2\beta r T_{m-1} \quad (2.2.86b)$$

with

$$Y = y + 2\beta r \quad (2.2.86c)$$

and

$$I_2(y) = \frac{2y^{m+1}}{(y+2\beta r)^{1/2}} A_{2m+2} \quad (2.2.87)$$

where

$$A_{2m+2} = \frac{2m(1+k_1^2) A_{2m} - (2m-1)A_{2m-2}}{(2m+1) k_1^2} \quad (2.2.88a)$$

with

$$A_2 = \frac{1}{k_1^2} [K(k_1) - E(k_1)], \quad (2.2.88b)$$

$$A_4 = \frac{1}{3k_1^4} [(2+k_1^2) K(k_1) - 2(1+k_1^2) E(k_1)] \quad (2.2.88c)$$

in which the modulus k_1 is given by

$$k_1^2 = \frac{y}{y+2\beta r}, \quad 0 < k_1^2 < 1 \quad (2.2.88d)$$

and $K(k_1)$ and $E(k_1)$ are complete elliptic integrals of the first and second kind.

The integral equation (2.2.53), then reduces to

$$\sum_{n=0}^N a_n A_n(y) = -u(y) \quad (2.2.89)$$

where $A_N(y)$ are known for all values of y in I . Choosing N suitable values of y , (y_1, y_2, \dots, y_N) for which $u(y)$ is known, we have the system of equations to determine a_n ,

$$a_1 A_1(y_1) + a_2 A_2(y_1) + \dots + a_N A_N(y_1) = -u(y_1),$$

$$a_1 A_1(y_2) + a_2 A_2(y_2) + \dots + a_N A_N(y_2) = -u(y_2),$$

.

$$a_1 A_1(y_N) + a_2 A_2(y_N) + \dots + a_N A_N(y_N) = -u(y_N),$$

which can be written in matrix notation as

$$[A] \{a\} = -\{u\}$$

or

$$\{a\} = -[A]^{-1} \{u\} \quad (2.2.90)$$

where

$[A] = [A_r(y_s)]$: is a $(N \times N)$ square matrix of known elements

$\{u\} = \{u(y_s)\}$: is a $(N \times 1)$ column matrix of known elements

$\{a\} = \{a_r\}$: is a $(N \times 1)$ column matrix of the unknown coefficients.

Hence $f'(y)$ is approximately determined, from which the geometry of the equivalent body of revolution may be found. The use of the above method has been illustrated in the "Numerical Application" later in the section.

Numerical Application

In order to illustrate the methods of solution for obtaining the shape of a body of revolution that will generate a specified signature at a given Mach number and lateral spacing from the body the following example is chosen.

Two of the specified pressure signatures as given by Barger (1968) have been selected - one with a finite rise and the other with a plateau with its peak same as that for the finite rise. The sole reason for selecting these pressure signatures at $M = 1.2$ and $r/l = 4.2$ is that with these conditions, the specified and experimentally measured pressure signatures agree very well with some rounding off of the corners.

These signatures have a stretch of 15.3 cms starting from zero strength at $x - \beta r = 0$ and coming back to zero strength at $x - \beta r = 15.3$ cms. The peaks of the signatures are obtained by joining straight lines rather than rounding them at the peaks (Barger, 1968). This is done only for mathematical convenience. The desired finite rise pressure signature at $r/l = 4.2$ and $M = 1.2$ is given by,

$$\begin{aligned}\frac{\Delta p}{p_o} &= \frac{0.0096}{4} x, \quad 0 \leq x \leq 4 \text{ cms.} \\ &= 0.0096 - \frac{0.0192}{7.5} (x-4), \quad 4 \leq x \leq 11.5 \text{ cms.} \\ &= -0.0096 + \frac{0.0096}{3.8} (x-11.5), \quad 11.5 \leq x \leq 15.3 \text{ cms.}\end{aligned}$$

and the desired plateau pressure signature at $r/l = 4.2$, $M = 1.2$ is given by,

$$\begin{aligned}\frac{\Delta p}{p_o} &= \frac{0.0096}{0.5} x, \quad 0 \leq x \leq 0.5 \text{ cms} \\ &= 0.0096, \quad 0.5 \leq x \leq 4 \text{ cms} \\ &= 0.0096 - \frac{0.0192}{7.5} (x-4), \quad 4 \leq x \leq 11.5 \text{ cms} \\ &= -0.0096 + \frac{0.0096}{3.8} (x-11.5), \quad 11.5 \leq x \leq 15.3 \text{ cms}\end{aligned}$$

These two signatures are plotted in Fig. 2.2.7. Since at these conditions the far-field theory given by Barger (1968) is adequate for determining the shape of the body of revolution, it is of no use to modify this far-field theory at this field $r/l = 4.2$ with $M = 1.2$ or any field away from $r/l = 4.2$. The body obtained by use of the far-field theory does not give any significant difference between the specified pressure signature and pressure signature obtained by use of the near-field theory (Sec. 2.2.1), or in other words, the far-field and near-field merge at $r/l = 4.2$ for this body at the given conditions. So the near-field theory is of use only for fields between $r/l = 0$ and $r/l = 4.2$ at $M = 1.2$. The numerical procedure adopted to illustrate this is as follows:

Barger's procedure is used to determine the shape of the body of revolution by the use of his far-field theory. This

procedure involves the construction of F-function and then the F-function integral is inverted to give the shape of the body of revolution. Then the Whitham's far-field theory (Whitham, 1952) is used to compute the pressure signature of this body at $r/\ell = 0.5$ and also the near-field theory (Sec. 2.2.1) is used to compute the same at $r/\ell = 0.5$. The two pressure signatures are plotted in Figure 2.2.8. It is seen that there is significant difference between the two signatures. This suggests that the far-field theory is not accurate enough in these near-field points. Of course, here the body is approximately 8-10% thick and thus it is expected that thicker bodies (about 20% thick) will give larger errors between the pressure signatures obtained by the use of far-field and near-field theories.

Now the far-field pressure signature at $r/\ell = 0.5$, $M = 1.2$ becomes the specified pressure signature in that field. We can use "method of collocation" or "direct numerical method" to determine the shape of the body of revolution. Since in the near-field points the F-function and pressure signature have no simple relationship as in the case of far-field points, the integral equation (2.2.60) is solved assuming that the characteristics are straight. The body obtained from this procedure is the first approximation and then the near-field theory (Sec. 2.2.1) is used to calculate the pressure signature at the above field $r/\ell = 0.5$ at $M = 1.2$. It is found that this signature and the specified signature do not coincide, thus suggesting that the characteristics are not straight at this field. Although the peaks of the signatures are the same, there is a shift in their

positions. Thus manipulating the starting signature and iterating, it is possible to get back the specified pressure signature at $r/l = 0.5$. After one or two careful iterations, it is possible to determine the body of revolution for the types of specified pressure signature described here.

In the method of collocation $f'(t)$ is assumed to be of the form

$$f'(t) = \sum_{n=1}^N a_n t^{\frac{n}{2}}$$

The choice of N is important, as this determines the size of the matrix $[A]$. When N is about 12, there is loss of accuracy in computation because of the type of matrices occurring here. To get around this difficulty and to use the "method of collocation" more powerfully, the series for $f'(t)$ is assumed to be different in different portions of the pressure signature and collocation is done at fewer points in each portion. The coefficients of the different series are found successively in the calculation procedure. Since we are seeking solutions for smooth bodies, the slopes of the area distribution are matched at the junction points in the calculation of the coefficients of the series.

We know from slender body theory that

$$f'(t) = \frac{S''(\tau)}{2\pi}$$

Two integrations of the series for $f'(t)$ with boundary conditions $S(0) = S'(0) = 0$ for bodies pointed at nose give the

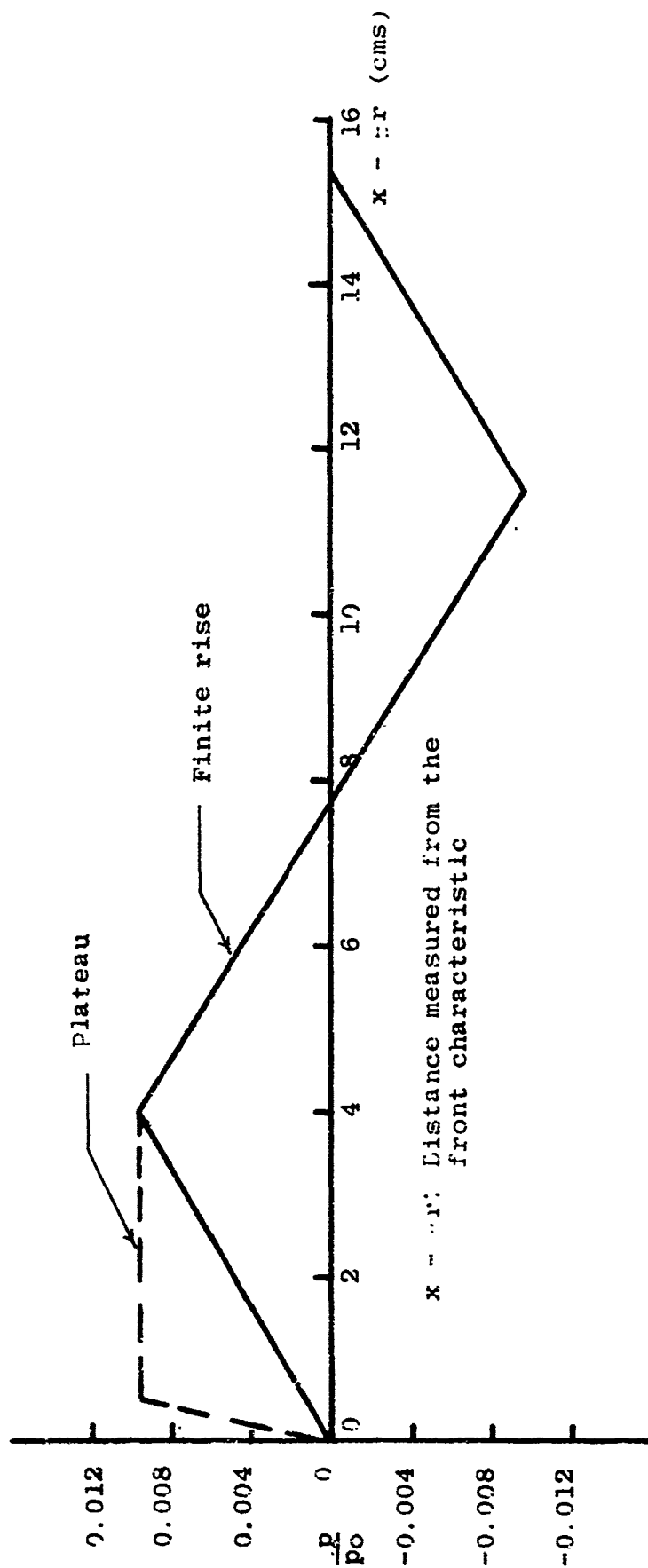


Figure 2.2.7: Specified pressure signatures at $r/l = 4.2$ and $M = 1.2$ (Barger, 1968)

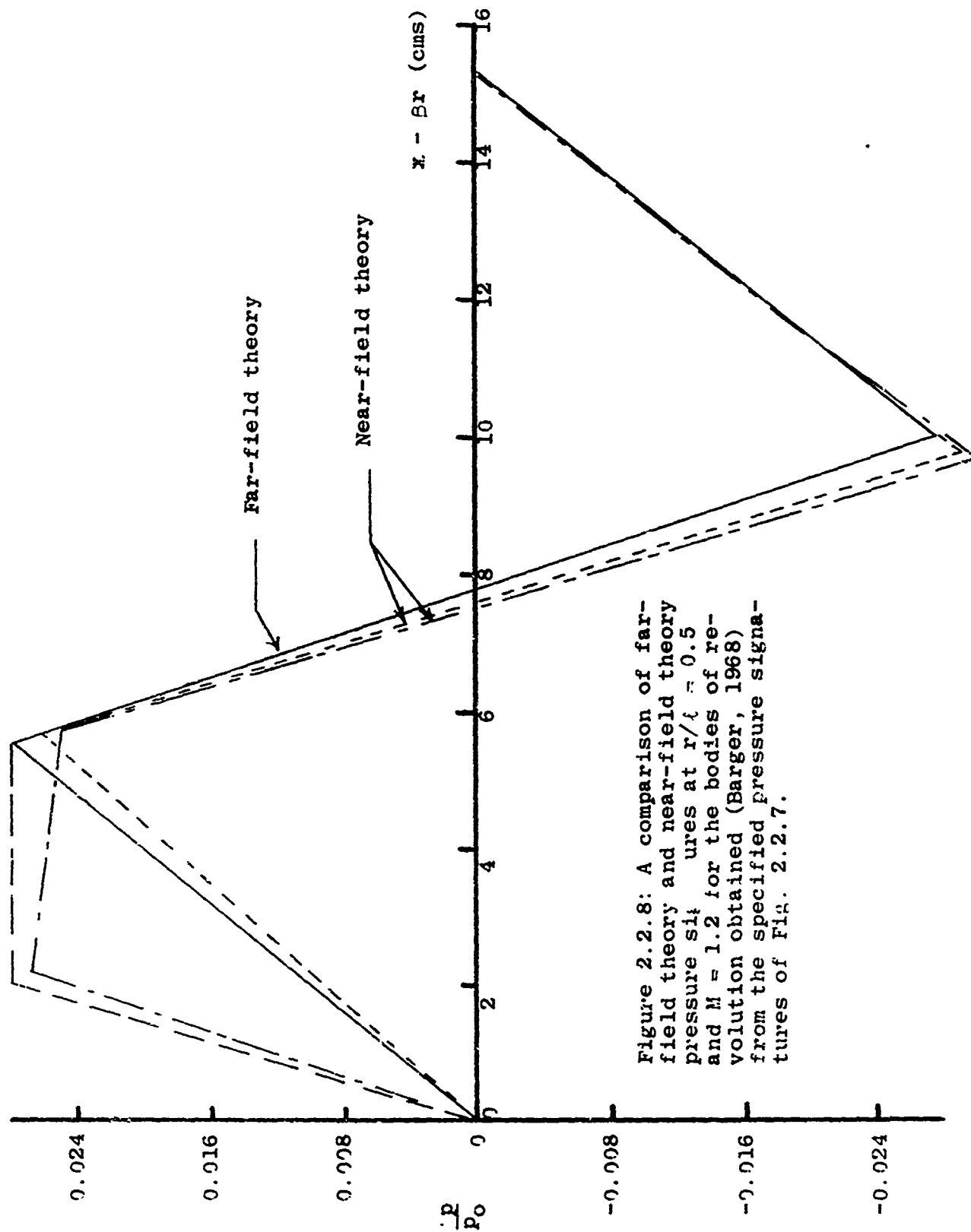


Figure 2.2.8: A comparison of far-field theory and near-field theory pressure signatures at $r/\xi = 0.5$ and $M = 1.2$ for the bodies of revolution obtained (Barger, 1968) from the specified pressure signatures of Fig. 2.2.7.

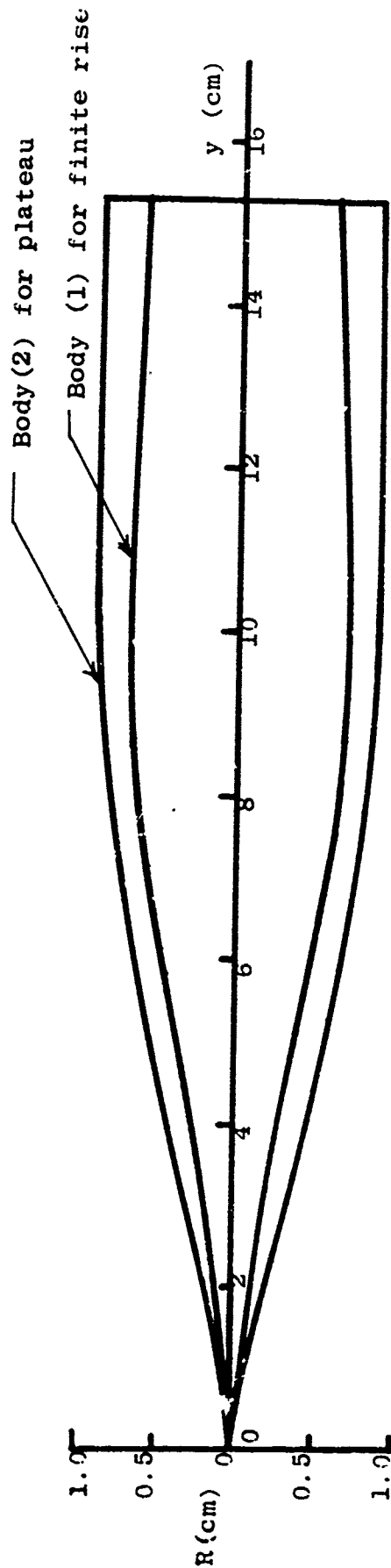


Figure 2.2.9: Profile of bodies of revolution obtained for the specified pressure signatures at $r/l = 0.5$ and $M = 1.2$ by the use of the present near-field theory.

area distribution and thus the distribution of the radius.

Conclusions

The designed bodies of revolution which produce the specified pressure signature at Mach number $M=1.2$ and a spacing $r/l=0.5$ away from the body axis have been plotted in Figure 2.2.9. It is seen from the plots that the body (1) of revolution due to the finite rise pressure signature is much sharper at the nose and thinner than body (2) due to the plateau pressure signature. This observation could otherwise have been made from the physical point of view, but the present analysis gives the exact shapes of the bodies. Although in the present example problem the far-field and near-field theories tend to merge at a field $r/l=4.2$ and $M=1.2$, for thicker bodies these two theories will give the same pressure signatures at distances more than $r/l=4.2$. It might be mentioned that the effect of Mach number on both theories will nearly be the same. In the present example, it has been checked by the author that although the pressure signatures due to the two bodies degenerate to N-waves at large distances, body (1) produces stronger front shock than body (2).

Recommendation

Since the near-field signature shape is sensitive to slight deviations in the shape of the generating body, an extensive study and suitable alterations of the near-field signature will make it possible to reduce sonic boom at far-field points to a desired level.

It also may be pointed out here that the same theory is applicable for a body of revolution at an angle of attack. Although the contribution of the thickness of the body to the pressure

signature is much more significant compared to that due to a small angle of attack, the work done in Secs. 2.2.1 and 2.2.2 may be applied to determine a body of revolution at an angle of attack for a desired pressure signature.

APPENDIX 2.2.1

The Simplification of the Integral Occurring in Equation (2.2.18)

$$L = \int_0^y \ln \left\{ \frac{N(r) - (y-t)^{1/2}}{N(r) + (y-t)^{1/2}} \cdot \frac{N(R) + (y-t)^{1/2}}{N(R) - (y-t)^{1/2}} \right\} f'(t) dt \quad (A.1)$$

where

$$N(r) \equiv N(y, t, 2\beta r) = (y-t + 2\beta r)^{1/2}, \quad (A.2)$$

$$N(R) \equiv N\{y, t, 2\beta R(y)\} = \{y-t + 2\beta R(y)\}^{1/2}$$

The integral (A.1) may be written as

$$L = L_1 - L_2 + L_3 - L_4, \quad (A.3)$$

where

$$L_1 = \int_0^y \ln \{ (y-t + 2\beta r)^{1/2} - (y-t)^{1/2} \} f'(t) dt, \quad (A.4a)$$

$$L_2 = \int_0^y \ln \{ (y-t + 2\beta r)^{1/2} + (y-t)^{1/2} \} f'(t) dt, \quad (A.4b)$$

$$L_3 = \int_0^y \ln \{ \{y-t + 2\beta R(y)\}^{1/2} + (y-t)^{1/2} \} f'(t) dt, \quad (A.4c)$$

$$L_4 = \int_0^y \ln \{ \{y-t + 2\beta R(y)\}^{1/2} - (y-t)^{1/2} \} f'(t) dt \quad (A.4d)$$

Integrating by parts we obtain from Eqs. (A.4)

$$L_1 = f(y) \ln(2\beta r)^{1/2} - f(o) \ln\{(y+2\beta r)^{1/2} - y^{1/2}\} - \frac{1}{2} \int_0^y \frac{f(t) dt}{(y-t)^{1/2} (y-t+2\beta r)^{1/2}} \quad (A.5a)$$

$$L_2 = f(y) \ln(2\beta r)^{1/2} - f(o) \ln\{(y+2\beta r)^{1/2} + y^{1/2}\} + \frac{1}{2} \int_0^y \frac{f(t) dt}{(y-t)^{1/2} (y-t+2\beta r)^{1/2}} \quad (A.5b)$$

$$L_3 = f(y) \ln\{2\beta R(y)\}^{1/2} - f(o) \ln\{[y+2\beta R(y)]^{1/2} + y^{1/2}\} + \frac{1}{2} \int_0^y \frac{f(t) dt}{(y-t)^{1/2} \{y-t+2\beta R(y)\}^{1/2}}, \quad (A.5c)$$

$$L_4 = f(y) \ln\{2\beta R(y)\}^{1/2} - f(o) \ln\{[y+2\beta R(y)]^{1/2} - y^{1/2}\} - \frac{1}{2} \int_0^y \frac{f(t) dt}{(y-t)^{1/2} \{y-t+2\beta R(y)\}^{1/2}}, \quad (A.5d)$$

Combining the expressions of (A.5) and cancelling terms yields

$$L = \ln \left[\frac{\{(y+2\beta r)^{1/2} + y^{1/2}\} \{(y+2\beta R(y))^{1/2} - y^{1/2}\}}{\{(y+2\beta r)^{1/2} - y^{1/2}\} \{(y+2\beta R(y))^{1/2} + y^{1/2}\}} \right] f(o) + \int_0^y \left[\frac{y-t+2\beta R(y)}{\{y-t+2\beta R(y)\}^{1/2} (y-t)^{1/2}} - \frac{y-t+2\beta r}{(y-t+2\beta r)^{1/2} (y-t)^{1/2}} \right] f(t) dt \quad (A.6)$$

Assuming the body to be pointed

$$f(o) = \frac{S'(o)}{2\pi} = R(o) R'(o) = 0,$$

since $R'(0)$ is finite and $R(0) = 0$.

We, therefore, obtain the form given in the text

$$L = \int_0^y \left[\frac{y-t+2\beta R(y)}{(y-t)^{1/2} \{y-t+2\beta R(y)\}} - \frac{y-t+2\beta r}{(y-t)^{1/2} (y-t+2\beta r)^{1/2}} \right] f(t) dt$$

The other integrals of equation (2.2.18) in which the logarithmic terms occur may similarly be treated.

APPENDIX 2.2.2

The kernel function

$$L_1(z, t) = -\frac{1}{2} \int_0^1 \frac{\xi^{1/2} d\xi}{(1-\xi)^{1/2} \{(z-t)\xi + 2\beta r\}^{3/2}} \quad (B.1)$$

Substituting $\xi = \sin^2 \theta$ and simplifying, we have

$$L_1(z, t) = -\frac{1}{(2\beta r)^{1/2}} \int_0^{\pi/2} \frac{d\theta}{(1+n^2 \sin^2 \theta)^{1/2}} \\ + \frac{(2\beta r)^{1/2}}{z-t} \int_0^{\pi/2} \frac{d\theta}{(1+n^2 \sin^2 \theta) (1+n^2 \sin^2 \theta)^{1/2}}, \quad (B.2)$$

where

$$\frac{z-t}{2\beta r} = n^2 > 0 \quad \text{for } z > t,$$

The two integrals of the second member of (B.2) can be reduced to standard forms in complete elliptic integrals of the first and second kind by introducing a variable χ in place of θ by means of the relation

$$\text{sn}^2 \chi = \frac{(1+n^2) \sin^2 \theta}{1+n^2 \sin^2 \theta}, \quad (B.3)$$

which reduces them to the following forms

$$\int_0^{\pi/2} \frac{d\theta}{(1+n^2 \sin^2 \theta)^{1/2}} = \kappa' \int_0^{\chi} d\chi = \kappa' K(\kappa)$$

and

$$\int_0^{\pi/2} \frac{d\theta}{(1+n^2 \sin^2 \theta)(1+n^2 \sin^2 \theta)^{1/2}} = \kappa' \int_0^{K(\kappa)} \frac{dn^2 \chi d\chi}{\chi} = \kappa' E(\kappa)$$

where

$$\kappa = \left(\frac{n^2}{1+n^2} \right)^{1/2} = \left(\frac{z-t}{z-t+2\beta r} \right)^{1/2}, \quad 0 < \kappa < 1,$$

and

$$\kappa' = (1-\kappa^2)^{1/2} = \left(\frac{2\beta r}{z-t+2\beta r} \right)^{1/2}$$

is the complementary modulus.

APPENDIX 2.2.3

1. Evaluation of

$$I_1(y) = \int_0^y \frac{t^m dt}{(y-t+2\beta r)^{1/2} (y-t)^{1/2}}$$

Changing the variable of integration by means of the relation $\xi = (y-t)^{1/2}$, $I_1(y)$ reduces to

$$I_1(y) = 2 \int_0^{y^{1/2}} \frac{(y-\xi^2)^m d\xi}{(\xi^2+2\beta r)^{1/2}}. \quad (C.1)$$

Now since

$$\begin{aligned} (y-\xi^2)^m &= \{Y - (\xi^2+2\beta r)\}^m \\ &= Y^m - \binom{m}{1} Y^{m-1} (\xi^2+2\beta r) + \dots + (-)^r \binom{m}{r} Y^{m-r} (\xi^2+2\beta r)^r \\ &\quad \dots + (-)^m (\xi^2+2\beta r)^m \end{aligned}$$

where

$$Y = y + 2\beta r$$

and, furthermore, since

$$T_m = \int_0^{y^{1/2}} (\xi^2+2\beta r)^{m-\frac{1}{2}} d\xi = \frac{y^{1/2} Y^{\frac{2m-1}{2}}}{2m} + \frac{(2m-1)}{2m} 2\beta r T_{m-1},$$

with

$$T_m = \int_0^{y^{1/2}} \frac{d\xi}{(\xi^2 + 2\beta r)^{1/2}} = \ln \left(\frac{y^{1/2} + y^{1/2}}{(2\beta r)^{1/2}} \right)$$

we have the result given in the text.

2. Evaluation of

$$I_2(y) = \int_0^y \frac{t^{\frac{2m+1}{2}} dt}{(y-t+2\beta r)^{1/2} (y-t)^{1/2}}$$

We change the variable of integration t by substituting $t = y \sin^2 \theta$, yielding

$$I_2(y) = \frac{2y^{m+1}}{(y+2\beta r)^{1/2}} \int_0^{\pi/2} \frac{\sin^{2m+2} \theta d\theta}{(1-k_1^2 \sin^2 \theta)^{1/2}} \quad (C.2)$$

where

$$k_1^2 = \frac{y}{y+2\beta r}, \quad 0 < k_1^2 < 1 \quad \text{for } y \neq 0.$$

Introducing the elliptic function $\text{sn } \chi$ to transform the variable of integration by means of the relation

$$\text{sn } \chi = \sin \theta$$

the integral on the right-hand side of (C.2) may be written as

$$A_{2m+2} = \int_0^{\pi/2} \frac{\sin^{2m+2} \theta d\theta}{(1-k_1^2 \sin^2 \theta)^{1/2}} = \int_0^{K(k_1)} \text{sn}^{2m+1} \chi d\chi \quad (C.3)$$

In reference (Byrd and Friedman, 1954) it is shown that

$$A_{2m+2} = \frac{2m(1+k_1^2) A_{2m} - (2m-1)A_{2m-2}}{(2m+1) k_1^2}, \quad m = 2, 3, 4, \dots$$

and the first two integrals A_2 and A_4 are easily evaluated to give

$$A_2 = \int_0^{K(k_1)} \text{sn}^2 \chi \, d\chi = \frac{1}{k_1^2} [K(k_1) - E(k_1)],$$

$$A_4 = \int_0^{K(k_1)} \text{sn}^4 \chi \, d\chi = \frac{1}{3k_1^4} [(2+k_1^2) K(k_1) - 2(1+k_1^2) E(k_1)],$$

where K and E are complete elliptic integrals of the first and second kind.

The above formulas will enable us to evaluate $I_2(y)$ in closed form.

2.3 SONIC BOOM REDUCTION BY FOCUSED LASER BEAM TECHNIQUES

by Mr. Ronald Kohl

2.3.1 The Problem

If a supersonic aircraft could be made sufficiently long and properly shaped and designed, more favorable ground pressure signatures could be obtained. In particular, if the aircraft's equivalent body of revolution has certain shapes, the over-pressure can be reduced or the shock waves in the signature can be eliminated and replaced with finite rates of pressure rise. The latter modification in a signature of given over-pressure reduces the power in the signature which occurs in the frequencies audible to the human ear (Hilton and Newman, 1966; Zepler and Harel, 1965; Kryter, 1965).

To obtain such pressure signatures, however, the aircraft lengths required for an aircraft of 350,000 lbs, flying at Mach number 2.7, at an altitude of 65,000 feet, range from 500 ft up depending on the effective bodyshape desired (McLean, Carlson, and Hunton, 1966). Still longer lengths are required for the planned SST cruising weight of about 600,000 lb. Aircraft structures of these lengths are considered too long for economical reasons. A means must be found to create airflows similar to those that would occur about the longer aircraft, but which keeps a structural aircraft length near the 300 ft. length considered for the present SST. (See Figure 2.3.1). To deflect the airflow without using structure, energy could be

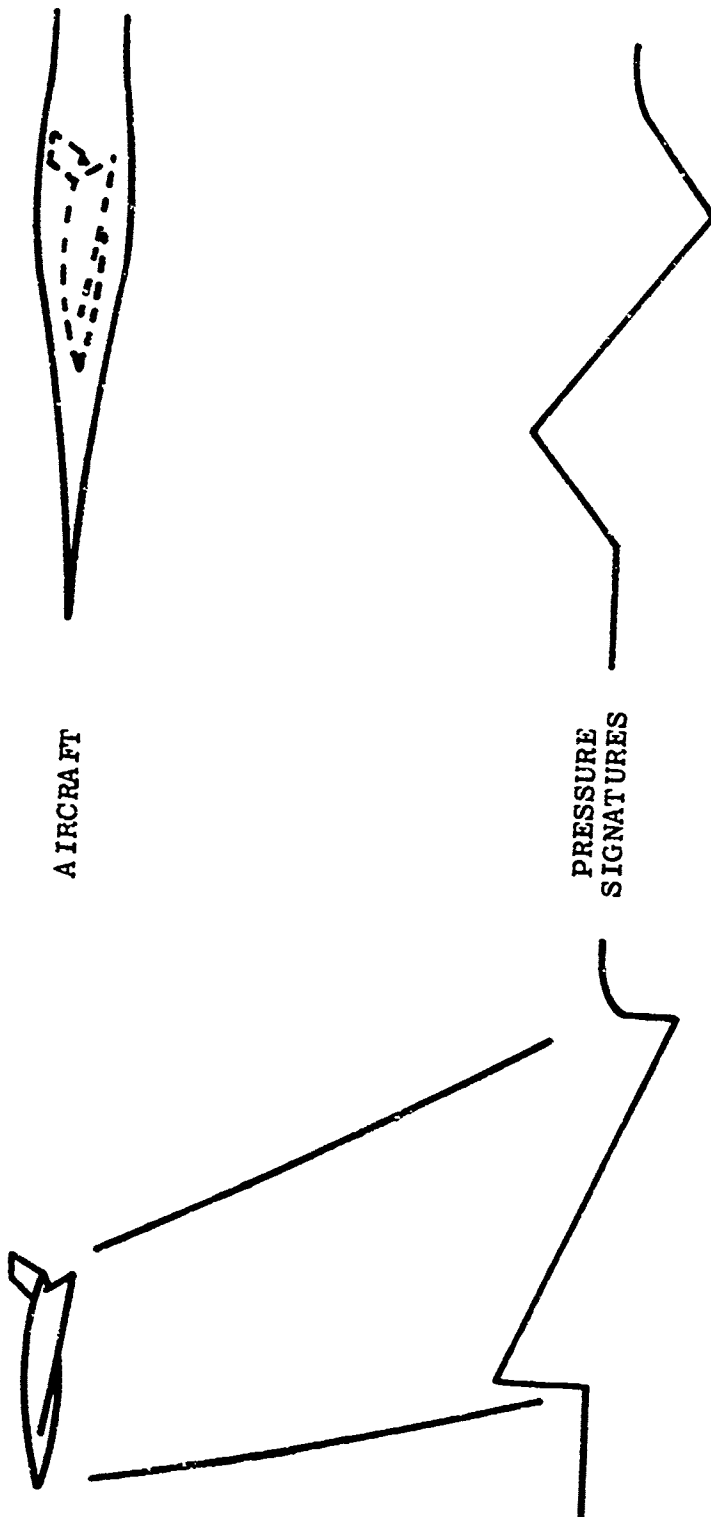


FIGURE 2.3.1. The Problem

introduced into the airflow and here this energy must be introduced at distances the order of 100 ft or more from the aircraft structure. To do this, novel means must be used.

The idea was advanced to use present or future lasers to accomplish this. The feasibility of the use of lasers depends on, among other things, the power required to be introduced into the airflow. Of particular interest is the power required in the region out in front of the aircraft where the front of the pressure signature would be affected and where the introduction of burning fuels may not be feasible.

2.3.2 The Method Used

In the presence of one of these uneconomically long noses of a desired shape, the flow streamtubes take certain forms. The flow outside of a streamtube, including the ground pressure signature, is completely determined by the streamtube. No matter what means are used to produce the streamtube, if the streamtube is produced, the desired ground pressure signature is obtained. The idea here is to produce the streamtube desired by adding heat to the flow inside the streamtube rather than having a nose of the desired shape located inside the streamtube. In this way there is a "phantom" nose present. To find the power requirements, we find the streamtube area developments and the pressures produced on the surfaces of the streamtubes by the uneconomically long nose of a desired shape. The input power required to duplicate the area development and surface pressures of a given streamtube is then found by considering the streamtube as a one dimensional channel and finding the heat addition required to duplicate the surface pressures which exist in the actual flow. For a given nose the calculation is done for several streamtubes of differing initial area to determine the effect on the streamtube power requirement of the initial streamtube size.

To obtain linear finite rates of ground signature pressure rise with a structural nose, application of Whitham's approach (Whitham, 1952) shows the well known axisymmetric area development $S = ax^{5/2}$ is required where x is the axial distance from the nose tip. The constant a is related to the desired rate of ground signature pressure rise dP/dt by

$$a = \frac{16 \sqrt{2\beta_\infty} r}{15M_\infty^2 [\gamma K_r K_a P_\infty U_\infty / (dP/dt) + (\gamma+1) M_\infty^2 r \beta_\infty^{-1}]}$$

where M_∞ , P_∞ and U_∞ are the upstream Mach number, static pressure, and velocity at the altitude of interest r . The quantity β_∞ is $\sqrt{M_\infty^2 - 1}$ and γ is the ratio of the specific heats for air. K_r is the reflection coefficient, the factor by which the magnitude of the pressure in the ground pressure signature is increased over the free stream pressure signature due to the presence of the ground. Here $K_r = 2$ was used. K_a is the correction coefficient of Kane (Kane 1966; Kane, 1967) which is the ratio of the pressure variation at sea level in the U. S. Standard Atmosphere to the pressure variation at sea level in a uniform atmosphere of pressure P_∞ . For an altitude of 60,000 ft. this factor is $K_a = 4.33$. For the purpose of this work the small differences in pressure signature lengths between the uniform and standard atmosphere signatures are ignored. (Hayes and Maefeli, 1968).

To find the streamtube area or radius development with x and the streamtube surface pressures for a given nose, the nose was replaced by flow sources on its axis in the usual slender body - perturbed flow approach. The streamfunction Ψ , when written in the form

$$\Psi / \rho_\infty U_\infty = \frac{1}{2} r^2 + \psi,$$

where ρ_∞ is the upstream density at the altitude of interest and r is the radial distance from the axis, was found to be given by

$$\psi = - \int_0^{\cosh^{-1}(\frac{x}{\beta r})} f(x - \beta r \cosh \sigma) \beta r \cosh \sigma d\sigma$$

where $f(x)$ is the usual axial source distribution in the slender body approach

$$f(x) = \frac{1}{2\pi} \frac{dS}{dx}.$$

The radius of a streamtube, selected upstream where $\psi = 0$, was then traced through the flow using the constancy of ψ . Pressures on the streamtube surface were found through the pressure coefficient

$$C_p = \frac{p - p_\infty}{\frac{1}{2} \rho_\infty U_\infty^2} = -2u - v^2,$$

where the flow velocity in the axial direction is $(1+u)U_\infty$ and in the radial, vU_∞ , with u and v given by the well known relations

$$u = - \int_0^{\cosh^{-1}(\frac{x}{\beta r})} f'(x - \beta r \cosh \sigma) d\sigma$$

$$v = \int_0^{\cosh^{-1}(\frac{x}{\beta r})} f'(x - \beta r \cosh \sigma) \beta \cosh \sigma d\sigma.$$

where $f'(x) = df/dx$. In order to calculate the heat addition required to obtain pressures in the streamtube-channel which match the known pressures at the surface of the streamtube, the inviscid equations of conservation of mass, momentum and energy, the equation of state (perfect gas) and the definition of the stagnation temperature T_0 are combined under the assumption of one dimensional dependence to obtain the power addition per unit axial length

$$\frac{dp}{dx} = \rho_{\infty} U_{\infty} A_{\infty} c_p \frac{dT_o}{dx}$$

where

$$\begin{aligned} \frac{1}{T_o} \frac{dT_o}{dx} &= [1 + (\gamma-1) M^2/2]^{-1} \frac{1}{A} \frac{dA}{dx} \\ &+ \beta^2 \gamma^{-1} M^{-2} [1 + (\gamma-1) M^2/2]^{-1} \frac{1}{p} \frac{dp}{dx} \end{aligned}$$

with $\beta^2 = M^2 - 1$ and M^2 the square of the Mach number. M^2 is found down the channel by applying

$$\begin{aligned} \frac{1}{M^2} \frac{dM^2}{dx} &= - \beta^{-2} [1 + (\gamma-1) M^2/2] (1 + \gamma M^2) \frac{1}{T_o} \frac{dT_o}{dx} \\ &+ 2\beta^{-2} [1 + (\gamma-1) M^2/2] \frac{1}{A} \frac{dA}{dx}. \end{aligned}$$

These expressions can be found in Table 8.2 of (Shapiro, 1953).

The calculation moved down the channel by steps of axial displacement Δx , the approximation to dx , which was chosen to be sufficiently small for the sake of accuracy, but not so small as to take unreasonable computer time. The quantity dA/A was used in the form $2dr/r$ where dr is known from

$$d(\Psi/\rho_{\infty} U_{\infty}) = 0 = r dr + \frac{\partial \Psi}{\partial r} dr + \frac{\partial \Psi}{\partial x} dx,$$

where

$$\frac{\partial \psi}{\partial r} = \int_0^{\cosh^{-1}(\frac{x}{\beta r})} f'(x - \beta r \cosh \sigma) \beta^2 r \cosh^2 \sigma d\sigma$$

$$- \int_0^{\cosh^{-1}(\frac{x}{\beta r})} f(x - \beta r \cosh \sigma) \beta \cosh \sigma d\sigma$$

and

$$\frac{\partial \psi}{\partial x} = - \int_0^{\cosh^{-1}(\frac{x}{\beta r})} f'(x - \beta r \cosh \sigma) \beta r \cosh \sigma d\sigma.$$

The change in streamtube radius Δr with axial displacement Δx from axial position x_1 was found by using Δr from a previous trial (beginning with the final value of Δr from the previous step) to obtain $r_a = r_1 + \Delta r/2$. This value was used with $x_a = x_1 + \Delta x/2$ in $\partial \psi / \partial r$ and $\partial \psi / \partial x$ to obtain a new trial Δr . This process was continued until the relative difference in succeeding trial Δr 's was less than $1:10^6$. The streamtube radius at $x_2 = x_1 + \Delta x$ was then $r_2 = r_1 + \Delta r$. To guard against wandering from the original streamtube in moving down the flow, the difference in the value of the actual and original stream function was monitored. The relative error in streamtube radius was always less than $1:10^3$.

The quantity dp/p is

$$\frac{dp}{p} = (C_p + \frac{2}{\gamma M_\infty^2})^{-1} dC_p.$$

Where the nose first begins to influence the streamtube ΔC_p

is the order of C_p , so $\Delta p/p$, which was always small, was used in the form

$$\frac{\Delta p}{p} = \frac{2(C_{p2} - C_{p1})}{C_{p2} + C_{p1} + 4/\gamma M_\infty^2}.$$

In moving down the streamtube, the numerator was monitored for possible loss of significant figures as C_{p2} approached C_{p1} .

Knowing $\Delta A/A$ and $\Delta p/p$, $\Delta T_o/T_o$ can be determined accurately by knowing M^2 at $x = x_a$. For small Δx , $M_a = (M_1 + M_2)/2$ and M_2 is found by successive trials, beginning with a trial value for M_a (initially M_1 was used), obtaining a trial $\Delta T_o/T_o$ and $\Delta M^2/M^2$ and thus a new value for M_2 and M_a . This was continued until successive trial values of M_a differed by less than $1:10^6$. This approach in obtaining M_a was also used in (Miller and Carlson, 1969).

A program was developed to calculate the desired quantities along the lines given above for phantom noses of area development $S = ax^n$ with $n \geq 2$. All integrands for such noses are finite. The integral evaluations in this program were done with a combination of Simpson's rule and Newton's 3/8 rule with the number of intervals adjusted for accuracy and speed.

To speed up the computer runs on conical noses ($n = 2$) the integrals were done analytically. The results obtained using numeric and analytic integrations always agreed to better than $1:10^3$. All computer runs were done on the IBM 1130 system here at the Institute.

To establish minimum power requirements, noses which produce finite pressure rises in the pressure signature were joined tangentially to the effective body of revolution of an SST so that the body was enclosed within the nose. See Figure 2.3.2. The power required to duplicate the flow caused by the presence of the phantom nose between the phantom nose tip and the SST body tip was then calculated by summing the power requirements per step down the channel until the characteristic from the SST body tip was reached. To duplicate the flow produced by the phantom nose behind the position of the SST body tip characteristic would require cooling the flow to compensate for the compression of the flow impinging on the SST. If no cooling is allowed and we still wish flow behind the SST body tip to have the characteristics of flow over the phantom nose, an even longer phantom nose would be required for a given rate of pressure signature rise. Thus for a given nose shape, the length of nose considered here, the distance from the phantom nose tip to the SST body tip, is a minimum and the power requirements obtained are minimum power requirements.

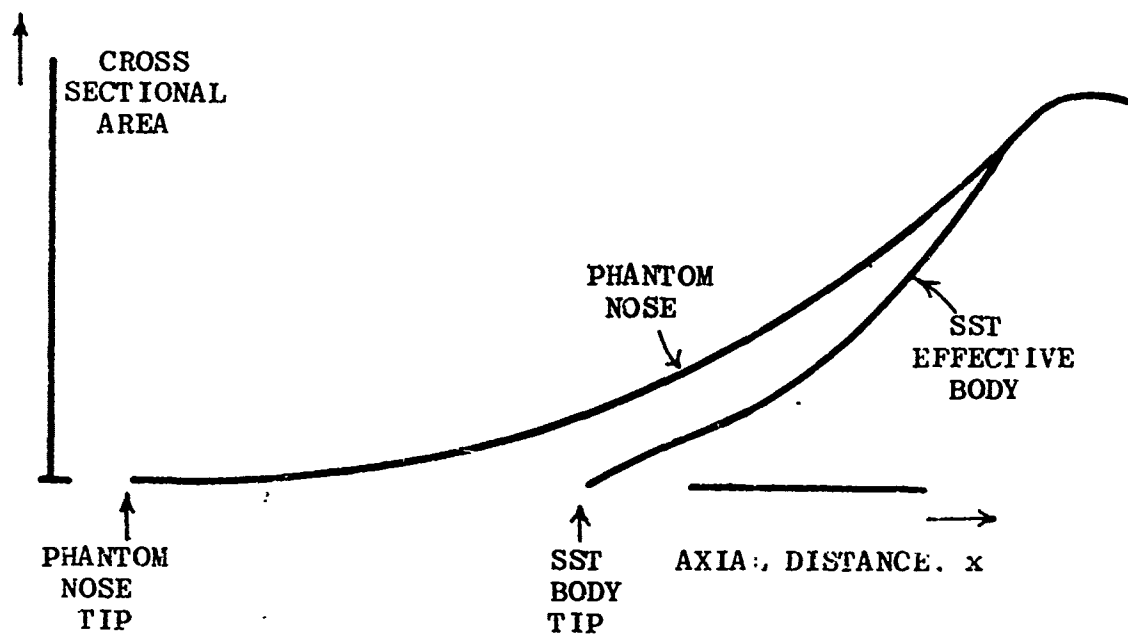


FIGURE 2.3.2. Establishment of minimum power requirements.

2.3.3 Results

Results for a typical case are given in Figures 2.3.3, .4, .5 and .6. In this case a phantom nose which produces a ground pressure rise of 2 lb/ft^2 in 10 msec from an altitude of 60,000 feet at a Mach number of 2.7 is joined to the effective body of a 600,000 lb. SST resulting in a phantom nose length of 249 feet to be duplicated by heat addition. In this example the streamtube of 100 ft^2 initial area is the one considered as shown in Figure 2.3.3. In Figure 2.3.4 the required power input per unit axial length, the required input power distribution, is plotted down the streamtube. Figure 2.3.5 shows the integral of the curve in Figure 2.3.4, or the total power required. Using the energy available from the combustion of a pound of jet kerosene and the SST cruise velocity of 1,780 m/hr, this quantity is given in pounds of fuel per mile of sonic boom abatement system operation. The power required to simulate the presence of the 249 foot nose is the power produced by combusting 43 pounds of fuel per mile or 420 Megawatts. Figure 2.3.6 shows that this result depends only slightly on the streamtube-channel chosen for the cross sectional heat addition. The input power distribution is also practically independent of streamtube area as shown in Figure 2.3.7.

A comparison of the power requirements for various phantom noses is shown in Figure 2.3.8. The power requirements are plotted against the rate of ground signature pressure rise produced by the noses. These rates range from a barely finite rate to a rate where the ground pressure does not reach 2 lbs/ft^2 , the

unmodified, predicted SST maximum overpressure, for 100 msec, which is one fourth the predicted SST pressure signature length. Thus, Figure 2.3.8 indicates that if a barely finite rate of pressure rise can be obtained, beneficial rates of rise can be obtained with an increase in power of the order of 50% or less.

A comparison of power requirements as a function of nose shape was also made to see if relaxing the phantom nose shape from the desirable $S = ax^{5/2}$ shape might bring a helpful reduction in the power requirement. Here a conical nose ($S = ax^2$) and a nose of area development $S = ax^3$, both of the same length and base area as the nose of Figure 2.3.3 are compared to the nose of that figure. A longitudinal cross section of the noses is shown in Figure 2.3.9. The resultant input power distributions are compared in Figure 2.3.10 for an initial streamtube area of 100 square feet. A comparison of the total power required to duplicate the effects of these noses, and noses similarly obtained, is shown in Figure 2.3.11. While the input power distributions are somewhat different, the total power required is practically the same for the various shapes. (One can show that for slender noses of area development $S = ax^n$, the linear rise or $S = ax^{5/2}$ nose shape produces a minimum average pressure rise and a minimum maximum pressure rise in a shockless signature, as well as being the shape which produces a shockless pressure signature at a maximum distance from the nose axis. A shape of $S = ax^n$ with n less than $5/2$ does not produce a shockless signature). The power requirements for the $S = ax^2$ and $S = ax^3$ noses, as with

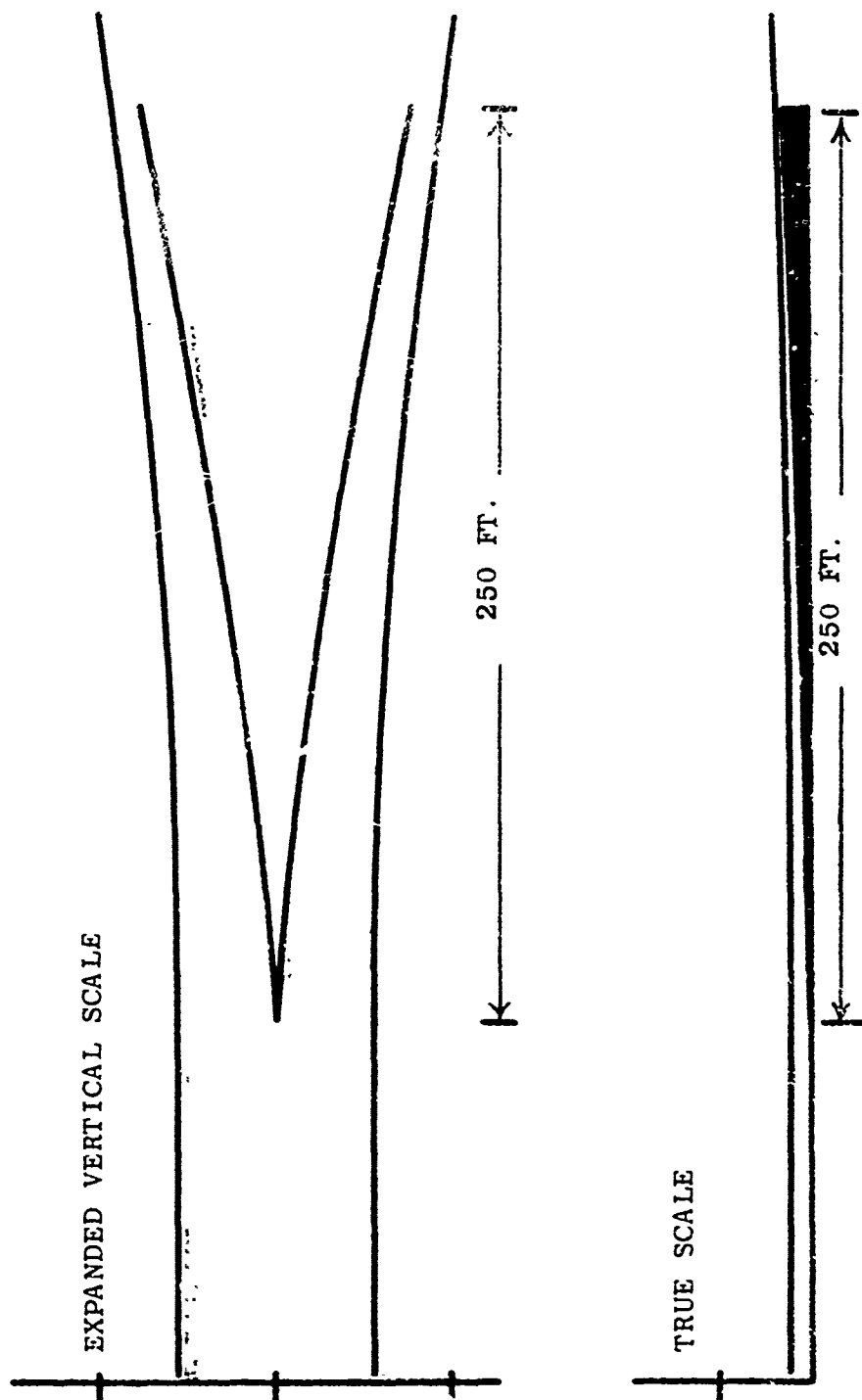


FIGURE 2.3.3. Longitudinal cross section of the phantom nose which produces a ground pressure rise of 2 lb/ft^2 in 10 msec from 60,000 ft at Mach number 2.7 and the resultant streamtube of 100 sq. ft. initial area.

$10^6 \frac{\text{FT. LB. SEC}}{\text{FT.}}$

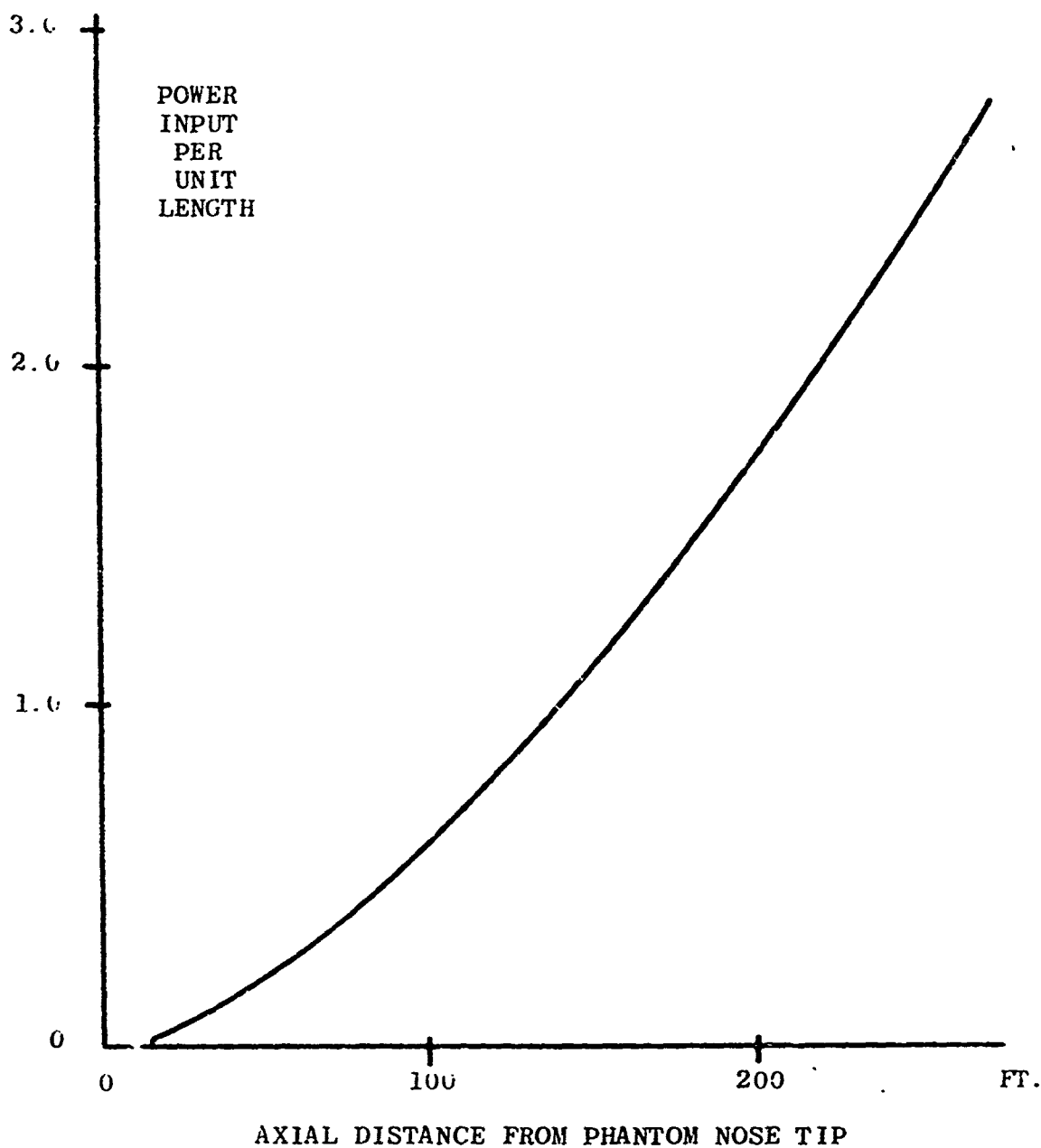


FIGURE 2.3.4. Input power per unit axial length. The input power distribution required to duplicate the nose and streamtube of Figure 2.3.3.

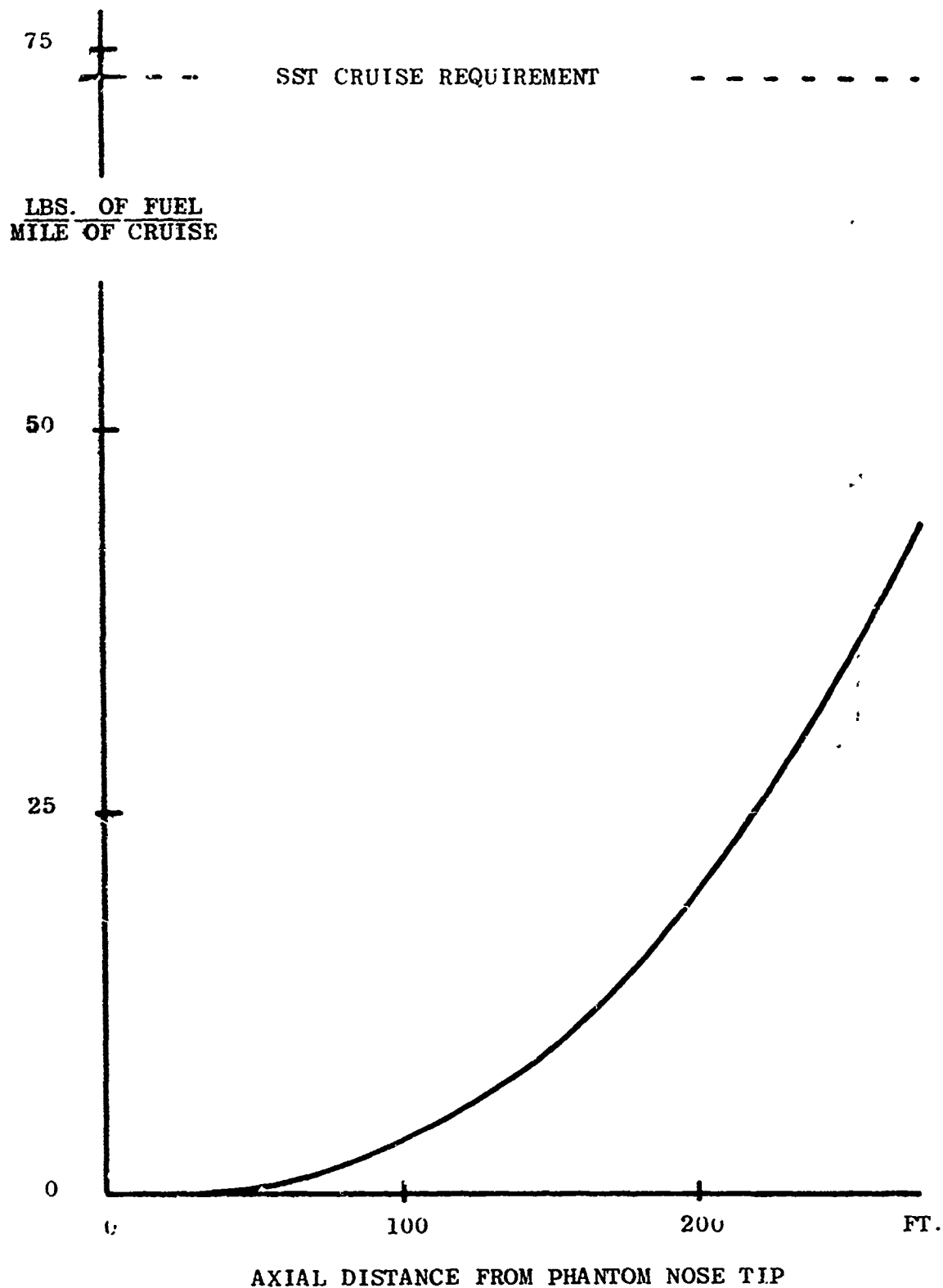


FIGURE 2.3.5. Total power required up to the axial position indicated. The integral of the curve in Figure 2.3.4 in lbs. of fuel/mile of SST cruise.

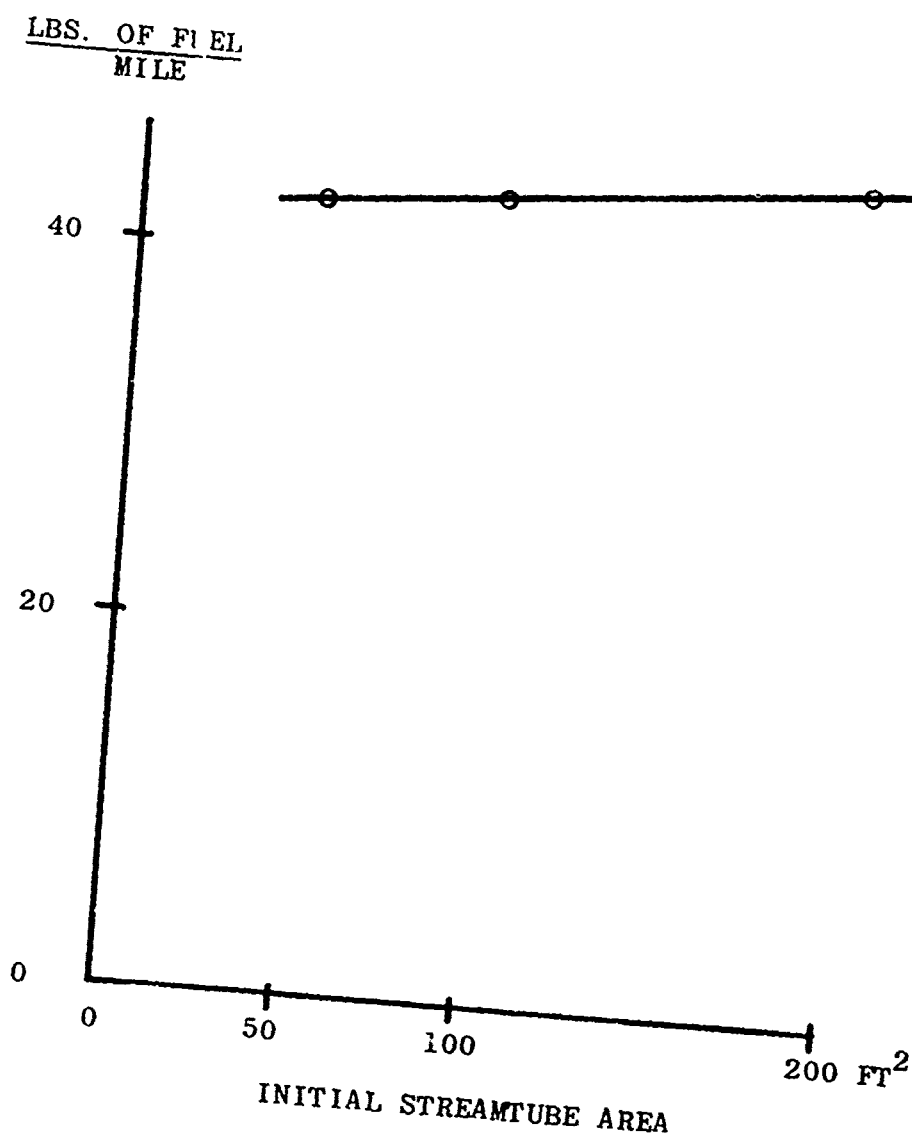


FIGURE 2.3.6. Power requirement vs. initial area of streamtube in which heat is added for phantom nose of Figure 2.3.3.

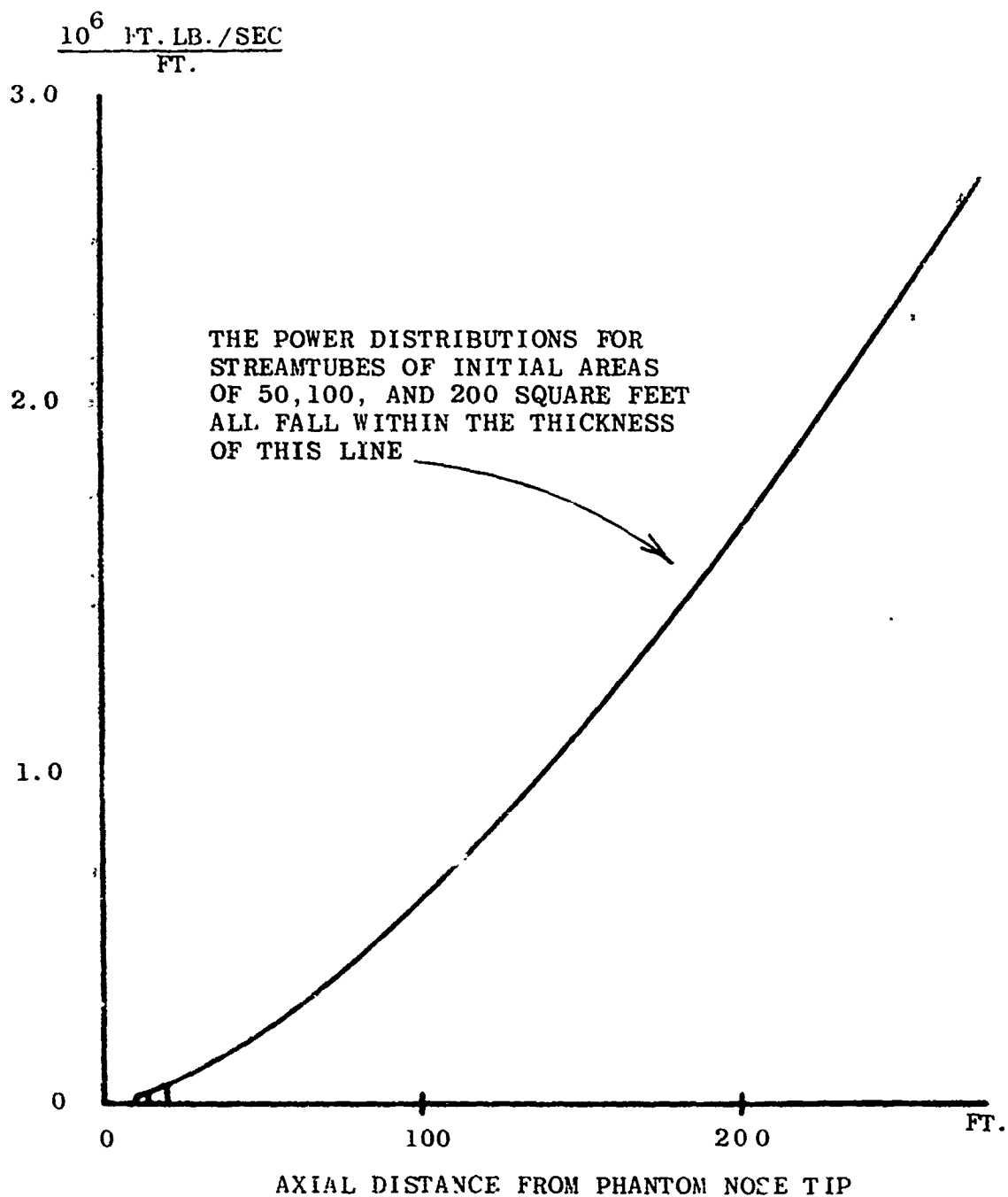


FIGURE 2.3.7. The input power distribution for various streamtubes and the phantom nose of Figure 2.3.3.

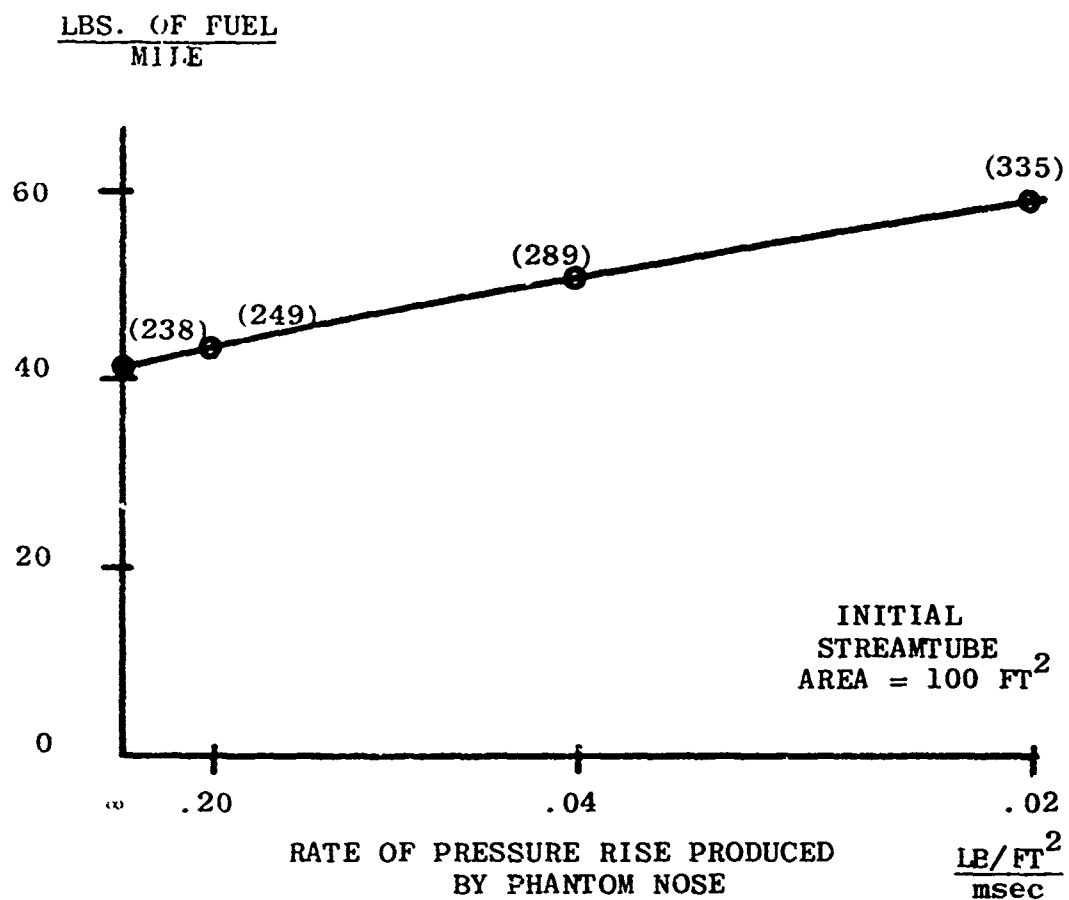


FIGURE 2.3.8. Power requirement vs. rate of ground signature pressure rise produced by phantom nose for SST of 600,000 lbs at Mach number 2.7. (The length of nose duplicated is indicated in parentheses in feet.)

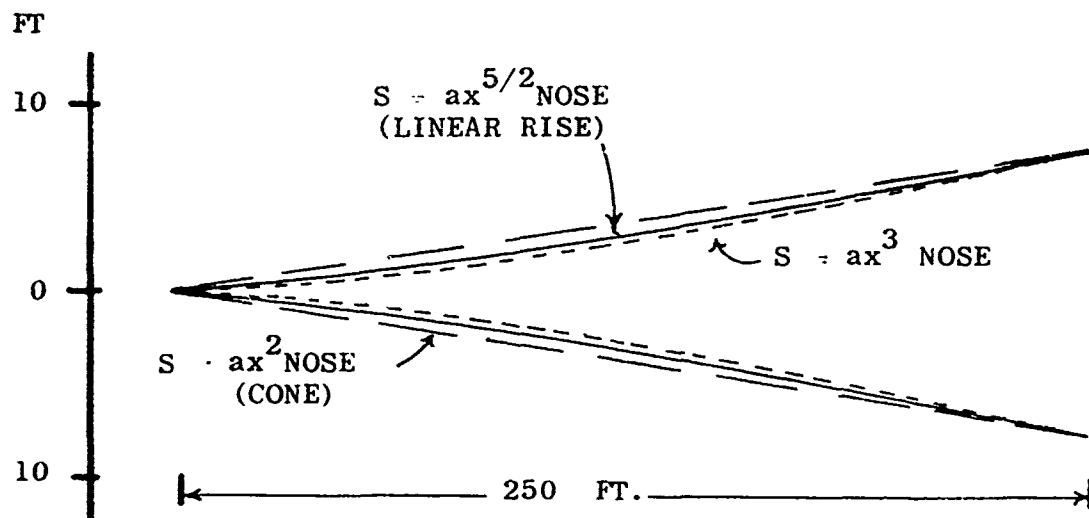


FIGURE 2.3.9. Comparison of nose shapes. Longitudinal cross sections of noses of the same length and base area. The linear rise nose is the nose of Figure 2.3.3.

$10^6 \text{ FT. LB. / SE.}$
 FT.

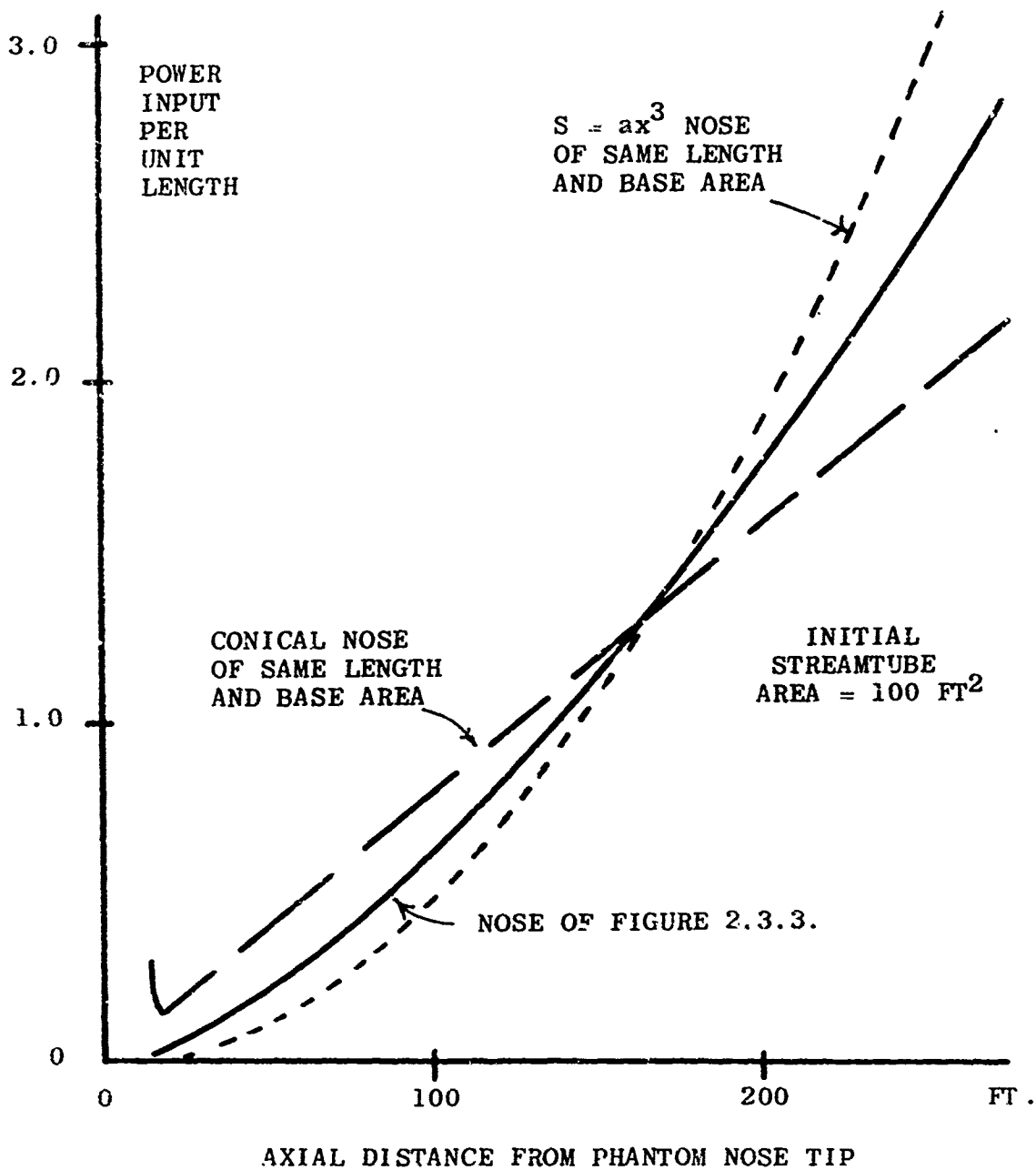


FIGURE 2.3.10. A comparison of the input power distributions required to duplicate the linear rise nose of Figures 2.3.3 through 2.3.6 and the ($S = ax^{5/2}$) and $S = ax^3$ noses of the same length and base area.

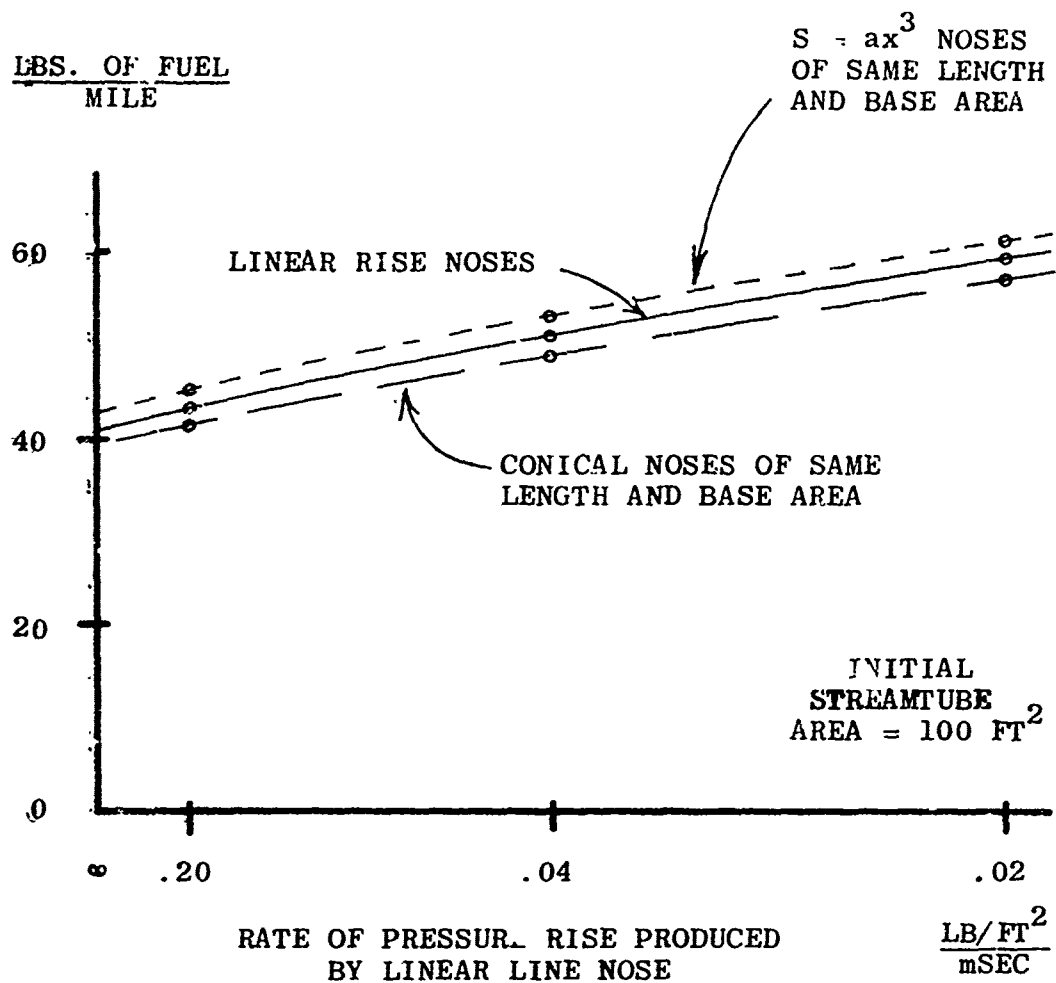


FIGURE 2.3.11. A comparison of the power required to duplicate the linear rise ($S = ax^{5/2}$) noses of Figure 2.3.8, and the conical ($S = ax^2$) and $S = ax^3$ noses of the same length and base area.

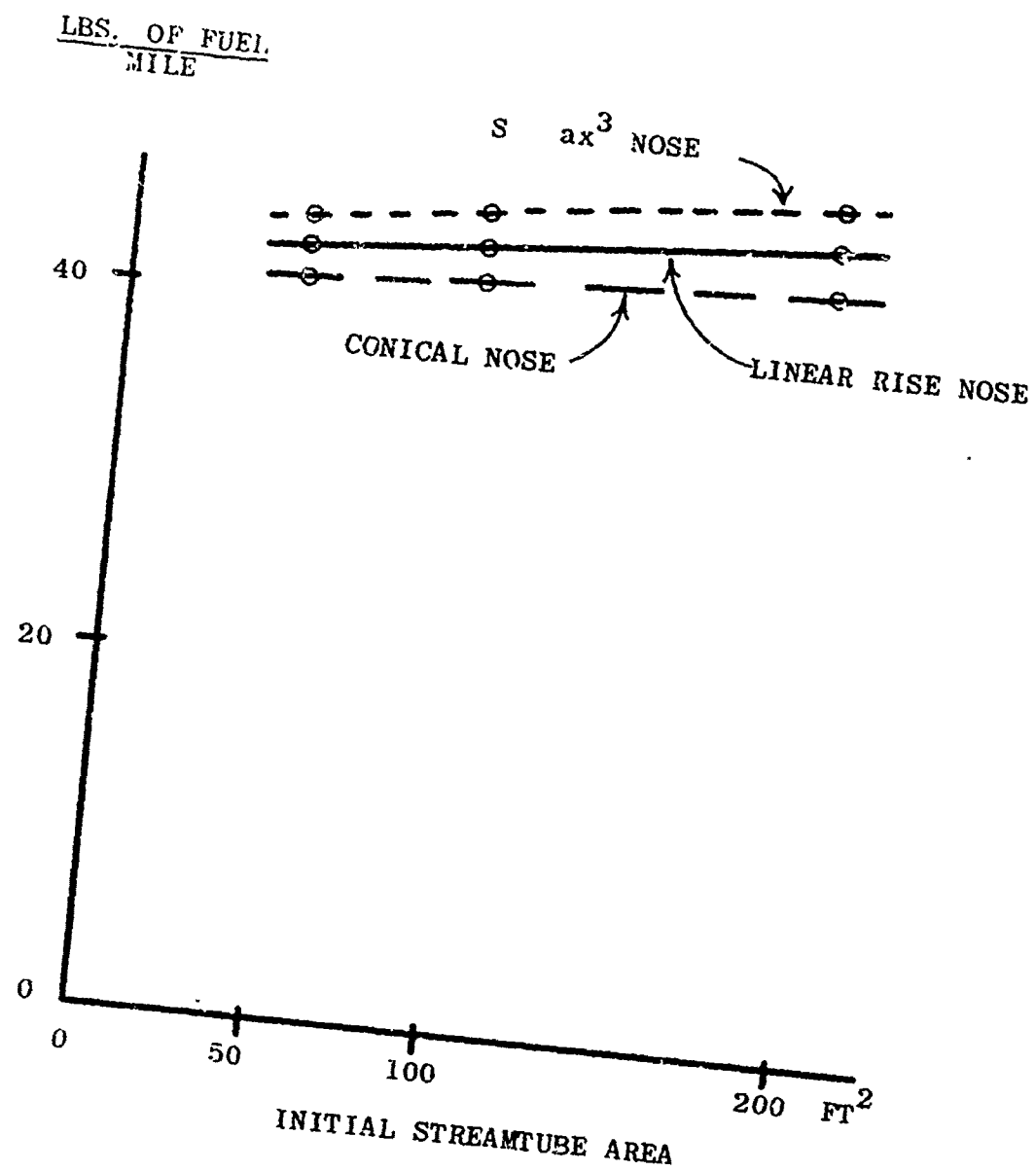


FIGURE 2.3.12. Power requirement vs. initial streamtube area for the noses of Figure 2.3.9.

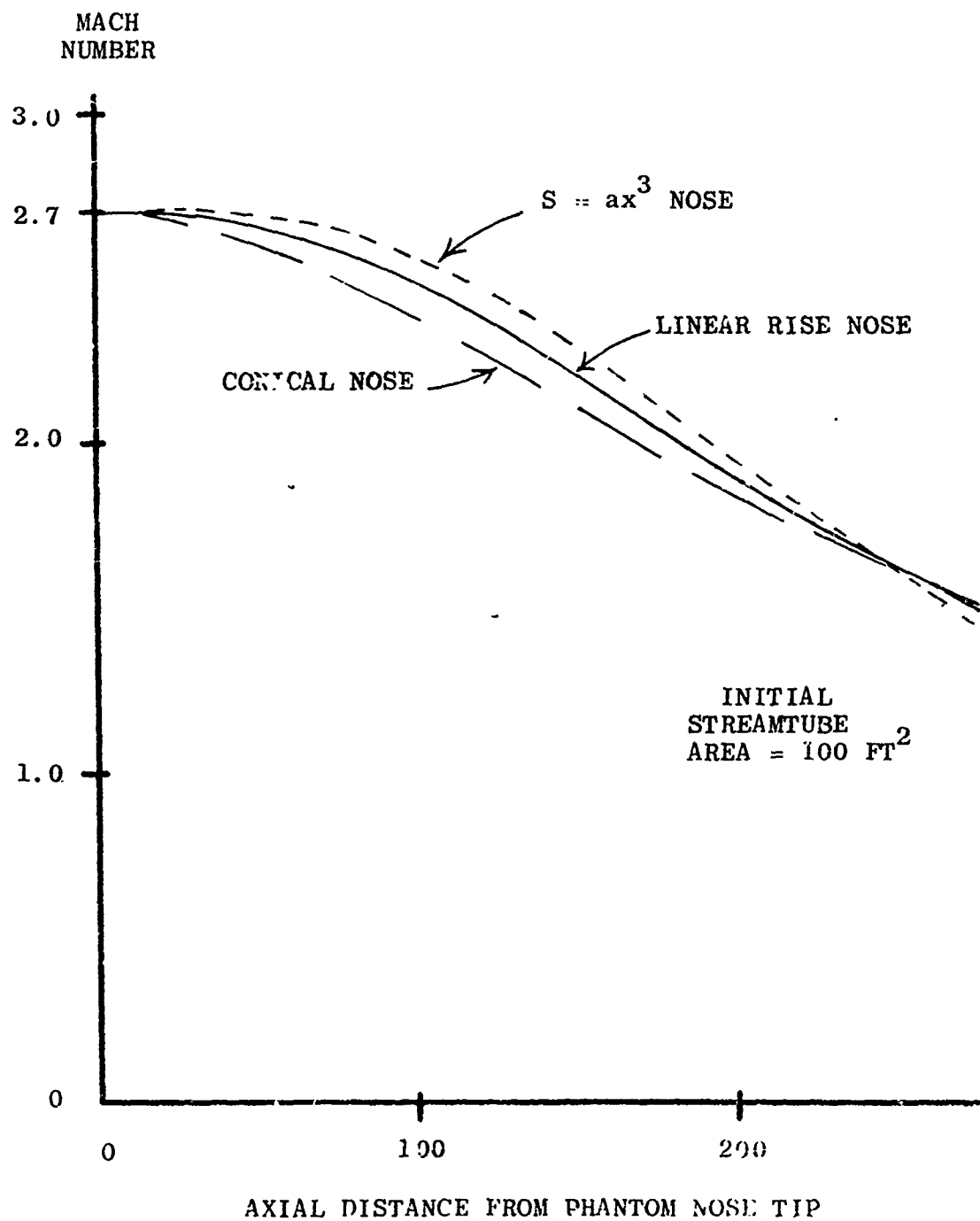


FIGURE 2.3.13. Streamtube - channel Mach number for the phantom noses of Figure 2.3.9.

the linear rise noses, do not depend very much on the particular streamtube-channel chosen as shown in Figure 2.3.12. For all the nose-streamtube combinations the Mach number in the streamtube-channel stayed above one. See Figure 2.3.13.

Consideration of the above results leads to an approximation scheme. In the expression for $T_o^{-1} dT_o/dx$ since the $p^{-1} dp/dx$ term is observed to be small compared to the $A^{-1} dA/dx$ term except near the region where the streamtube considered is first affected by the nose, and as M and T_o undergo small changes in that region compared to the changes occurring further down the streamtube, we neglect the effect of the $p^{-1} dp/dx$ term and write

$$\frac{dT_o}{T_o} \cong [1 + (\gamma-1)M^2/2]^{-1} \frac{dA}{A}$$

and

$$\frac{dM^2}{M^2} \cong - \frac{dA}{A}$$

Thus $M^2 A$ is a constant which can be evaluated upstream to give $M^2 = M_\infty^2 A_\infty/A$ where A_∞ is the upstream, or initial, streamtube area. Then

$$\frac{dT_o}{T_o} = [A + (\gamma-1) M_\infty^2 A_\infty/2]^{-1} dA$$

and $T_o[A + (\gamma-1) M_\infty^2 A_\infty/2]^{-1}$ is a constant. This implies that the power addition per unit streamtube-channel length is

$$\frac{dp}{dx} = \frac{\rho_{\infty} U_{\infty}^2 c_p T_{0\infty}}{1 + (\gamma - 1) M_{\infty}^2 / 2} \frac{dA}{dx} = \rho_{\infty} U_{\infty}^2 c_p T_{\infty} \frac{dA}{dx}$$

where T_{∞} is the upstream static temperature. Since the streamtubes considered here are sufficiently close to the axis compared to the phantom nose surface, slender body theory should apply and the rate of streamtube area change at a given cross sectional plane should be determined to a sufficient approximation by the axial flow sources at the intersection of the plane and axis. That is,

$$\frac{dA}{dx} = 2\pi f(x) = \frac{dS}{dx}$$

where, as above, S is the cross sectional area of the phantom nose. The channel heat addition per unit length can then be written as

$$\frac{dp}{dx} = \rho_{\infty} U_{\infty}^2 c_p T_{\infty} \frac{dS}{dx}$$

This last expression essentially reproduces the curves of Figure 2.3.10 except for the spike at the front of the conical nose curve which is due to the steep, but small, increase in pressure there, a feature one would not wish to duplicate in any event. This last expression was derived by Swigart and Lubard (Swigart and Lubard, 1969) in a different approach and the above discussion shows the circumstances under which the answers obtained by their approach will agree with those obtained

by a one dimensional channel approach as used here and elsewhere (Miller and Carlson, 1969; Siegelman, 1970). Relating the mass source per unit length represented by the axial sources, $S_L = 2\pi\rho_\infty U_\infty f(x)$, to the equivalent heat sources per unit length, $Q_L = c_p T_\infty S_L$ (Tsien and Beilock, 1949; Willmarth, 1957), one has $dP/dx = Q_L$ to the above approximation.

2.3.4 Discussion

The power requirements as obtained above have serious consequences for the use of any laser system. For the purpose of this discussion we shall use the 420 Megawatt power requirement figure for the phantom nose of Figure 2.3.3 which gives a finite rate of pressure rise of $0.2 \text{ (lb/ft}^2\text{)/m sec}$, equivalent to the attainment of 2 lb/ft^2 in 10 milliseconds. The power requirement for this rate of rise is compared to those of other rates of rise in Figure 2.3.8.

Many laser systems rely on electric energy as their initial energy source either through the use of flashlamps or through electrical discharges of various types. Questions of laser efficiency aside, the generation of 420 Megawatts of electrical power carries a severe weight penalty. At these power levels magnetohydrodynamic (MHD) generators offer the smallest equipment weight per kilowatt, but turbo-alternators offer the lowest specific fuel consumption assuming environmental air is used as the oxydizer (Cooper, 1971). The MHD equipment weight is about 0.2 pounds per kilowatt or 84 thousand pounds for the generation

of 420 Megawatts. This weight is 30% of the nonfuel takeoff weight of the commercial version of the Boeing SST (Aviation Week, 1970). The MHD generator specific fuel consumption is about 1.1 (lb/sec)/MW or 930 lb of fuel per mile of sonic boom abatement operation during SST cruise. With the turbo-alternator, which will involve higher equipment weight, this figure is 470 lb of fuel per mile. Both figures assume the use of environmental air as the oxydizer.

There are laser systems, recently announced in the literature, which do not require the generation of electric power. These are the purely chemical or direct combustion laser (Cool and Stephens, 1969) and gas dynamic laser (Gerry, 1970; Meinzer, 1971). Putting questions of suitability for heating the airflow aside, these carry severe weight penalties also. The chemical laser referenced here requires no electric discharge to attain partial dissociation of the reactants, a procedure which is used on other chemical lasers and typically requires an electrical input power many times the laser output power (Spencer et. al., 1970). But the laser type referenced here does require a non-cycling mass flow. According to the article cited, this flow would have to be so large that any practical application is fully unfeasible. There are unclassified, unconfirmed reports of the attainment or future attainment of 100 kilowatts per pound of flow per second from a direct combustion laser, but this would still leave an unfeasibly large flow requirement.

With gas dynamic lasers the specific power figure of 2 to 3 kilowatts per pound of flow per second is still far too small for a single use flow. In gas dynamic lasers the mass flow can

be cycled. The laser output would then originate in the compressor driving the flow circuit (Hertzberg, Johnston, and Ablstrom, 1971). The best mechanical power generation to equipment weight ratio has recently moved from 5.0 kW/lb (Wood, 1968) to 6.5 kW/lb (Aerospace Association, 1970). Even at the latter figure, however, 65,000 pounds of equipment 24% of the nonfuel SST takeoff weight, would be required to generate 420 Megawatts of mechanical power for the compressor. This figure does not include the weight of the compressor itself. It is to be kept in mind that the sonic boom reduction by means of lasers can be readily restricted to sensitive parts of the overflight terrain by means of turning on and off the laser equipment.

2.3.5. Conclusions and Recommendations

It is concluded that large amounts of power will be required to produce desirable finite rise time pressure signatures. This is shown in subsection 2.3.3. It is also concluded, as discussed in subsection 2.3.4, that at present there exists no system which can generate such power in laser emission without severe weight penalties.

In view of the amazing advance in the maximum average output power of lasers in this past decade, laser progress should be informally monitored for the discovery of a system which obtains its output chemically from its fuel with power output to mass flow ratios approaching those available from the combustion of commercial fuels. It should be borne in mind that heating of the airstream by laser emission can be accomplished not only by gas breakdown,

so far achieved only by Q switched or gain switched lasers using some form of direct or indirect electrical excitation, but also by absorption in an atmospheric absorption band such as the CO₂ band at 4.3 μ m.

2.4. ENGINE-AIRFRAME INTEGRATION WITH SPECIAL EMPHASIS ON NON-CIRCULAR ENGINE EXHAUSTS AND JET FLAPS

2.4.1 Pressure Distribution of Deflected Two-Dimensional Jets Behind Wings

by Dr. B. H. Goether¹, assisted by Dr. Heinz Gruschka and UTSI Student Mr. Philip Kessel

One major part of the sonic boom signature is produced by the lift of an aircraft; this part is usually much larger than the sonic boom part due to the solid displacement of the aircraft structure. Thus, the major effort of this study was directed towards determining which sonic boom alleviations can be obtained by appropriately utilizing the lift component of deflected exhaust jets of turbojet or ramjet engines.

On Figures 2.4.1 to 2.4.4 some fundamental relationships in the formation of the sonic boom signature for two-dimensional lifting surfaces are depicted. It is demonstrated on Figure 2.4.1 that the downward momentum behind a wing without ground effect corresponds to one-half of the total lift on either side of the wing. On the other hand, if the pressure and expansion waves impinge upon the ground, the total impulse submitted to the ground is equal to the full amount of the lift. As Figure 2.4.2 also indicates, the dividing streamline behind the wing approaches again the undisturbed position after passing through the reflected wave system, because all waves cancel each other at large distances.

On Figures 2.4.3 and 2.4.4 it is demonstrated that the sonic boom signature on the ground spreads over a larger distance and has a smaller pressure peak when the lifting wing has a larger chord; that is when the lift is spread over a larger distance in the flight direction.

The purpose of this investigation is to show that the distribution of the lift in the flight direction can occur not only by means of stretching the wing chord, but also by having a part of the total lift produced by the deflected exhaust jet of the engine (see Figure 2.4.5). In the case of a deflected exhaust jet, it is to be understood that the entire vertical component of the deflected jet, that is the lift component, is transferred to the wing at the deflection point of the jet, that is in the exhaust nozzle. However, as far as the action on the flow and particularly also on the wave system which finally impinges on the ground is concerned, the lift component of the jet is distributed over a distance downstream of the exhaust nozzle.

This phenomenon has not been fully recognized in the past. Therefore, on Figure 2.4.6, various force equilibrium sketches are prepared which show that the reaction on the flow behind the wing, equivalent to the vertical lift component of the jet, is caused by the aerodynamic pressure difference between the upper and the lower surfaces of the deflected jet. In effect, the deflected jet acts like a solid plate in the flow which is curved according to the jet.

A theoretical two-dimensional calculation was conducted as shown in principle on Figure 2.4.7 and on pages 2.167 a and b.

A numerical evaluation of the pressure distribution curves is shown on Figure 2.4.8. The rearward shifting of the lift is larger the larger the Mach number is and the larger the jet momentum coefficient is.

A comparison of the jet lift was conducted with respect to the lift generation by means of wings and mechanical flaps (see Figure 2.4.9).

A jet flap operating at a Mach number of $M = 3$ with a momentum coefficient of $C_{\mu} = 1.4$ has the same lift-producing effectiveness as a wing in supersonic flow. In subsonic flow, a jet momentum coefficient of approximately $C_{\mu} = 1.9$ is required to produce the same lift as a wing.

At a jet momentum coefficient of $C_{\mu} = .5$, figure 2.4.9 shows that in flight at Mach number 3, the jet flap would be identical in effectiveness as a mechanical flap with a flap chord of approximately 35 percent of the main wing. The same jet momentum coefficient $C_{\mu} = .5$ in subsonic flow would have the same lift effectiveness as a flap of 13 percent chord length.

In the following, some applications of the new theory on lift shift and performance changes due to jet flap deflection are shown for the Mach number range up to $M = 12$.

JET FLAP IN SUPERSONIC FLOW

Free jet

Centrifugal
pressure
gradient

$$\frac{dP}{dh_j} = -\frac{\rho_j v_j^2}{R} = \frac{\rho_j v_j^2}{(ds/d\delta)s}$$

Centrifugal
pressure
difference

$$P_{j \text{ lower}} - P_{j \text{ upper}} = \Delta P_s = -h_j(\rho_j v_j^2) \cdot \left(\frac{d\delta}{ds}\right)_s$$

External flow

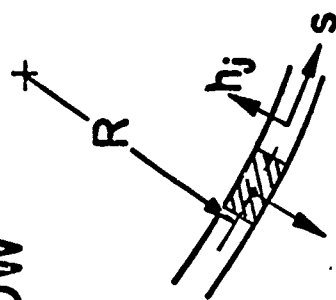
$$P_{j \text{ upper}} - P_\infty = -\frac{\rho_\infty}{2} v_\infty^2 \frac{2\delta}{\sqrt{M_\infty^2 - 1}}$$

$$P_{j \text{ lower}} - P_{j \text{ upper}} = \frac{\rho_\infty}{2} v_\infty^2 \frac{4\delta}{\sqrt{M_\infty^2 - 1}}$$

Pressure equilibrium

$$-h_j \rho_j v_j^2 \left(\frac{d\delta}{ds}\right)_s = \frac{\rho_\infty}{2} v_\infty^2 \frac{4\delta}{\sqrt{M_\infty^2 - 1}}$$

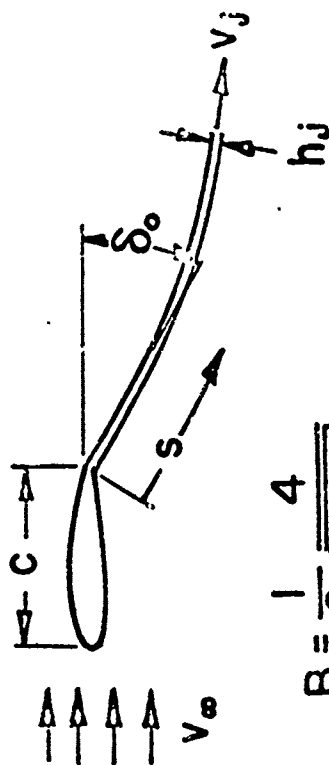
$$\left(\frac{d\delta}{\delta}\right)_s = -\frac{\rho_\infty v_\infty^2}{\rho_j v_j^2} \frac{ds}{h_j} \frac{2}{\sqrt{M_\infty^2 - 1}}$$



JET FLAP IN SUPERSONIC FLOW

Jet angle (by integration)

$$\frac{\delta}{\delta_0} = \exp\left(-\frac{s}{c}\right) B$$



$$B = \frac{1}{C_\mu \sqrt{M_\infty^2 - 1}}$$

$$C_\mu = \frac{\rho_j V_j^2 \cdot h_j}{\rho_\infty V_\infty^2 \cdot c} = \text{jet momentum coefficient (based on unit span)}$$

$$J_m = \rho_j V_j^2 \cdot h_j = \text{jet momentum}$$

Pressure difference

$$\Delta P_s / \rho_\infty V_\infty^2 = \delta_0 \frac{4}{\sqrt{M_\infty^2 - 1}} \exp\left(-\frac{s}{c}\right) B$$

Free jet lift (by integration)

$$\Delta L / \left(c \frac{\rho_\infty V_\infty^2}{2}\right) = C_\mu \delta_0^2, \text{ and } \Delta L = J_m \delta_0$$

Thrust loss (by integration)

$$\Delta T / \left(c \frac{\rho_\infty V_\infty^2}{2}\right) = \frac{1}{2} C_\mu \delta_0^2 \approx C_\mu (1 - \cos \delta_0), \text{ and } \Delta T = J_m (1 - \cos \delta_0)$$

2.4.2 SHIFT OF LIFT BEHIND SOLID WING AND AIRCRAFT PERFORMANCE CHANGES DUE TO DEFLECTED JETS

Figure 2.4.10 shows the airframe and propulsion system data used in this study. The Lift Over Drag (L/D) ratios from various configuration studies were plotted and a boundary curve drawn which is believed to be representative of the most optimistic L/D ratio obtainable. The curves in Figure 2.4.10 give also ramjet and turbojet performance and the values of air specific impulse, I_{air} , as a function of Mach number. This data is used to calculate the exhaust momentum to thrust ratio and also the jet momentum coefficient, C_{μ} .

$$\frac{J_m}{T} = 1 + \frac{v_{\infty}}{g} \frac{1}{I_{air}}$$

J_m = exhaust momentum

v_{∞} = flight velocity

g = gravitation constant

T = thrust

I_{air} = air specific impulse.

The data from Figure 2.4.10 was used to calculate the ratio of jet lift to wing lift. This data is plotted in Figure 2.4.11. The effect of jet flap on aircraft L/D and range is shown in Figure 2.4.12. In these plots the advantage of exhaust deflection at high Mach numbers shows quite plainly. It is also obvious that for every Mach number there is an optimum exhaust deflection, measured from the horizontal, which will maximize range. The optimum range factor varies between +0.7% at 6° for Mach 2, to +27% at 13.5° for Mach 12.

The expression for pressure distribution along a jet flap can be rearranged in terms of aircraft and propulsion parameters by substituting the engine mass flow and aircraft geometry factors we get:

$$\frac{B_j \Delta P_x}{B_{te} W/S} = \frac{B_j}{B_{te}} \delta_o \frac{4q}{\alpha} \frac{1}{W/S} e^{-\frac{x}{L_{te}}} \frac{4q_{\infty}}{\alpha} \frac{B_{te}^2}{\dot{m} u_e} \frac{B_j}{B_{te}}$$

where

$\frac{B_j \Delta P_x}{B_{te} W/S}$	=	Non-dimensional flap lift
B_j	=	Width of jet flap
B_{te}	=	Trailing edge span
W/S	=	aircraft wing loading
ΔP_x	=	pressure across flap at status x
δ_o	=	jet flap deflection
q_{∞}	=	dynamic pressure
α	=	$\sqrt{M_{\infty}^2 - 1}$
\dot{m}	=	engine mass flow
u_e	=	engine exhaust velocity

The pressure distribution for some typical aircraft are shown in Figure 2.4.13, 2.4.14, and 2.4.15.

A lift discontinuity exists at the trailing edge of the wing due to the abrupt change in the direction of the airflow caused by the jet flap. The extent of this

discontinuity can be limited by decreasing the span of the jet flap. Since momentum considerations insure that the total lift must remain the same, we can predict that the lift distribution of the jet with smaller span must extend further behind the aircraft.

In these figures the width of the jet is varied from 0.25 to 1.0 times the trailing edge span. The approximate lift distribution on the wing is also plotted in order to show graphically the order of magnitude effect of the lift on the flap. For this purpose the thickness effects and the fuselage effects, if any, are ignored which results, using conical flow theory, in a constant spanwise averaged lift distribution.

As aircraft Mach numbers increase, the exhaust volume flow from conventional engines becomes larger due to the decrease in air specific impulse. At Mach 12 the mass flow from two cylindrical exhausts would fill the entire base of the aircraft. Engine cowl drag would become a predominant factor in this case and would obviously force a compromise between cowl drag and expansion ratio. The lift distribution for aircraft having two cylindrical exhausts is shown in Figure 2.4.16. Note that at Mach 12 the width of the jet exhaust, L_j , is equal to the trailing edge span and hence the jet flap is shifting "lift" far behind the trailing edge of the wing.

2.4.3 FINITE ASPECT RATIO EFFECTS

The preceding calculations have been conducted with the assumption that the downwash behind the wing can be neglected as in two-dimensional theory. If the downwash is taken into consideration, however, the exhaust jets are more slowly bent into the direction of the undisturbed horizontal flow. In frictionless flow, and with exhaust jet spans smaller than the trailing edge span of the wing, the jet flow is completely imbedded in the downwash flow and will asymptotically reach not the direction of the undisturbed flow but the direction of the downwash flow behind the wing. At very large distances, the downwash and the jet will eventually impinge upon the ground and will be turned into the horizontal direction.

The turning of the downwash flow at the impingement on the ground will produce a pressure phenomenon which can be integrated as a secondary sonic boom signature which moves along the ground with the Mach number of the aircraft, but with much larger rise times than are experienced in the primary sonic boom. (See Figure 2.4.17).

The slower turning of the jet flow in the downwash has the result that the jet lift is shifted much further behind the solid surfaces of the wing than is shown in figures 2.4.13 to 2.4.16. Consequently, the sonic boom alleviation effects are more pronounced when the finite aspect ratio effects are taken into consideration. It is recommended to examine numerically the effects of downwash on the lift shift behind the wing and the secondary sonic boom signature in the impingement region of the downwash on the ground.

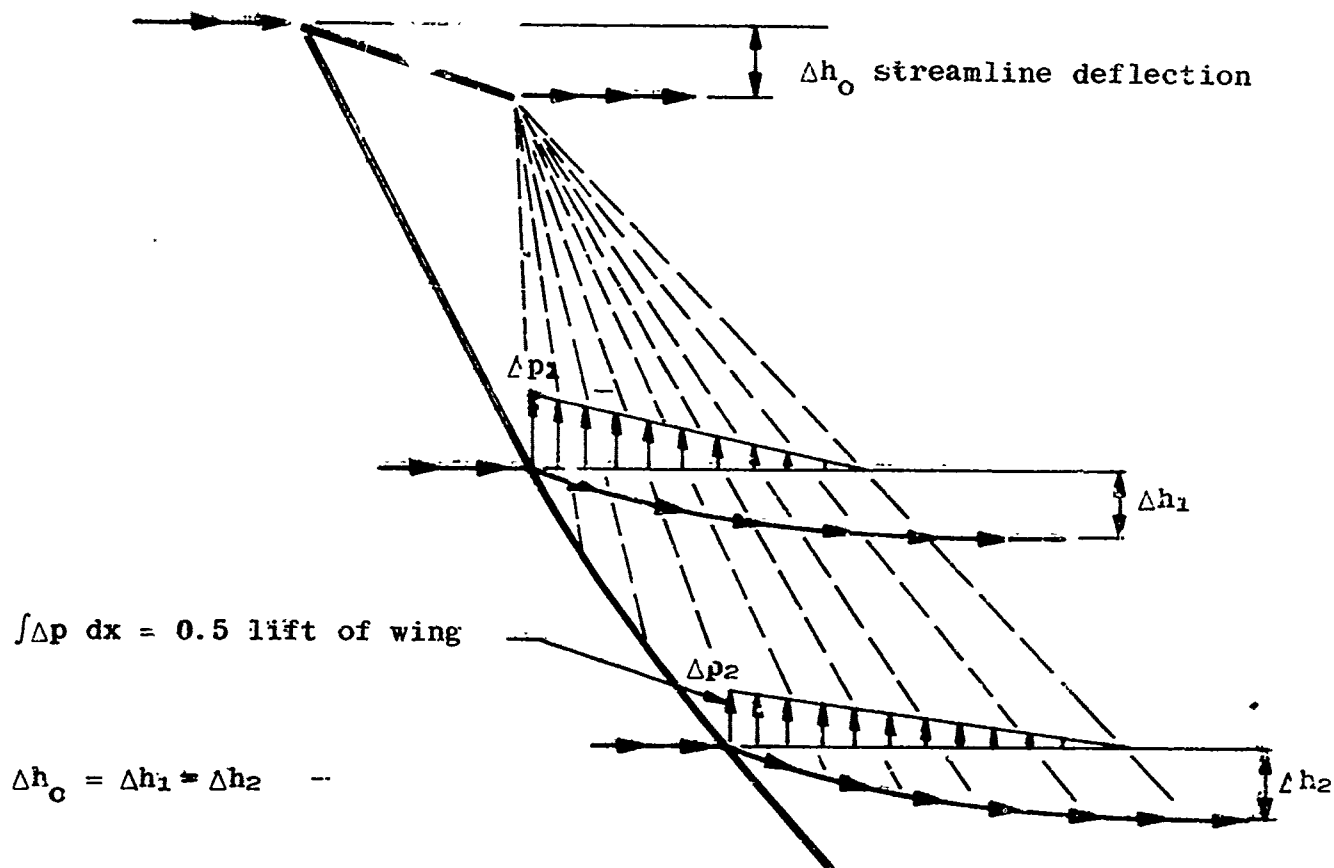


FIGURE 2.4.1. 2 Dimensional flat plate at small angle of attack

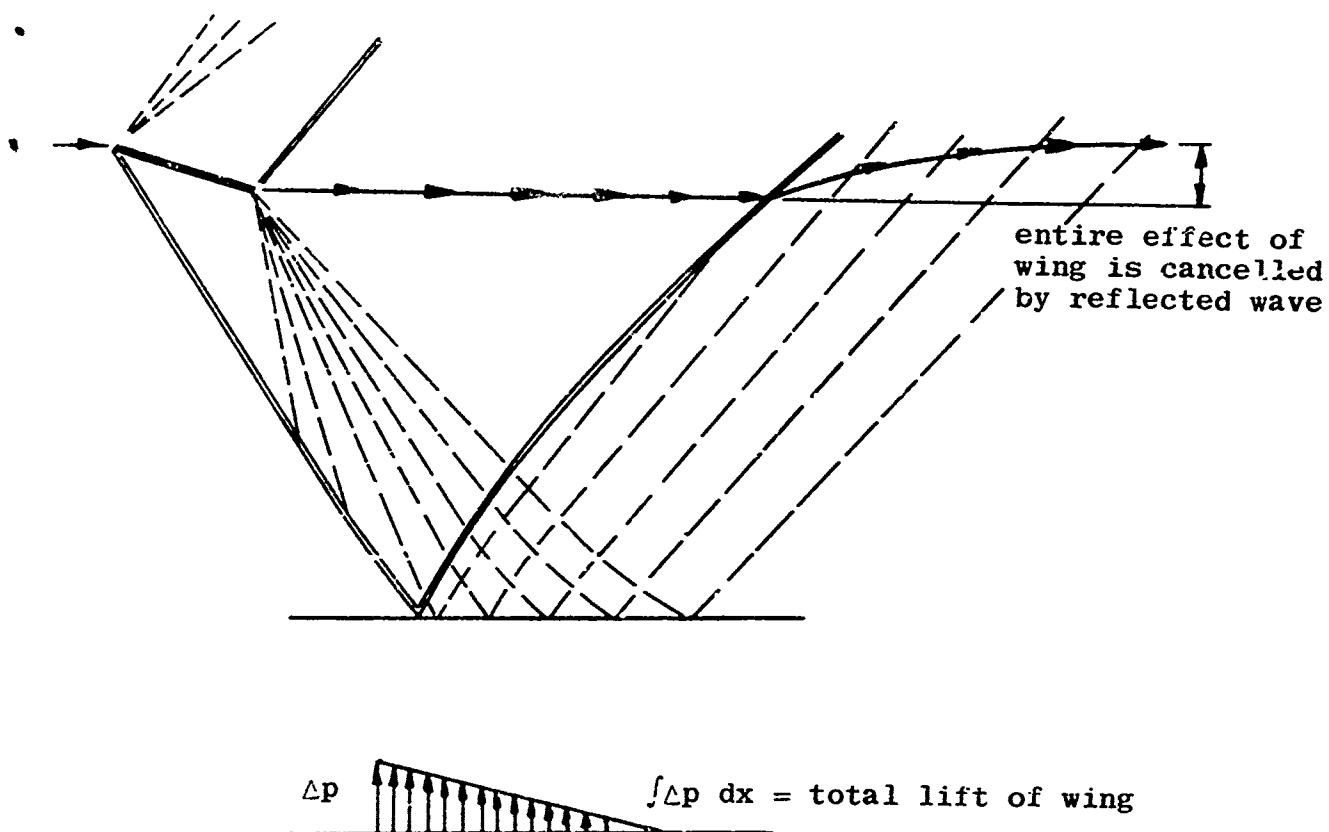


FIGURE 2.4.2. 2 Dimensional flat plate in ground effect

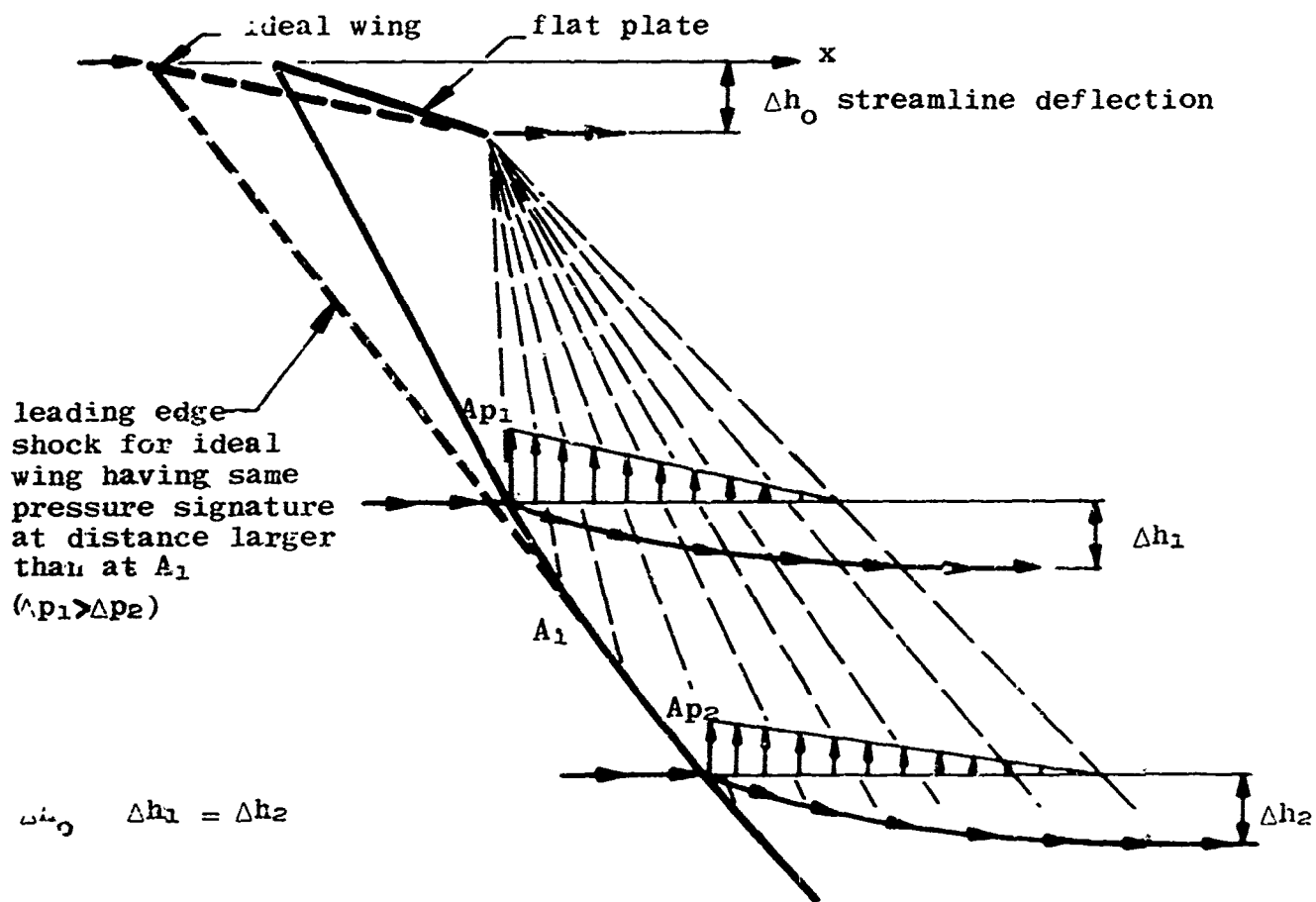


FIGURE 2.4.3. 2 Dimensional flat plate at small angle of attack

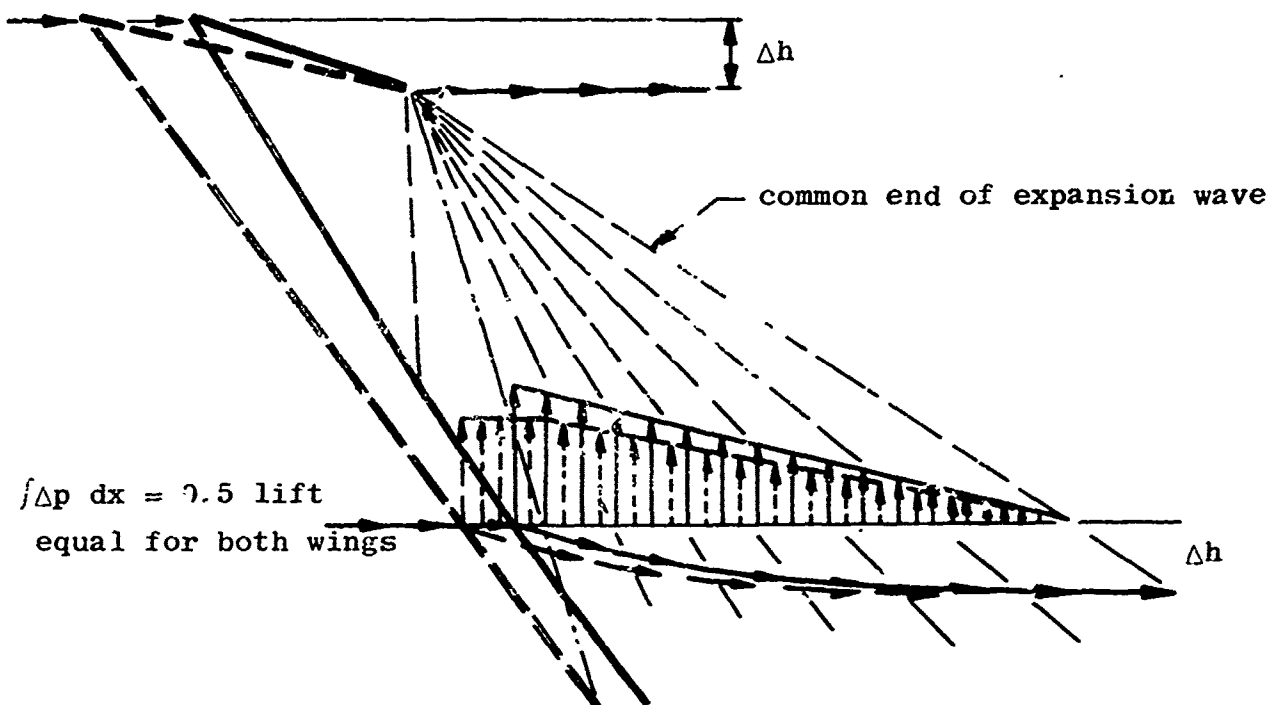


FIGURE 2.4.4. Lift on 2 dimensional wings of various chord lengths and same lift

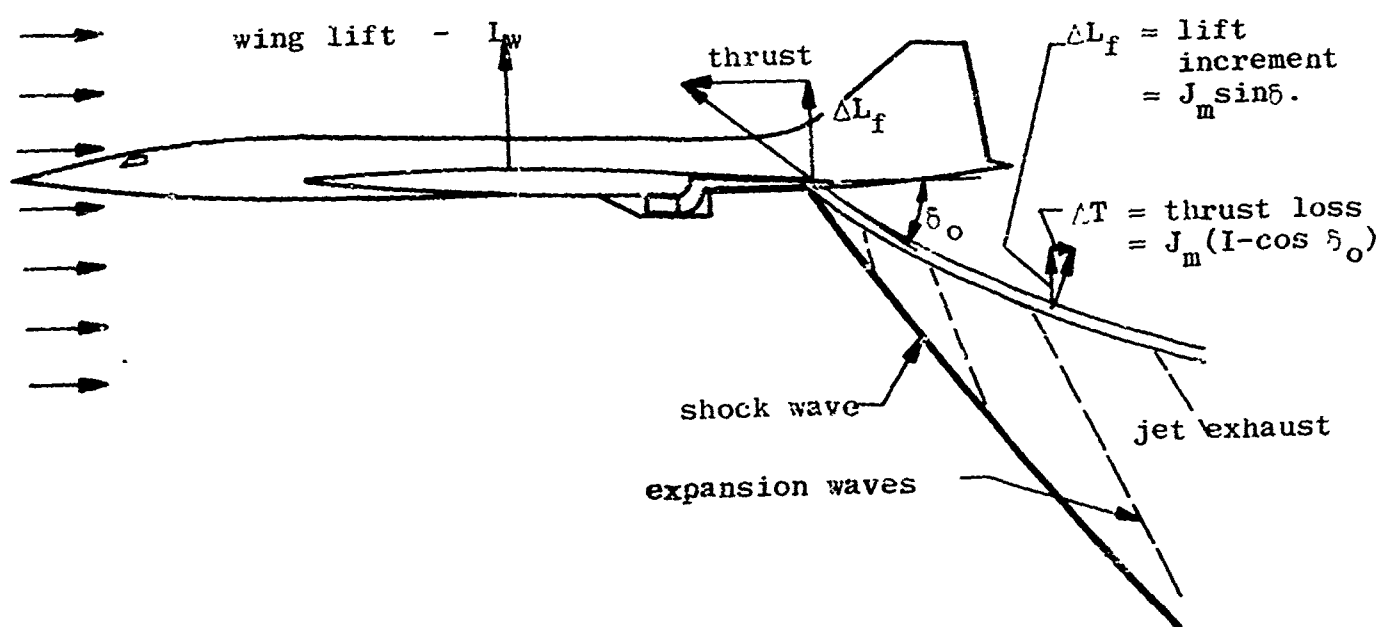
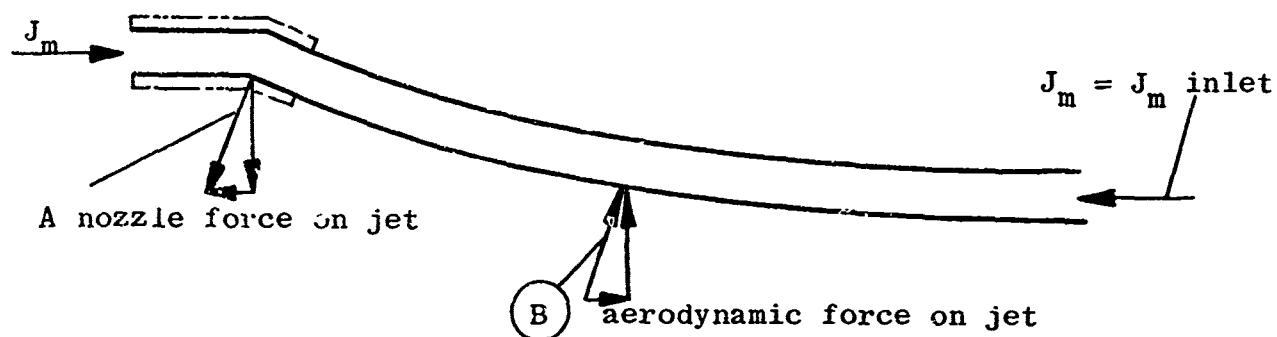
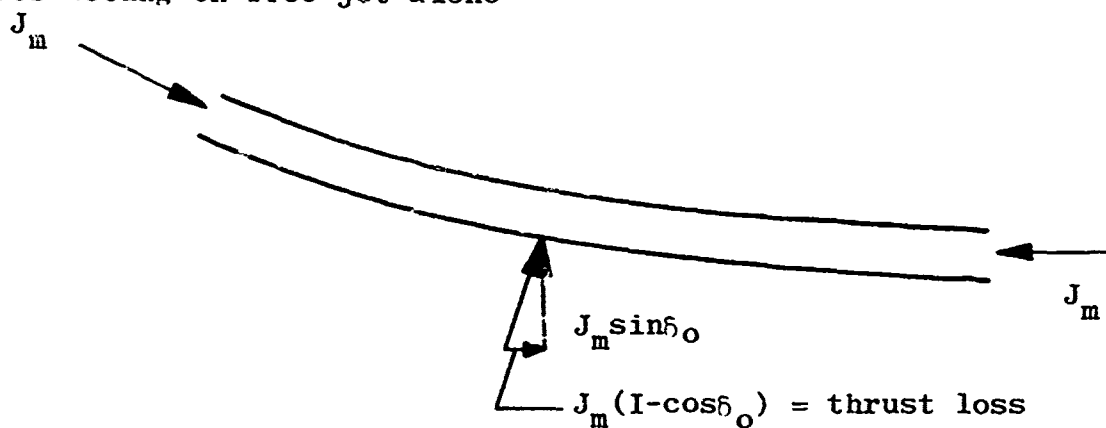


FIGURE 2.4.5. Jet flap principles

Forces acting on jet in supersonic flow



Forces acting on free jet alone



Aerodynamic forces acting on exterior of jet nozzle and free jet

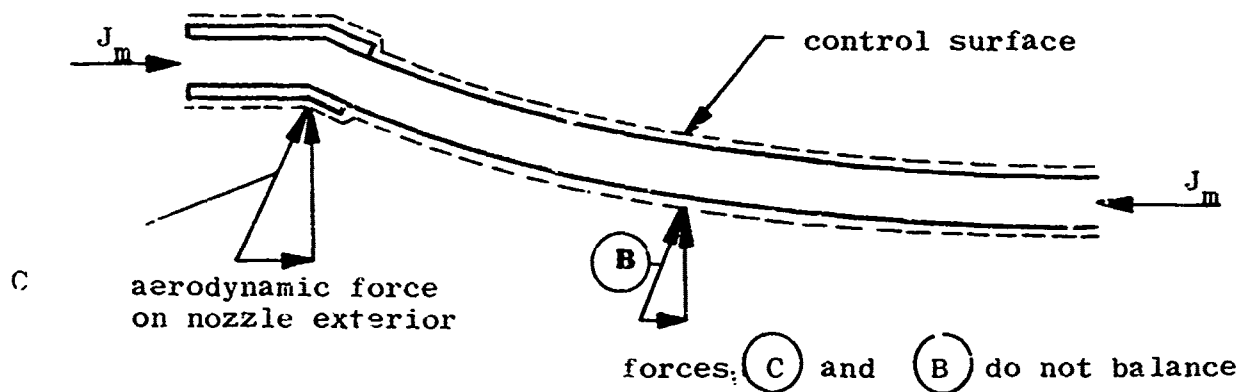


FIGURE 2.4.6.

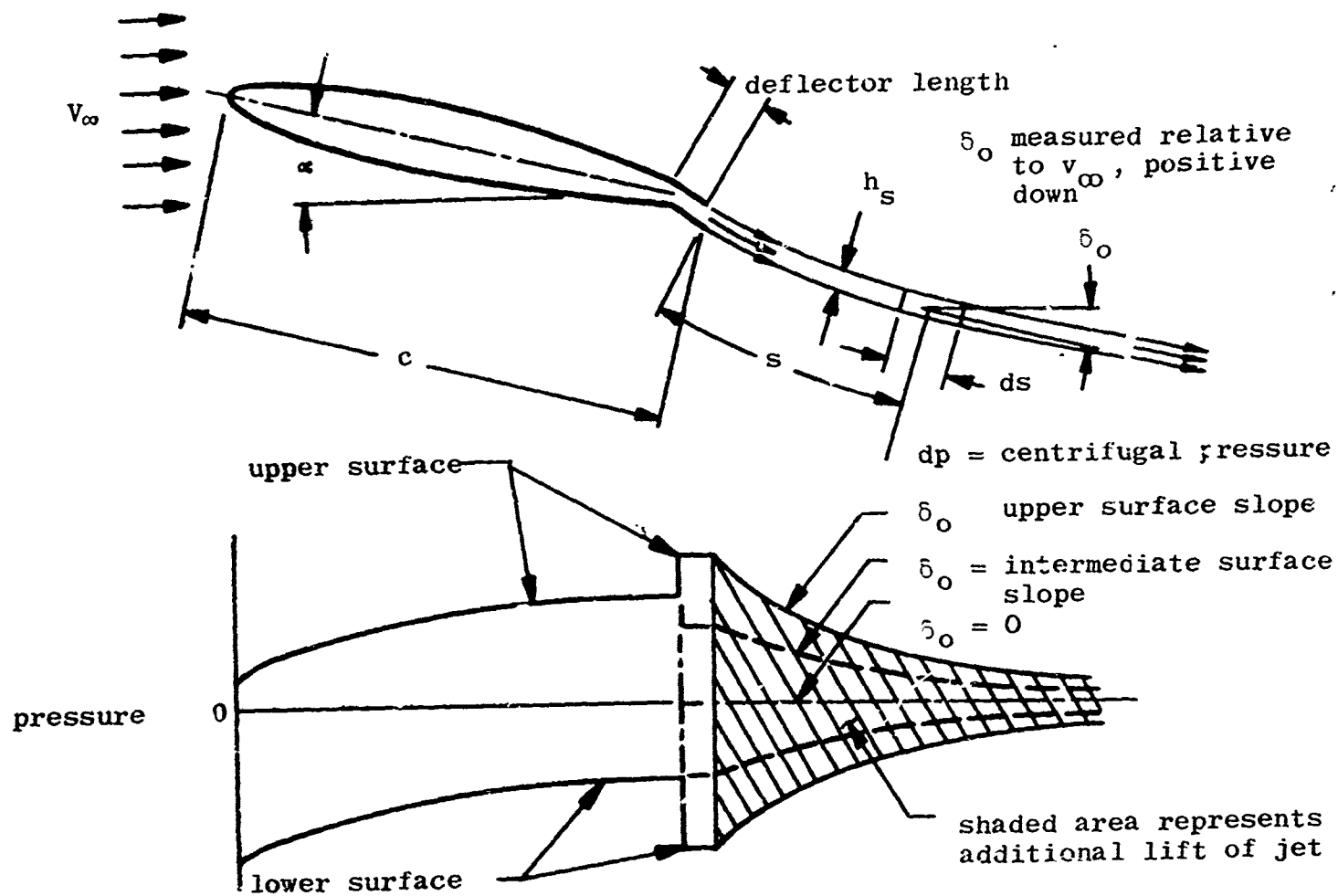
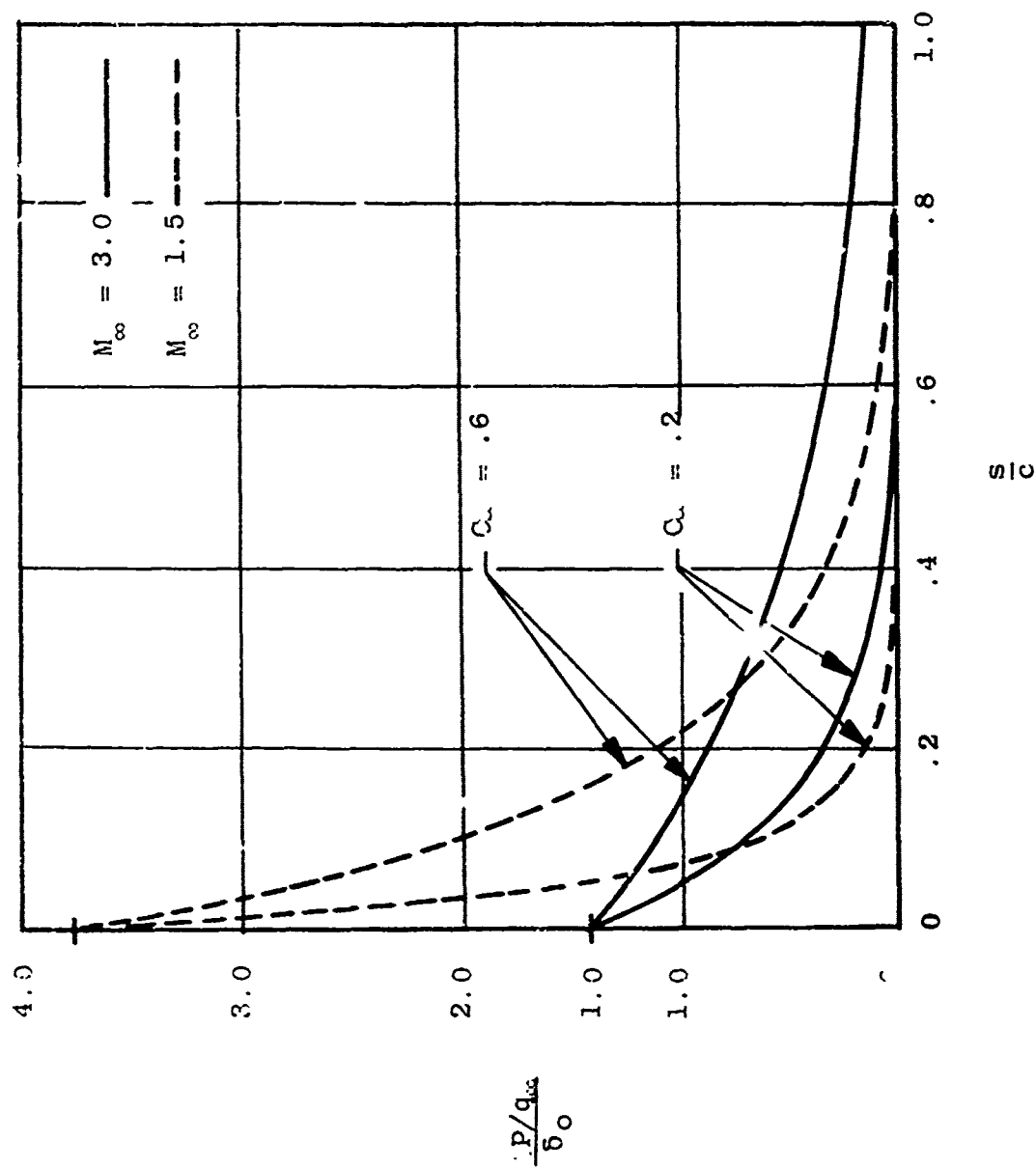


FIGURE 2.4.7. 2 Dimensional jet flap in supersonic flow



$$\frac{P/q_\infty}{\gamma_0} = \frac{4}{M_\infty^2 - 1} \exp\left(-\frac{s}{R}\right)$$

$$B = \frac{1}{C_1} \sqrt{M_\infty^2 - 1}$$

Q_j = jet momentum coefficient

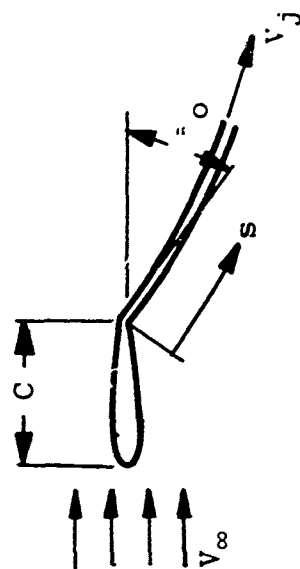


FIGURE 2.4.8. Pressure distribution along a 2-dimensional jet

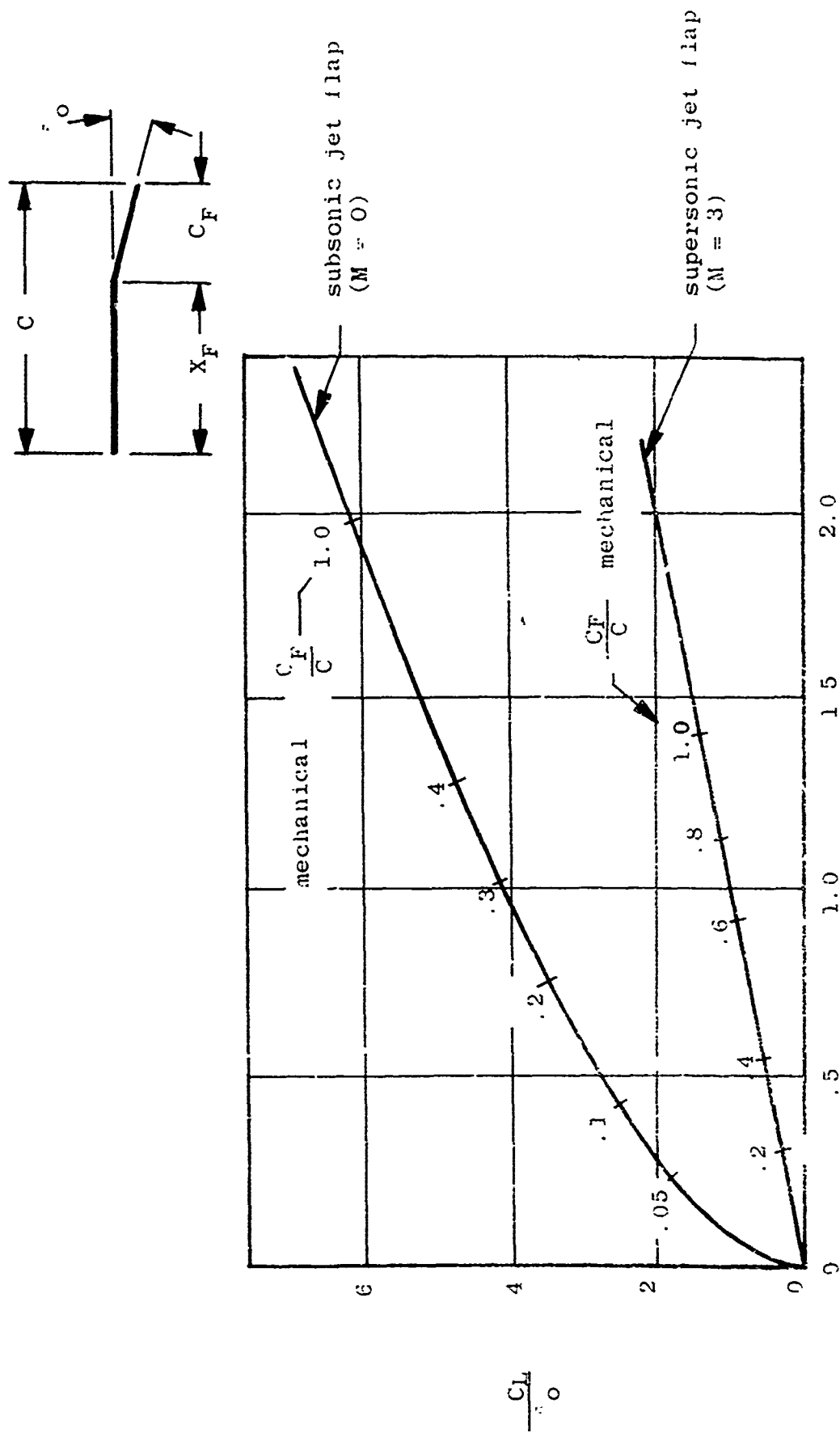


FIGURE 2.4.9. Jet lift augmentation

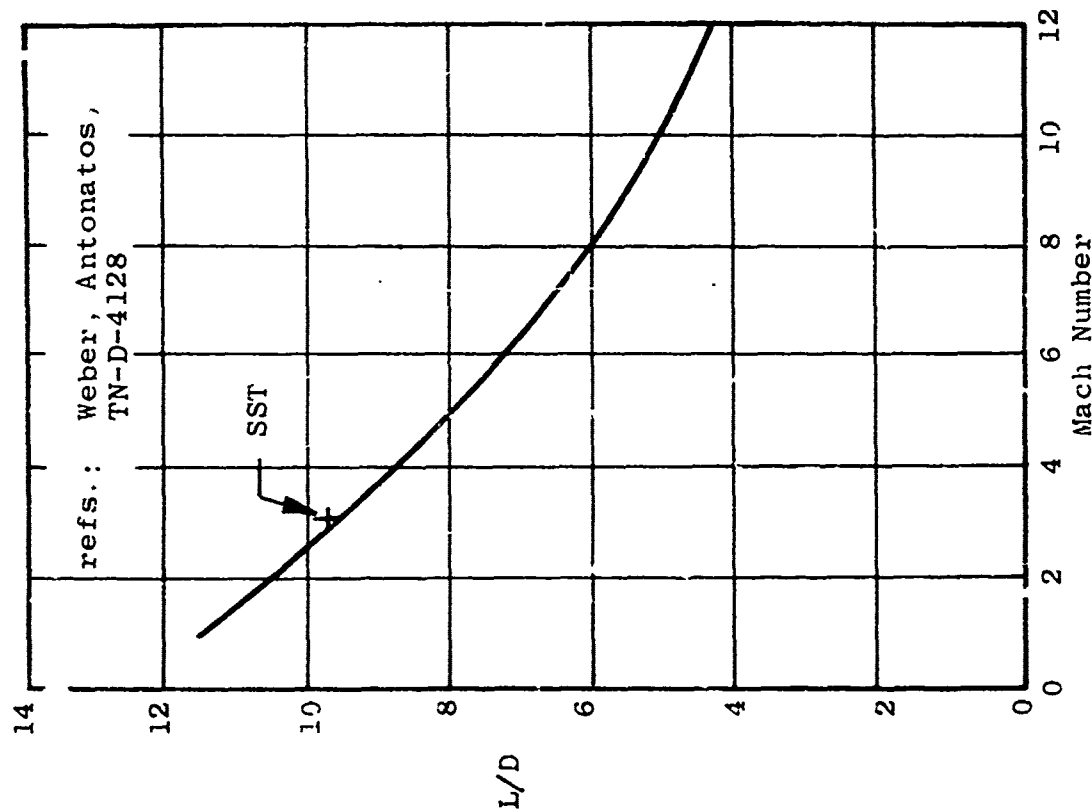
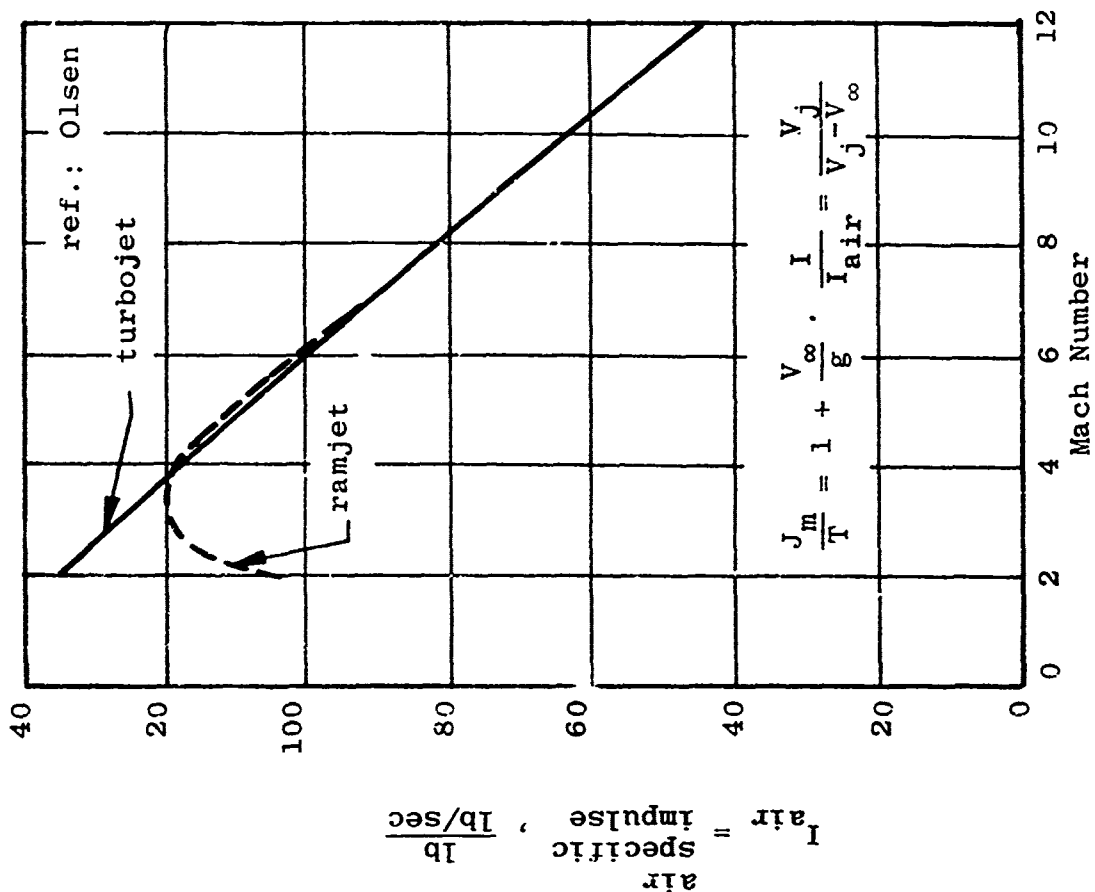


FIGURE 2.4.10. Lift/drag ratio and specific air impulse

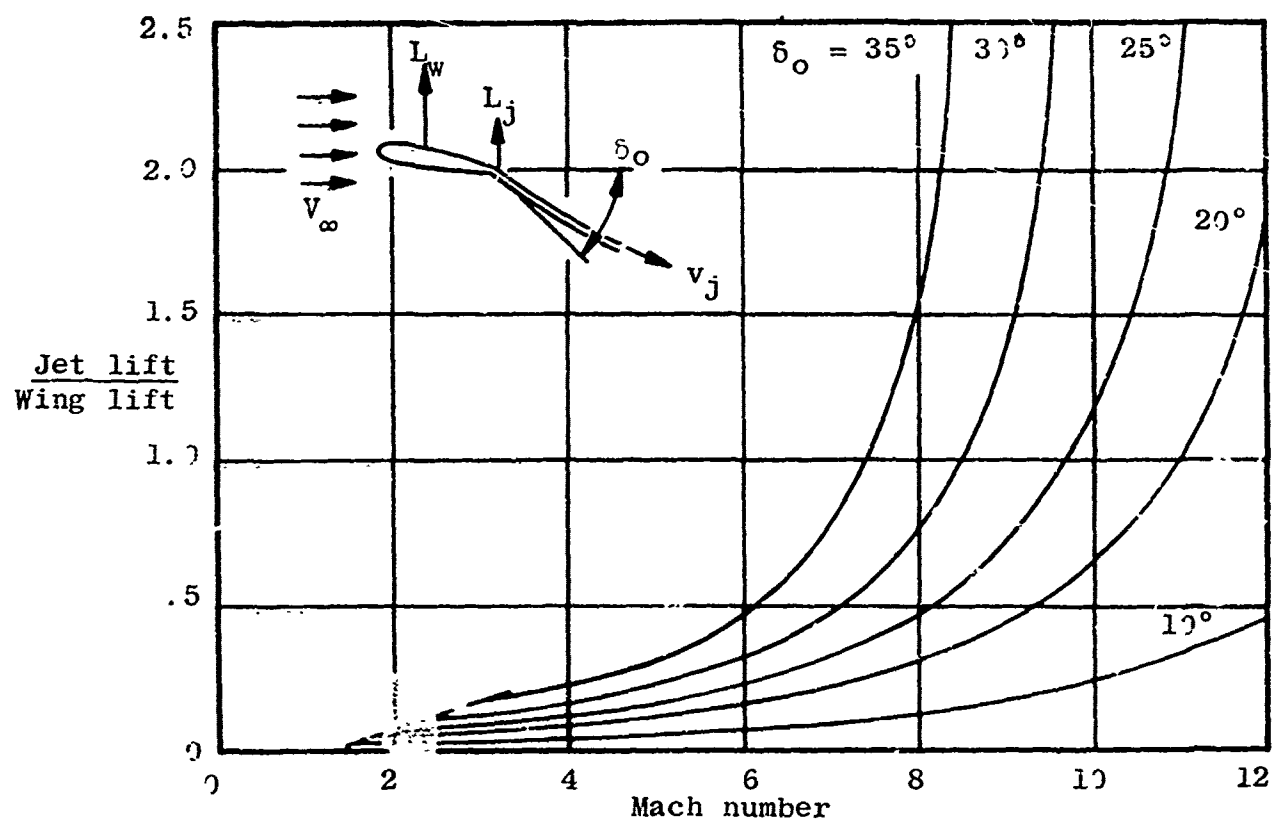


FIGURE 2.4.11. Ratio of jet lift to wing lift

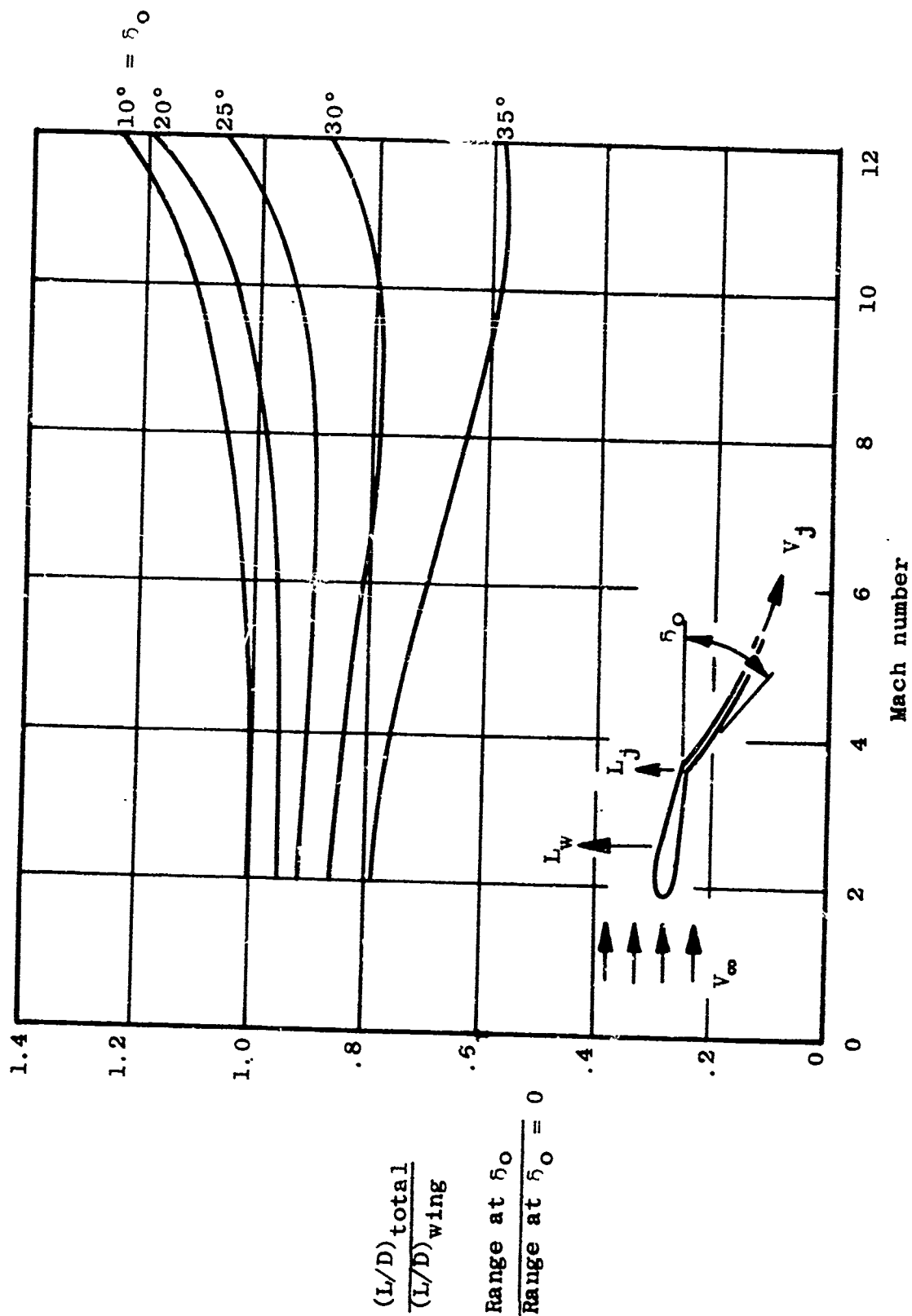


FIGURE 2.4.12. Total lift/drag ratio and aircraft range ratio

Mach number = 6
 Jet deflection = 20°
 $\frac{\text{Jet lift}}{\text{Wing lift}} = .163$

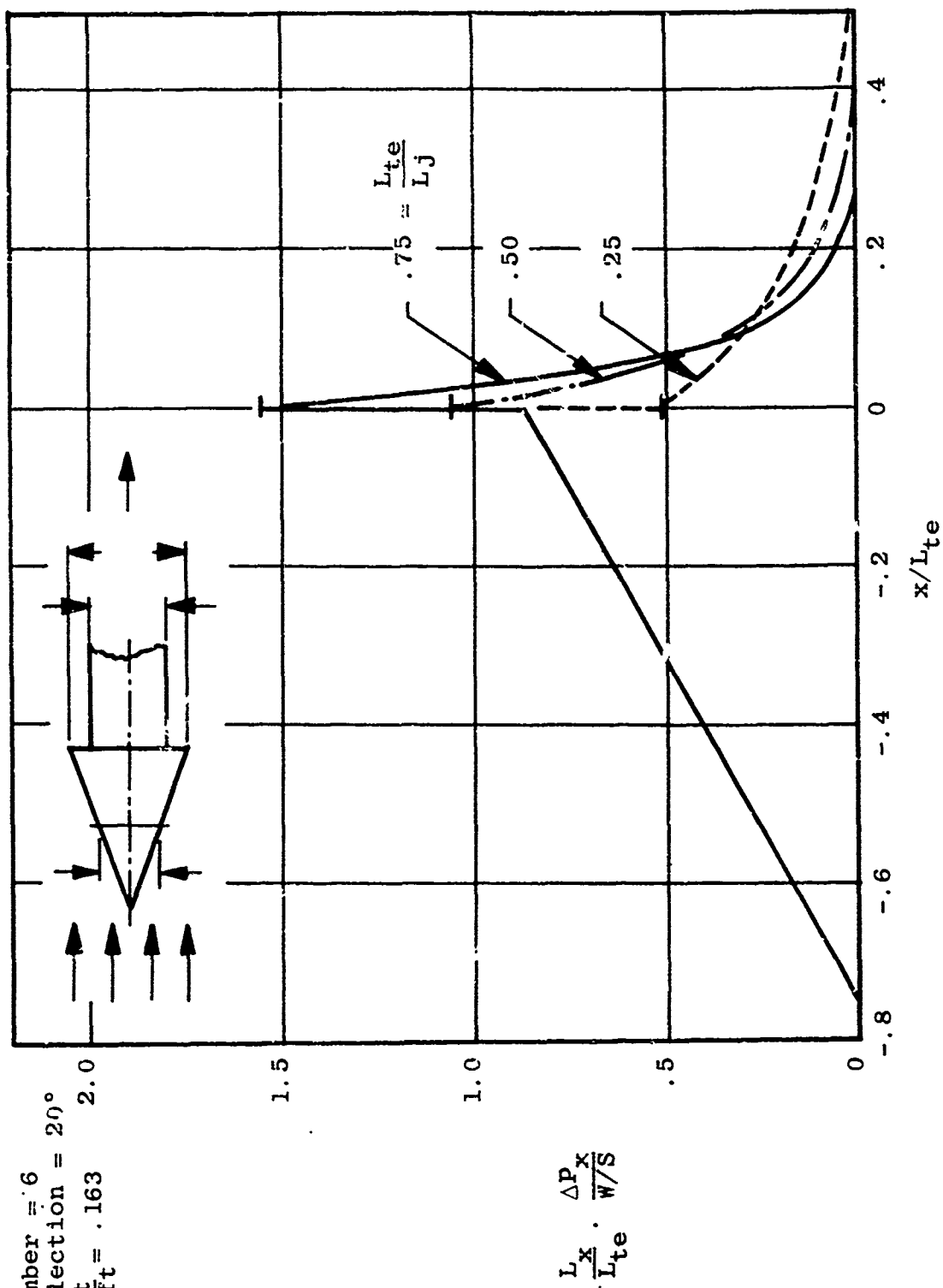


FIGURE 2.4.13. Jet flap pressure distribution without downwash

Mach number = 3
 Jet deflection = 20°
 $\frac{\text{jet lift}}{\text{wing lift}} = .07$

$$\frac{L_x - P_x}{L_{te} W/S}$$

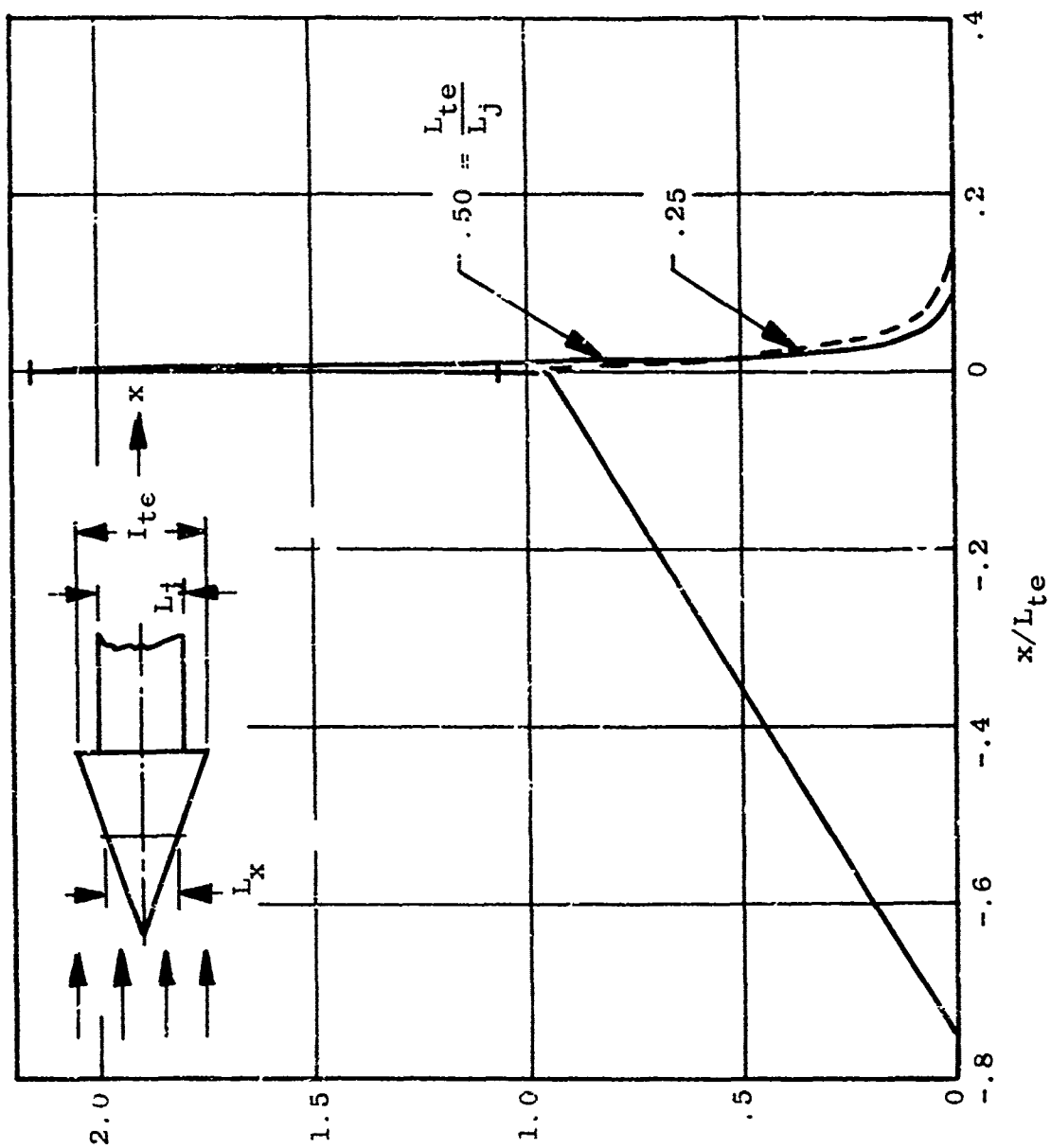


FIGURE 2.4.14. Jet flap pressure distribution without downwash

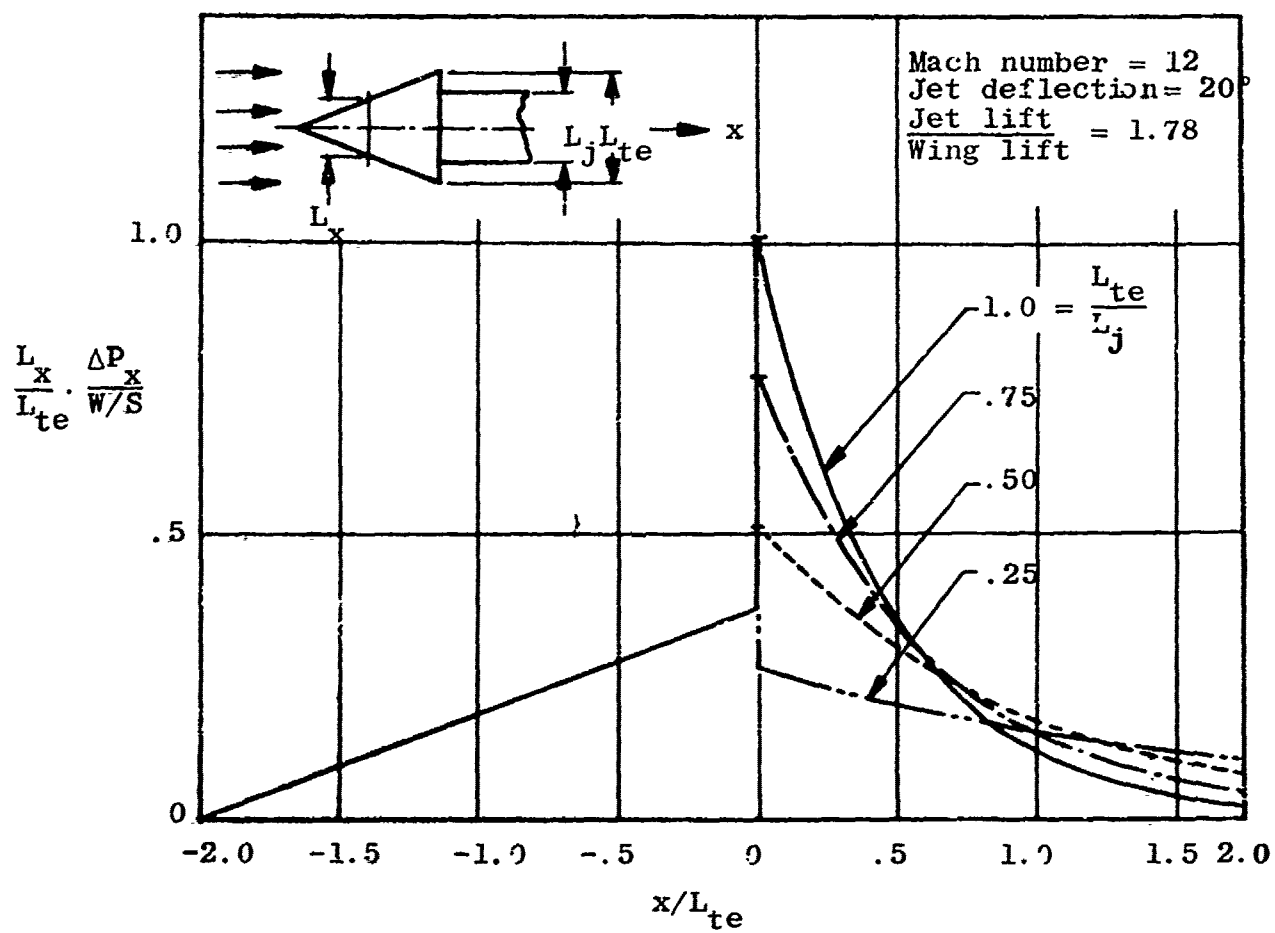


FIGURE 2.4.15. Jet flap pressure distribution without downwash

(Full expansion at 20° jet deflection)

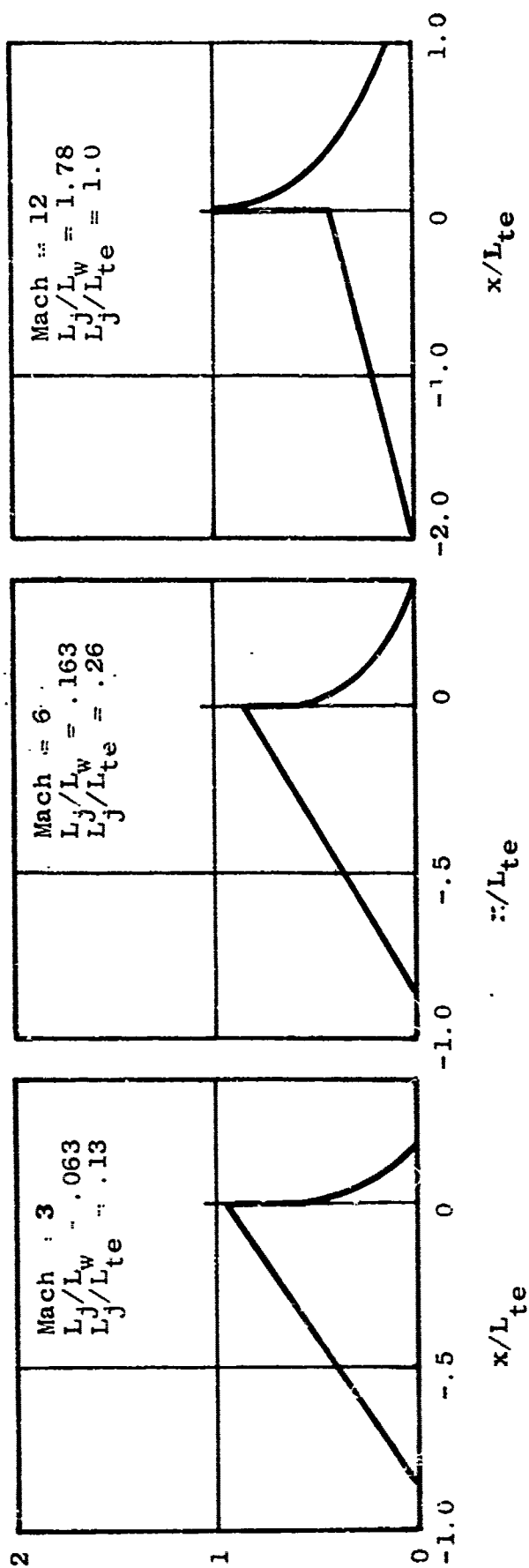
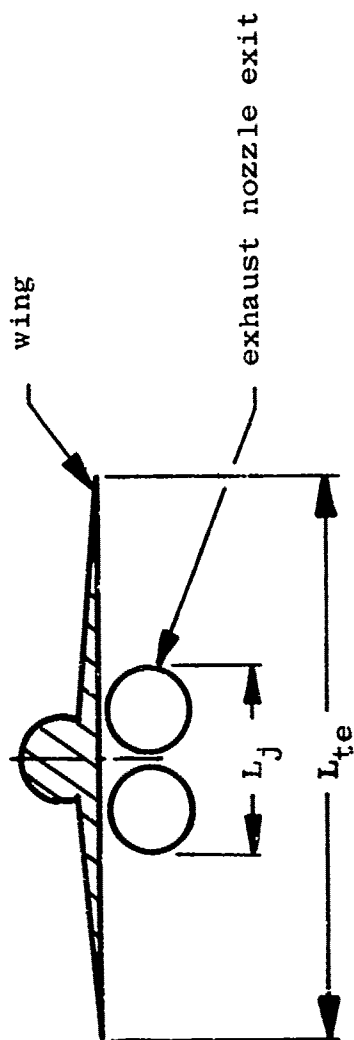


FIGURE 2.4.16. 2 Cylindrical jet exit configuration

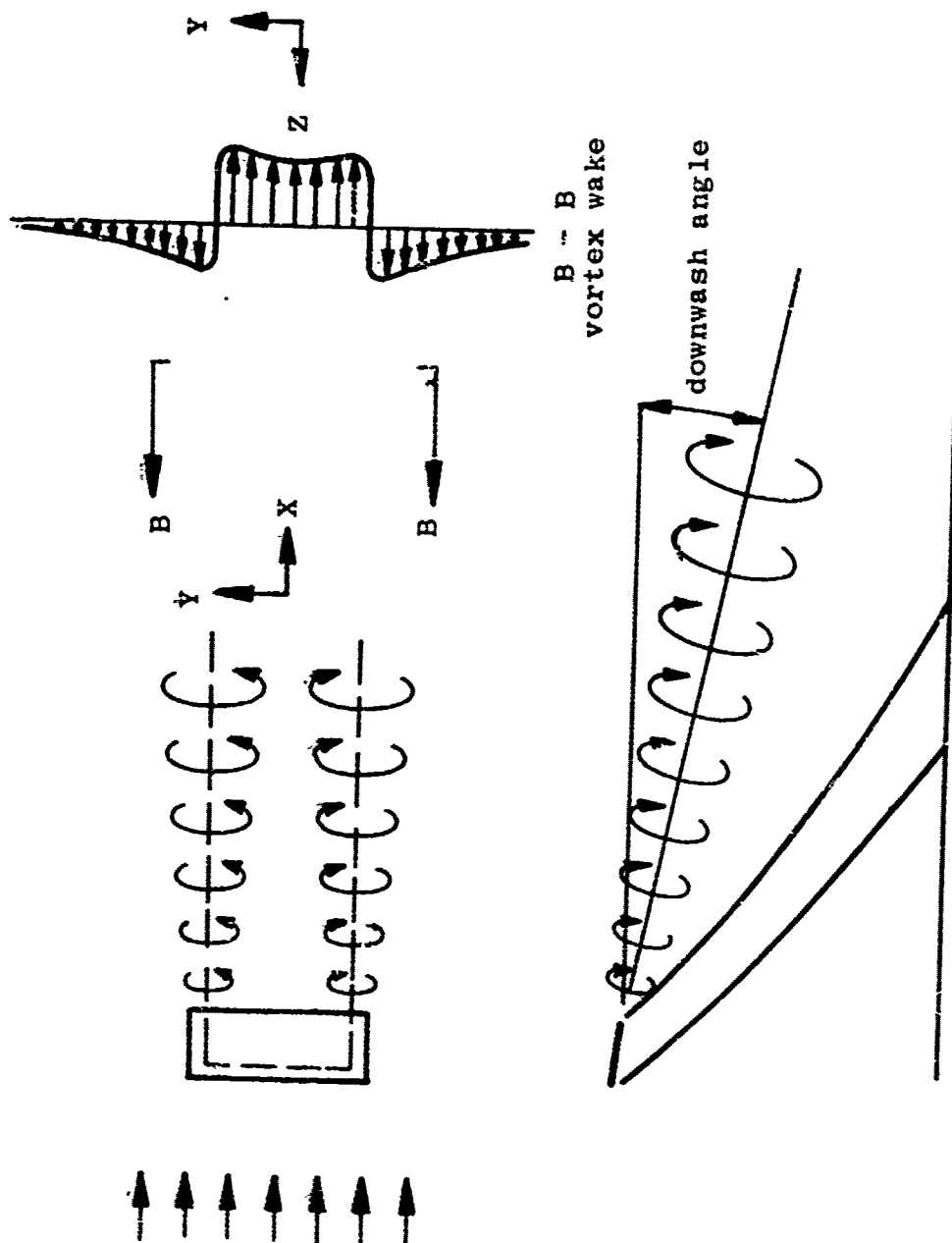


FIGURE 2.4.17. Finite aspect ratio effects

3. CONCLUSIONS AND RECOMMENDATIONS

3.1 Considerable progress was made in this contract in developing a new theory which permits the use of normal size models in wind tunnel tests to determine the sonic boom on the ground by measuring the pressure signature in the wind tunnel test section. The theory has been developed for axisymmetric flow conditions, and a start has been made on the theory for non-symmetric lifting configurations. It is recommended that the non-symmetric lifting theory be completed and that procedures for checking the theory in a wind tunnel be developed and suitable verification tests conducted.

3.2 Some calculations were carried out by means of an improved method for determining aircraft contours with desirable finite pressure rise times; included also was the determination of phantom body shapes which have predetermined finite rise times which can be simulated by heat addition to the flow upstream of the aircraft, for instance by lasers.

Concerning the application of laser beams to produce a desired heat input distribution through the mechanism of focusing laser beams and ionization of the flow, a few experimental test points, from previous tests with different objectives, are available. It is recommended that brief laboratory tests be designed and conducted in order to determine to what extent the control of the heat input at desired specific locations can be accomplished in laboratory and in flight operations.

3.3 Many previous investigations have shown that deviations from the conventional circular engine exhaust can cause dramatic improvements of the maximum lift coefficient and large effects on the noise level of engine exhausts. The research under this contract has shown that a slot-type engine exhaust has the unique capability of shifting lift from the solid surfaces of the wing to the region behind the wing, as far as the effects on the external flow and on the sonic boom are concerned. These results, which for the first time have clarified an important characteristic of slot nozzles, have been developed for two-dimensional flow conditions. It was shown that not only a shifting of the lift on the main wing and an associated reduction of the sonic boom was achieved, but also favorable effects on the performance of the aircraft in certain flight regimes and configurations were obtained. In view of the current interest in the application of non-circular engine exhausts for maximum lift and noise attenuation purposes, it is recommended that the two-dimensional theory for the slotted nozzle exhaust effects be extended to the three-dimensional theory, to be used as the basis for subsequent verification testing in wind tunnels and eventually in flight.

4. REFERENCES

- Aerospace Industries Association, Inc. (1970), Aerospace Year-book (48th Edition)
- Aviation Week and Space Technology (1970), Vol. 92, No. 1, January 5
- Barger, R. L. (1968), "Design of Bodies to Produce Specified Sonic-Boom Signatures", NASA TND-4707
- Batdorf, S. B. (1969), Aerospace Corporation ATR-70 (S9900)-1
- Bauer, R. C. (1971), Private Communication with Y. S. Pan
- Borner (1968), "Lectures on Cauchy's Problems in Linear Partial Differential Equations", Yale University Press
- Byrd, Paul F., and Friedman, Morris D. (1954), "Handbook of Elliptic Integrals for Engineers and Physicists", Springer-Verlag
- Carlson, H. W. (1964), "Correlation of Sonic-Boom Theory with Wind-Tunnel and Flight Measurements," TR R-213, NASA
- Cool, T. A. and Stephens, R. R. (1969), J. Chem. Phys. 51, 517.
- Cooper, R. (1971), Air Force Aero Propulsion Laboratories (private communication)
- Courant, R. and Friedrichs, K. O. (1948) Supersonic flow and Shock Waves, Interscience, New York, Chapters 3 and 4
- Gerry, E. T. (1970), IEEE Spectrum 7, 51; and elsewhere
- Hadamard (1909), "Integral Equations", Cambridge University Press
- Hayes, W. D. (1947), Linearized Supersonic Flow, thesis, California Institute of Technology
- Hayes, W. D. and R. C. Haefeli, (1968), NASA SP-180, 151
- Hayes, W. D. and Probststein, R. F. (1966) Hypersonic Flow Theory, Vol. 1, Academic Press, New York, Chapter 7
- Hertzberg, A., Johnston, E. W. and Ahlstrom, H. G. (1971), AIAA Paper 71-106
- Hildebrand, F. B. (1956), "Introduction to Numerical Analysis", McGraw Hill Book Co.
- Hilton, D. A. and Newman, J. W., Jr. (1966), J. Acoustical Soc. Am. 39, S31

- Hunton, Lynn W. (1968), "Current Research in Sonic Boom", NASA SP-180, Second Conference on Sonic Boom Research held at the NASA, Washington, D. C., May 9-10.
- Kane, E. J. (1967), NASA SP-147, 49
- Kane, E. J. (1966), J. Acoustical Soc. Am. 39, S26
- Kryter, K. D. (1965), J. Acoustical Soc. Am. 39, S65
- Kutler, Paul (1971), Private Communication with Y. S. Pan
- Kutler, P. and Lomax, H. (1971), "A Systematic Development of the Supersonic Flow Fields Over and Behind Wings and Wing-body Configurations using a Shock-Capturing Finite-Difference Approach", AIAA Paper No. 71-99.
- Laitone, E. V. (1947), "The Linearized Subsonic and Supersonic Flow About Inclined Slender Bodies of Revolution", Jour. Aero. Sc., 14.
- Lighthill, M. J. (1945), "Supersonic Flow Past Bodies of Revolution", Br. A.R.C., R&M No. 2003.
- Lighthill, M. J. (1948), "Supersonic Flow Past Slender Pointed Bodies of Revolution at Yaw", Quart. Jour. Mech & Appl. Math., L, Part 1.
- Lomax, H. (1955), "The Wave Drag of Arbitrary Configurations in Linearized Flows as Determined by Areas and Forces in Oblique Planes", RM A55 A18, NACA.
- Lomax, H. and Heaslet, M. A., (1956), "A Special Method for Fine Body Distortions that Reduce the Wave Drag of Wing and Body Combinations at Supersonic Speeds," Report 1282, NACA.
- McLean, F. Edward (1965) "Some Nonasymptotic Effects on the Sonic Boom of Large Airplanes", NASA TND-2877
- McLean, F. E., H. W. Carlson, and L. W. Hunton, (1966), NASA TND-3587
- Meinzer, R. A. (1971), AIAA Paper 71-25
- Miller, D. S. and Carlson, H. W. (1970), AIAA Paper 70-903
- Miller, D. S. and Carlson, H. W., (1969), NASA TND-5582
- Morris, O. A., Lamb, M. and Carlson, H. W. (1970), "Sonic-Boom Characteristics in the Extreme Near Field of a Complex Airplane Model at Mach Number 1.5, 1.8, and 2.5", TN D-5755, NACA

- Pan, Y. S. (1970a), "Application of Whitham's Theory to Sonic Boom in the Mid- or Near-Field," AIAA Journal, Vol. 8, No. 11, pp 2080-2082.
- Pan, Y. S. (1970b), "Extension of Whitham's Supersonic Projectile Theory," UTSI Report, DOT FA 70 WA-2260.
- Pan, Y. S. (1970c), "On Supersonic Wind Tunnel Wall Reflection", UTSI Report, DOT FA 70 WA-2260
- Pan, Y. S. (1971), "A Method for Wind Tunnel Investigations of Sonic Boom Based on Large Models," AIAA Paper, No. 71-184.
Also, "A Method for Wind-Tunnel Investigation of Sonic Boom," AIAA Journal, Vol. 10, No. 11, pp. 1408-1414 (1972)
- Pan, Y. S. and Varner, M. O. (1971), "Design of Bodies to Produce Specified Sonic-Boom Signatures without Shock Waves," UTSI Report, DOT FA 70 WA-2260
- Shapiro, A. H. (1953), The Dynamics and Thermodynamics of Compressible Fluid Flow, The Ronald Press Co., Vol. I
- Siegelman, D. (1970), J. Aircraft 7, 280
- Siegelman, D. (1967), "Pressure Signature of an Axisymmetric Body at Angle of Attack", AIAA Journal, Vol. 5, No. 12, pp 2280-2281.
- Spencer, D. J., Mirels, H., Jacobs, T. A. and Gross, R.W.E. (1970), Appl. Phys. Letters 16, 235
- Swigart, R. and Lubard, S. (1969), Aerospace Corporation, ATR-69 (S8125)-1
- Tricomi, F. G. (1957), "Integral Equations", New York, Interscience Press
- Tsien, H. S. and Beilock, M. (1949), Aeron. Sci. 16, 756
- Tsien, H. S. (1938), "Supersonic Flow Over an Inclined Body of Revolution", Journ. Aero. Sc. 5
- Van Dyke, M. D. (1951), "First- and Second-Order Theory of Supersonic Flow Past Bodies of Revolution", J. Ae. Sc., 18
- von Karman, T., and Moore, N. B. (1932), "The Resistance of Slender Bodies Moving with Supersonic Velocities with Special Reference to Projectiles", Trans. ASME 54
- Ward, G. N. (1955), Linearized Theory of Steady High-Speed Flow, Cambridge University Press, London, Chapters 8 and 9

Ward, G. N. (1949), "Supersonic Flow Past Bodies of Revolution", Quart. Jour. Mech. & Appl. Math., 2, Part 1.

Watson, G. N., (1966), A Treatise on the Theory of Bessel Functions, 2nd ed., Cambridge University Press, pp. 79-80, 202-203

Whitham, G. B. (1952), Commun. Pure Appl. Math. 5, 301

Willmarth, W. W. (1957), Rand Corporation, RM-2078 (AD 150681)

Wood, K. D. (1968), Aerospace Vehicle Design, Vol. I, Aircraft Design (Third Edition)

Zepler, E. E. and Harel, J.R.P. (1965), J. Sound Vib. 2, 249